UNIVERSITY OF LONDON THESIS

Degree PhD Year 2006 Name of Author TOWNSEND Benjamin Robert

Primary motor cortical – cerebellar interactions in the control of precision grip

Benjamin Robert Townsend

Institute of Neurology
University College London

Submitted for PhD (Neuroscience)
January 2006

Supervisor: Professor R. N. Lemon

ProQuest LLC
789 East Eisenhower Parkway
P.O. Box 1346
Ann Arbor, MI 48106-1346

Abstract

Primary motor cortical – cerebellar interactions in the control of precision grip

Benjamin Robert Townsend

The primary motor cortex (M1) and cerebellum are strongly interconnected structures. For control of the arm and hand, the cerebellum must influence other parts of the motor network with direct access to the spinal cord, since it has no descending projections to the lower cervical cord itself. One important control pathway involves interactions of the cerebellum with M1. This thesis describes findings from simultaneous recording of neuronal activity in these structures, with the aim of addressing how they interact.

Recordings were made from M1 and cerebellar dentate nucleus in macaque monkeys performing a precision grip task. Multiple single units and local field potentials (LFP) were sampled, concurrent with EMG from hand muscles. A variety of approaches were then taken to assess M1-cerebellar communication.

Correlations of neural discharge in M1 and cerebellum with muscle activity were evaluated. Evidence was found for linear encoding of muscle activity in both areas.

Different output pathways of M1 to cerebellum were identified and studied at the single neuron level. Neurons in each pathway were interconnected and showed similar activity patterns.

Functional connectivity between the two structures was investigated, by compiling spike-triggered averages (SpTAs) of local field potentials, and stimulus-triggered averaging of single units.

Finally, firing rates and LFP activity within these structures were monitored across different load conditions during blocked and randomized trial sequences. M1 and cerebellar activity was dissociated between these conditions, highlighting the role of the cerebellum in predictive control of grip force. Coupling of oscillatory LFP activity between these structures was consistently observed across task conditions. It is suggested that SpTA effects and coherent LFPs represent communication across short and broad time scales respectively.

Overall, this research demonstrates how simultaneous recordings can provide new insights into the roles of M1 and cerebellum in the control of hand movements.

Contents

Abbreviations

1DI – First Dorsal Interosseous
AbDM – Abductor Digiti Minimi
AbPB – Abductor Pollicis Brevis
AbPL – Abductor Pollicis Longus
AdP – Adductor Pollicis
BMI – Brain-Machine Interface
CCH – Cross-Correlation Histogram
CPN – Cortico-Pontine Neuron
CP – Cerebral Peduncle
CM – Corticomotoneuronal
DoM – Depth of Modulation
ECR – Extensor Carpi Radialis
EDC – Extensor Digitorum Communis
EEG – Electroencephalogram
EMG – Electromyogram
EPSP – Excitatory Post-Synaptic Potential
FDP – Flexor Digitorum Profundus
FDS – Flexor Digitorum Sublimis
FCU – Flexor Carpi Ulnaris
ICP – Inferior Cerebellar Peduncle
IFR – Instantaneous Firing Rate
IPSP – Inhibitory Post-Synaptic Potential
ISI – Inter-Spike Interval
LFP – Local Field Potential
M1 – Primary Motor Cortex
MCP – Middle Cerebellar Peduncle
MEG – Magnetoencephalogram
PSF – Post-Spike Facilitation
PSTH – Peri-Stimulus Time Histogram
PT – Pyramidal Tract
PTN – Pyramidal Tract Neuron
SD – Standard Deviation
SH – Spike History
STA – Stimulus Triggered Average
STC – Spike-Triggered Covariance
SpTA – Spike Triggered Average
UID – Unidentified neuron

Declaration of conjoint work

The work presented in this thesis is my own original work completed without assistance, apart from the following.

1. Critical stages of the surgical procedures were performed by Prof R N Lemon.
2. The experimental work was performed in collaboration with Prof R N Lemon, with technical assistance from members of his research group.
3. Data analysed from monkey M36 was collected from a previous experiment by Andy Jackson, Prof R N Lemon and collaborators.
4. The analysis in Chapter 3 was developed and applied in collaboration with Liam Paninksi, Department of Statistics, University of Columbia.
5. Spike discrimination software was supplied by Dr S N Baker, University of Newcastle upon Tyne.
6. Post mortem histology was performed with assistance from Prof R N Lemon and Jim Dick, Sobell Department of Motor Neuroscience and Movement Disorders, Institute of Neurology.
7. MRI analysis software was supplied by Dr R Richards, University College London.

Acknowledgements

I would like to extend my most sincere thanks to all the people who helped make this possible:

Roger Lemon, for giving me the opportunity to do my own research within such a fascinating area of neuroscience, and for his dedicated, expert supervision throughout the project.

Liam Paninski and Thomas Brochier, superb mentors and friends, who have provided continued assistance, guidance and advice.

Sam Shepherd, for her excellent technical assistance with all the experimental work.

Thanks also to Eric Schmidlin, Rachel Spinks and Gita Prabhu for their help with recording sessions, and for making the lab a fun place to work.

Stuart Baker, for providing crucial advice on statistical issues; Lee Miller at Northwestern University, for his expert tutelage on cerebellar recordings, and Andy Jackson for helping me to get started at the beginning.

The staff of the Sobell department including Peter Kirkwood, Victor Baller, Ed Bye, Chris Seers, Linda Greensmith, Deborah Hadley and Kully Sunner for their help.

All my family, for their massive support and understanding, especially during the difficult bits – I don't think I can thank you enough!

Last but not least, huge thanks to Bea for her support and thanks to my friends, you all provided an excellent balance between work and play!

Chapter 1: Introduction

1.1 Background

Early anatomists proposed theories of cerebellar function based on the fact that it is distinct from the rest of the brain. Eristratus (304BC – 250BC) thought it to be the seat of intelligence, since it is so highly convoluted. However, since the first part of the 20th century, neuroscientists have recognised the importance of understanding the precise role of the cerebellum, by studying how it interacts with the rest of the brain. Connections from cerebral cortex to cerebellum by way of the pontine nuclei had been noted by Cajal in 1909 (Cajal 1952), while the cerebellar nuclei were known to project to the motor cortex by way of the thalamus, according to Vogt (reviewed in Henneman et al., 1952) . A further motivation for studying interactions between the two was the concomitant enlargement of cerebrum, posterior cerebellum and the pons in higher primates (Matano et al. 1985a, b).

While Flourens and Babinski noted the importance of the cerebellum in the coordination of movement, many investigators realised from an early stage that this involved an important relationship with the motor cortex. The work of Rossi (1912) and Moruzzi (1941) showed that cerebellar stimulation could affect cerebral motor functions. This was supplemented by Walker (1938) who showed that cerebellar stimulation changed the amplitude and frequency of electrical cerebro-cortical activity - particularly in the motor cortex. Aring (1936) observed that cerebellar tremor was alleviated by ablation of motor cortical areas. Taken together, these findings suggested a dynamic influence of the cerebellum on the motor cortex.

Further stimulation experiments indicated that certain regions of the cerebellum affected the same cortical areas as they were influenced by (Henneman et al., 1952; Snider and Eldred, 1952). Thus, it also became apparent at an early stage that the connectivity between cerebral cortex and cerebellum was reciprocal, which led to speculation about the possible functions of these loops.

Since then, significant advances in our understanding of voluntary movement control by the primary motor cortex (M1) and the role of the cerebellum have been made. It is now possible to decode the activity of single neurons in M1 in terms of the major parameters of a voluntary movement, such as direction, force and velocity. An interesting synthesis of neurophysiological recordings and theoretical modelling has facilitated the development of elaborate theories of cerebellar computation (Ito, 2005). Yet the precise nature of the interplay between the motor cortex and the cerebellum during the control of voluntary movements remains unclear. Recent advances in techniques to record neural activity in multiple brain areas simultaneously (Brown et al., 2004) have now provided us with the tools to begin to tackle this issue experimentally.

Before describing more recent findings about M1-cerebellar interactions, a review of what is currently understood about the structure, connectivity and function of M1 will be conducted, followed by cerebellum. The case will be made that both structures have prominent roles in the control of skilled finger movements.

1.2 The corticospinal system and primary motor cortex

1.2.1 The corticospinal tract

The capacity of primates to produce relatively independent movements of the fingers during grip is considered to be critically dependent on the cortico-motoneuronal component of the corticospinal tract (CST). Axons from pyramidal cells in layer V of the primary motor cortex (M1) constitute the bulk of the fibres in the CST (around 60% in man), with the other cortical sensorimotor areas making less substantial contributions. These fibres pass through the medullary pyramid before decussating and terminating in contralateral spinal segments, and are referred to as pyramidal tract neurons (PTNs). Early studies utilising electrical stimulation of the pyramid suggested the existence of this projection, e.g. the demonstration of evoked antidromic gross potentials in ipsilateral M1 of the rabbit (Woolsey and Chang 1948; Chang 1954) and the generation of antidromic action potentials in cat M1 Betz cell intracellular recordings (Phillips 1956). A key feature of the CST is that single axons give rise to multiple collaterals in the cord in cat and monkey (Shinoda et al., 1979; Shinoda et al., 1981; Lawrence et al., 1985; Shinoda et al., 1986). These in turn exert an excitatory monosynaptic influence on multiple motoneurons controlling different hand and arm muscles, as revealed by stimulation studies (Lemon et al., 1987) and spike triggered averaging of multi-unit EMG (Cheney and Fetz, 1980; Buys et al., 1986; McKiernan et al., 1998). Such divergence is thought to facilitate the activation of small groups of synergic muscles needed for fractionated patterns of muscle activity which underlie skilled hand function. The importance of the CST is

underscored by the severe impact on finger movements caused by complete, bilateral lesions to the pyramidal tracts (Lawrence and Kuypers, 1968).

1.2.2 Intrinsic connectivity of M1

In the macaque monkey, the primary motor cortex (MI, or Brodmann's area 4) lies immediately anterior to the central sulcus and is characterised by giant pyramidal "Betz" cells in lamina V and an absent layer IV (Geyer et al., 2000). The intrinsic structure and connectivity of M1 have been studied extensively in both cat and monkey.

The pyramidal cells (including Betz cells) provide most of the cortico-cortical and sub-cortical connections, as well as a substantial proportion of local excitatory connections (Thomson and Deuchars, 1997). Their morphology has been described by intracellular iontophoresis of HRP in monkey M1 (Ghosh and Porter, 1988). All pyramidal cells except those in lamina VI give off ascending dendrites that terminate in layer I in a tuft, and all except those in laminae II and VI give rise to intra-cortical axon collaterals.

Pyramidal tract neurons (PTNs) in macaque M1 produce axon collaterals which arborise predominantly in laminae V and VI of the cortex (Ghosh and Porter, 1988a). Two types of collaterals are seen; short collaterals which arborise in the vicinity of the soma, and long collaterals which spread over distances of approximately 1mm. These collaterals are excitatory: stimulating neighbouring pyramidal tract neurons (PTNs) or the pyramidal tract itself, evokes EPSPs in single fast PTNs (Kang et al., 1988, 1991). But it can also induce IPSPs (Renaud and Kelly, 1974; Renaud et al., 1974), for example in slow PTNs or other M1 pyramidal cells (Ghosh and Porter, 1988b) which are disynaptic, indicating that they are mediated through local inhibitory interneurons of which there are a variety in the neocortex (Thomson and Deuchars, 1997).

The radial spread of these axon collaterals gives rise to functional properties of M1 investigated through intra-cortical microstimulation (ICMS) mapping. These maps reflected multiple representations of simple movements about a single joint, with significant overlap between the representations (Lemon, 1988; 1999). Huntley and Jones (1991), combining ICMS with cortical injections of horseradish peroxidase in macaque M1, found that identical movements could be elicited from multiple non-contiguous sites, and that collateral connectivity linked regions giving movement of same joint/region. This organisation has been confirmed for hindlimb and face areas of M1 (Tanji and Wise, 1981; Huang et al., 1989).

1.2.3 Afferent connectivity of M1

Quantitatively, premotor and supplementary motor areas dominate the inputs to M1, but there are projections also from Brodmann's areas 3a (SI)1, 2 and 5 (Ghosh et al., 1987), premotor cortex and supplementary motor area (Dum and Strick, 2005), as well as callosal inputs from contralteral M1 (Jones 1986). Short-latency peripheral inputs, especially from muscles, reach the motor cortex through the projection from area 3a. Movement related neurons in M1 have receptive fields similar to SI neurons, except that they are often larger and multimodal. In M1, the rostral part receives mainly non-cutaneous ("deep") inputs while the caudal part receives mainly cutaneous inputs (Tanji and Wise, 1981); this organization applies to the hand area of M1. Furthermore, the afferent input to this area exhibits the same patchy and overlapping features seen in the motor output (Lemon, 1981).

The rostral part of M1 is innervated chiefly by the nucleus ventralis lateralis pars oralis (VLo), plus smaller contributions from rostral nucleus ventralis posterior lateralis (VPLo) and the VPLo-VLc (nucleus ventralis lateralis pars caudalis) complex. The caudal part of M1 receives its greatest input from VPLo, with a small contribution from VLo (Matelli et al., 1989). As described below, VPLo and VLc receive major inputs from the cerebellum (Asanuma et al., 1983a,b) while VLo receives major input from the basal ganglia (Schieber, 1999). These thalamocortical afferents terminate in all cortical laminae, but are densest in lamina III and the deep part of lamina V (Geyer et al., 2000).

1.2.4 Efferent connectivity of M1

Corticothalamic connections arise from pyramidal cells in laminae V and VI; the latter projection is the largest (Jones, 1986). Within lamina V corticostriatal projections arise from the superficial part of the layer; corticotectal, corticopontine and corticobulbar projections arise from the intermediate and deeper parts. Pyramidal cells in the deeper part of lamina III are the main source of callosal axons connecting M1 with its contralateral counterpart (Jones 1986). Finally, axons forming the corticospinal tract arise from medium to large sized pyramidal neurons with somata also in the deeper parts of lamina V (Jones and Wise, 1977). Direct corticopontine projections are supplemented by collaterals of the corticospinal tract (Ugolini and Kuypers, 1986), providing 2 pathways of efferent motor cortical-cerebellar connectivity (see below).

1.2.5 Functional organisation of M1 output

There is a gross somatotopy in M1, as demonstrated by electrical stimulation of the motor cortex. The face is represented laterally close to the Sylvian fissure, the leg medially close to the midline (extending on the mesial wall of the hemisphere), and the arm in between. Proximal parts of the extremities and axial body parts are primarily represented on the exposed cortical surface, whereas distal parts of the extremities and acral parts of the face (lips and tongue) are mainly represented in the rostral bank of the central sulcus (Geyer et al., 2000). The ordered mapping of the body onto M1 to produce a motor "simisculus" or "homunculus", would suggest that spatially separate parts of the cortex control individual body parts.

But at smaller spatial resolution, this concept breaks down. ICMS can evoke movements of the same joint or part of body at multiple locations (Gould et al., 1986; Huntley and Jones, 1991) and multiple muscles can be activated from the same site (Donoghue et al., 1992). This divergence seen in the ICMS effects is consistent with the divergence of single corticospinal axons to innervate multiple hand muscle motoneurons, described above. Corresponding observation of spike-triggered average effects in multiple hand muscle EMGs from a single CM cell defines the "muscle field" of the CM cell, which typically comprises 2-3 different muscles (Cheney and Fetz, 1980; Buys et al., 1986; McKiernan et al., 2000). Likewise, input from multiple CM cells converges onto single motoneurons, and these colonies of CM cells originate in overlapping areas of M1 (Andersen et al., 1975). The topography of M1 output is complex and highly fractionated.

1.2.6 Nature of movement representation in M1

There is evidence of functional modulation of CM connectivity during task performance. For example, CM cells discharge at higher rates when the target muscle on which they exerted maximum PSF is most active relative to other muscles (Bennett and Lemon, 1996); and CM cells with similar muscle fields show more synchronised activity (Jackson et al., 2003). Thus it has been suggested that the activity of individual CM cells contributes towards the fractionation of hand muscle activity underlying skilled movements of the fingers (Porter et al., 1993).

In light of these important findings, it would seem natural to conclude that the function of the motor cortex is the control of muscle activity. This has been investigated by studying the relationship of M1 unit discharge to the time course of EMG recorded from hand and forearm muscles during reaching tasks. (Holdefer and Miller, 2002) found that the activity of single M1 neurons could be described in terms of their correlations with a number of muscles, such that cells could be divided into distinct clusters which were thought to be cortical representations of "functional muscle synergies". Furthermore, Morrow and Miller (2003) were able to reconstruct the time course of EMG activity in single muscles from the combined spiking of small ensembles of up to 15 neurons.

However, arguing against this hypothesis of M1 control is a wealth of data demonstrating correlations between neuronal activity and a variety of other movement parameters.

Firstly, the work of Schieber and colleagues moves a step up from relating spiking to muscle activity, and correlates discharge of M1 neurons with finger movements. They have found multiple, overlapping representations of finger movements from

studying the discharge of single M1 neurons (Schieber and Hibbard, 1993). It has been suggested that, at least for the M1 hand area, these cells comprise a distributed network comprising diverse neuronal elements – individual neurons code for neither single muscles or movements – which allows for many combinations of muscle activity that can produce a huge variety of movements (Poliakov and Schieber, 1999).

An alternative approach has been to study the relationship of neuronal discharge to extrinsic movement parameters. The first demonstration of this was the correlation of discharge with force exerted at the wrist (Evarts, 1968). Humphrey and collaborators (1970) correlated the spiking of M1 neurons with position, velocity and force information during a wrist tracking task and were able to predict the time course of these variables from the spike rates of small groups (~5) of these cells. Georgopoulos et. al. (1986) observed that the discharge of single M1 neurons varied with the direction of movement in a centre-out reaching task, such that cells were tuned to a particular direction. These tuning curves, frequently observed for M1 neurons during arm reaching (Moran and Schwartz, 1999) and hand tracking (Paninski et al., 2004c), are often described as "cosine" due to their sinusoidal appearance in polar coordinates. As well as position, single unit discharge can also be correlated with hand velocity (Fu et al., 1995; Paninski et al., 2004a,c) enabling the full time varying hand-trajectory to be reconstructed from the activity of neuronal ensembles (Serruya et al., 2002; Hatsopoulos et al., 2004; Truccolo et al., 2005).

Finally, tuning of M1 neurons to static and dynamic force has also been extensively demonstrated, in wrist movement and precision grip tasks (Cheney and Fetz, 1980; Wannier et al., 1991; Porter et al., 1993; Hepp-Reymond et al., 1999).

The key feature linking all the above studies is that they are correlative in nature. It is not clear whether any of these parameters are explicitly encoded by M1 neurons, and thus the function of M1 in terms of its neural "code" for movement remains unclear.

Theoretical studies have attempted to clarify the situation. For example, a model proposed by Todorov (2000) assumed that M1 PTNs contribute additively towards the activation of muscles; correlation of neuronal discharge with kinematic parameters then emerges due to compensations made by the M1 output for each muscle's state dependence.

This theory has not fully resolved the issue, since it only accounts for the activity of identified M1 output neurons, yet these correlations are observed throughout the M1 hand and arm area. Also, a similar "encoding dilemma" exists in terms of cerebellar movement representations. Here again, tuning of cerebellar neurons, both in the cortex and the deep nuclei, can be demonstrated for muscle activity (Wetts et al., 1985) direction of reaching (Fortier et al., 1989) position and/or velocity (Mano and Yamamoto, 1980; Fu et al., 1997) and force (Smith and Bourbonnais, 1981).

It can be argued that the dichotomy between intrinsic versus extrinsic movement parameters is a false one, because fundamentally the control of muscles cannot be separated from the control of movements. The issue is the "level of explanation" which is necessary for a full description of how movements are controlled by groups of neurons within M1 and cerebellum. For example, is it better to study the contribution that these areas make by studying control at the level of muscles, or at the level of the trajectory of the hand? It is possible, of course, that control by these structures incorporates features that have been covered by all the major encoding theories, which operate at multiple levels (Scott, 2000). Support for this point of

view is provided by findings that neurons in both M1 and cerebellar dentate nucleus combine information about multiple movement features, such as patterns of muscle activity and kinematics (Thach, 1978; Kakei et al., 1999).

1.2.7 M1 Plasticity

The motor map which has been described for M1 is not rigid; it can be modified, such that the underlying cortical representations of movement are reorganised over time. This can include reorganisation over long time scales, related to changes in the state of the motor system. For example, Donoghue and Sanes (1988), through stimulation mapping/ICMS, observed increased representation of proximal (i.e. shoulder) and vibrissal movements in rat M1 2-4 months after amputation of the contralateral forelimb, which was due to changes in the underlying cortico-cortical connectivity.

It can also include plasticity over shorter time scales. Using trans-cranial magnetic stimulation to activate the motor cortex non-invasively in human subjects, Pascual-Leone and collaborators found an increased cortical representation of finger movements after 5 days' daily training on a 5-finger piano exercise in the contralateral hand. These changes paralleled improved task performance but were only evident approximately 20 mins after each training session, suggesting that acquisition of the necessary motor skills was associated with a short term change in the cortical outputs to the hand muscles (Pascual-Leone et al 1995; see Pascual-Leone et al., 2005). This "use dependent plasticity" has also been observed in a repetitive thumb movement task (Classen et al., 1998). These short-term changes

might underlie the initial acquisition of a motor skill and could involve temporary modification of existing connectivity in the cortex, perhaps by the unmasking of excitatory intra-cortical connections through altered intra-cortical inhibition (Jacobs and Donoghue, 1991). Training effects can be enhanced in humans using TMS with a theta burst stimulation paradigm (Hummel and Cohen, 2005). At the single cell level, M1 neurons in the monkey can show shifts in their "preferred direction" during performance of a centre-out reaching task; these shifts correlate with learning of altered task dynamics (Shadmehr and Mussa-Ivaldi, 1994) i.e. development of an internal model (Li et al., 2001). Therefore these observed changes in cortical movement representations may involve changes in the neural coding of movement parameters.

Longer term changes (Donoghue and Sanes, 1988) would involve formation of new connections, underlying the long term acquisition of a motor skill. Thus motor learning can be seen as a two step process (Pascual-Leone et al., 2005).

1.3 The cerebellum

1.3.1 Anatomy of the cerebellum

Mammalian cerebella all have the following structural features:

1. Cerebellar cortex, which is relatively uniform throughout
2. A white matter core "corpus medullare" – compact mass of myelinated axons surrounded by cortex
3. Deep cerebellar nuclei within the white matter, which receive the cortical outputs
4. Three cerebellar peduncles which connect the cerebellum to the brain stem and carry cerebellar afferent and efferent projections.

The cerebellar cortex is a highly folded sheet, with leaf-like plates or "folia" running transversely across the cerebellum. There is a fundamental pattern of 10 lobules divided by long transverse fissures (Palay and Chan-Palay, 1987; Voogd, 1967). Its gross anatomy is described according to this transverse arrangement, giving the flocculo-nodular lobe (lobule X), the anterior lobe (lobules I-V) and the posterior (lobules VI-IX) lobe. The latter, which is massively enlarged in primates, comprises medial and lateral sections. The cerebellum can also be divided up in a longitudinal fashion based on the presence of postulated phylogenetic differences (Voogd, 1967), comprising cerebellar vermis in the middle and hemispheres laterally, with an intermediate or paravermal zone in between. The hemispheres correspond to the lateral part of the posterior lobe.

In the macaque, the deep cerebellar nuclei comprise four distinct subnuclei bilaterally (Chan-Palay, 1977). Most medial is the fastigial nucleus which sits at the crown of the 4th ventricle; followed by the interpositus nucleus which itself consists of two distinct parts (anterior and posterior); most laterally is the nucleus dentatus or lateralis. In primates, the size of the dentate nucleus is expanded greatly in parallel with the expansion of the posterior lobe, particularly its more lateral part.

In general, afferent inputs to the cerebellum course through the inferior and middle cerebellar peduncles. The inferior cerebellar peduncle contains ascending projections carrying spinal, vestibular, reticular and olivary inputs, while the middle cerebellar peduncle contains projecting fibres from the pons, comprising pontocerebellar input from the pontine nuclei and the pontine reticular formation. The superior cerebellar peduncle carries mainly efferent projections from the cerebellar nuclei which connect with a range of targets in the midbrain. An afferent projection passes through this peduncle in the form of fibres from the anterior spinocerebellar tract which are relayed to the anterior lobe (Palay and Chan-Palay, 1987) .

Throughout the cerebellum the cortical sheet is organised into 3 basic layers – the molecular layer which is the most external, followed by a single layer of Purkinje cells, and finally the granular layer which borders the white matter. In each folium, cells and their processes within these layers have a highly regular organisation with respect to the transverse and parasagittal dimensions of the folium.

The granular layer contains an immense number of granule cells – $10x10^{11}$ in humans (Thach 2000) – which are extremely densely packed. Granule cell axons ascend to the molecular layer, where they bifurcate in a "T" shape and run longitudinally in the folium in parallel with each other (Palay and Chan-Palay, 1987). The dendritic trees of the Purkinje cells, arranged in orderly longitudinal

rows, push up into the molecular layer. As these parallel fibres course along the folium they pass through the Purkinje arborisation at right angles, making extensive synaptic contacts so that each Purkinje cell receives up to 200,000 parallel fibre synapses in humans (Llinas, 1981). Parallel fibre input is excitatory and mediated by glutamate (Voogd and Glickstein, 1998). These fibres run up to 6mm in monkey cortex, thus each one contacts many hundreds of Purkinje cells along its course.

The two main inhibitory interneurons of the molecular layer are the stellate cells and the basket cells, which both provide GABAergic feed-forward inhibition of Purkinje cells. Their dendritic trees are also contacted by parallel fibres. Golgi cells are found in the granular layer: these extend dendrites into the molecular layer which are contacted by parallel fibres, and provide GABAergic feedback inhibition onto the granule cells (Voogd and Glickstein, 1998).

One source of afferent input to the cortex is via the climbing fibres, derived from axons of neurons in the contralateral inferior olive (see below). As a rule each Purkinje cell also receives input from a single climbing fibre. En route to the molecular layer, collaterals of climbing fibres contact both Golgi and granule cells (Palay and Chan-Palay, 1987).

The second source is through the mossy fibres, axons derived from precerebellar nuclei that relay vestibular, pontine, reticulo-spinal and spinal inputs to the cortex. In the granular layer, these fibres ramify into branches and form synaptic complexes (rosettes) via which mossy fibres make glutamatergic contacts with granule and Golgi cells.

Purkinje cells axons provide the sole output of the cortex, inhibiting neurons of the deep cerebellar nuclei. This output is organised in a pattern of parallel longitudinal zones: Purkinje cells of a zone or pair of non-contiguous zones project to the same

target nucleus. Climbing fibre input from the inferior olive follows the same organisation, so that subnuclei of the inferior olive project to a single Purkinje cell zone or pair of zones which share the same target nucleus. These climbing fibres also pass collaterals to the corresponding target nucleus, leading to the concept of a cerebellar "microzone" (Voogd and Glickstein, 1998; Sugihara and Shinoda, 2004). In contrast, mossy fibre input is organised transversely (Voogd, 1967).

1.3.2 Main mossy fibre afferent inputs

Inputs from muscle spindles, Golgi tendon organs, pressure and tactile organs in the skin and deeper tissues of the forelimb are conveyed to the cerebellum through the cuneocerebellar and rostrocerebellar tracts. Axons in these tracts originate from cells in the dorsal column nuclei and project to the ipsilateral cerebellar cortex through the inferior cerebellar peduncle (ICP), terminating as mossy fibres chiefly in the pars intermedia and vermis of lobules V, anterior VI, posterior IV, and VIIIA (Bloedel and Courville, 1981; Palay and Chan-Palay, 1987).

Indirect input from spinal cord and cerebral cortex is relayed to the cerebellum from neurons in the precerebellar reticular nuclei, through the ICP (Figure 1). The paramedian nucleus and lateral reticular nucleus receive direct ascending spinal inputs, while nucleus reticularis tegmenti pontis (NRTP) receives direct input from the descending pathways including input from cerebral cortex. Its major input, however, is from the contralateral cerebellar nuclei via the superior cerebellar peduncle (Carpenter and Nova 1960; Brodal and Bjaalie 1992). In turn, NRTP

projects strongly to lateral hemispheres and dentate nucleus (Bloedel and Courville, 1981; Gerrits and Voogd, 1987).

In the monkey, the pontine grey receives dense projections from contralateral M1, premotor cortex (Brodmann's area 6) and the supplementary motor area. Visual projections are also received from contralateral dorsal stream visual areas 7a, LIP (lateral intra-pareital), MST (medial superior temporal), MT (middle temporal) and the frontal eye fields (Allen and Tsukahara, 1974; Glickstein, 1985, 2000, Stein and Glickstein 1992). In contrast, there are either sparse inputs or none at all from primary visual cortex (V1), or inferior temporal cortex (IT). In addition, there is a modest input from medial prefrontal cortex but little or none from the lateral prefrontal areas (Glickstein 2006). These projections decussate and enter the cerebellum via the middle cerebellar peduncle (MCP) terminating as mossy fibres particularly in lateral cerebellar cortex and nuclei (Voogd and Glickstein, 1998). As will be described below, there is substantial input via this route from the primary motor cortex (M1). Mossy fibres from the pontine nuclei, NRTP and the lateral reticular nucleus send excitatory collaterals to the deep cerebellar nuclei (Shinoda et al., 1992; Holdefer et al., 2005). There is evidence from anatomical tracing studies that the strength of collaterals from NRTP is somewhat greater than those from the pontine nuclei (Mihailoff 1993; Gerrits and Voogd 1987).

Proprioceptive and somatosensory information from the forelimb is also relayed from the dorsal column nuclei to the contralateral inferior olive.

1.3.3 Efferent connections

The cerebellar nuclei contain a heterogenous group of projection neurons: excitatory neurons which use glutamate and/or aspartate as their neurotransmitters, and inhibitory neurons using GABA and/or glycine (Chen and Hillman 1993; DeZeeuw and Berrebi 1995). Output projections from dentate nucleus and interpositus pass through the SCP, decussate and divide into ascending and descending parts (Figure 2). Ascending excitatory projections from both nuclei terminate in the magno- and parvocellular portions of the red nucleus (Chan-Palay, 1977), and ventrolateral (VL) thalamus (Asanuma et al., 1983a,b) which is an important relay for cerebellar inputs to the motor cortex (Hoover and Strick, 1999). Descending excitatory projections are sent to reticular tegmental nucleus and NRTP. Dentate also sends strong *inhibitory* projections to the principle olive (Chan-Palay, 1977).

Finally, injections of horseradish peroxidase into cat and monkey cerebellar cortex have demonstrated dentate-cortical projections (Tolbert et al., 1976, 1978) which also ramify in the granular layer as mossy fibres (Chan-Palay, 1977); both nucleo-cortical and nucleo-olivary projections are collaterals of nucleo-fugal axons . Thus there exist multiple internal loops between nuclei and cortex, termed "corticonuclear complexes" (Ito, 1984).

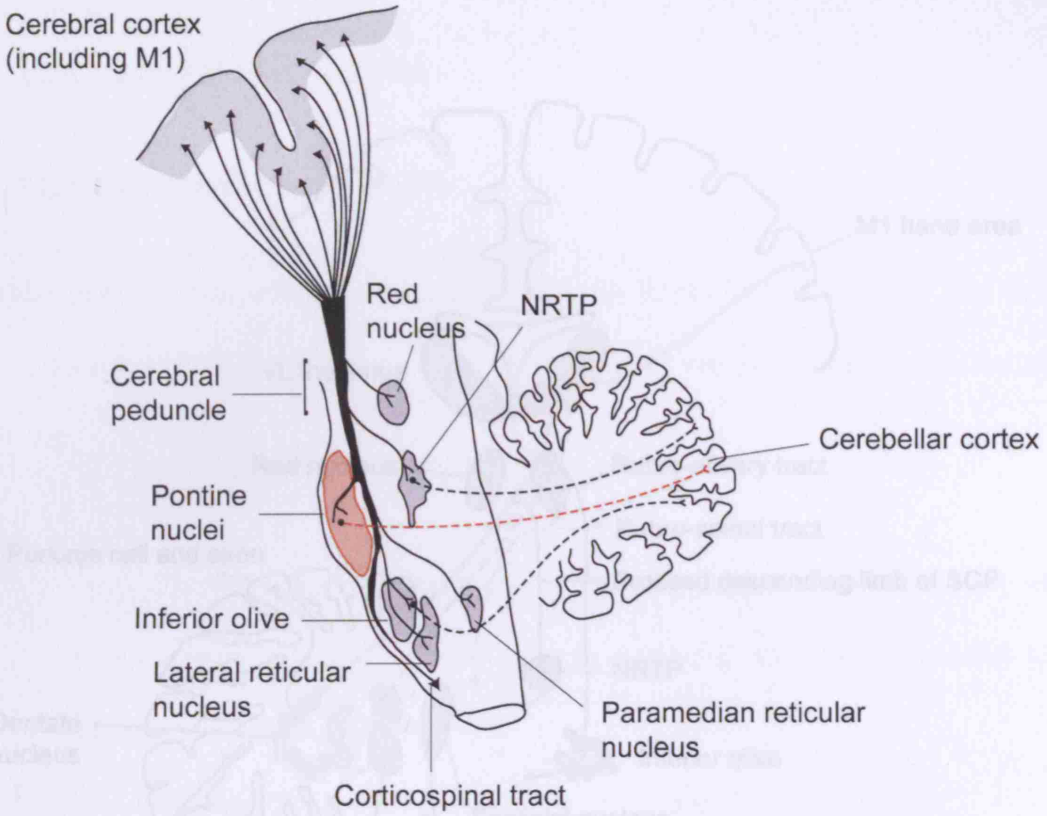

Figure 1.1. Cerebellar afferent connectivity
Simplified diagram of cerebellar afferent connectivity, including corticopontine and corticospinal pathways, in the human brain, adapted from Brodal (1981). Nuclei and pathways of interest are highlighted. N.B not all projections to pontine nuclei are collaterals of corticospinal tract (see text below). NRTP = nucleus reticularis tegmenti pontis.

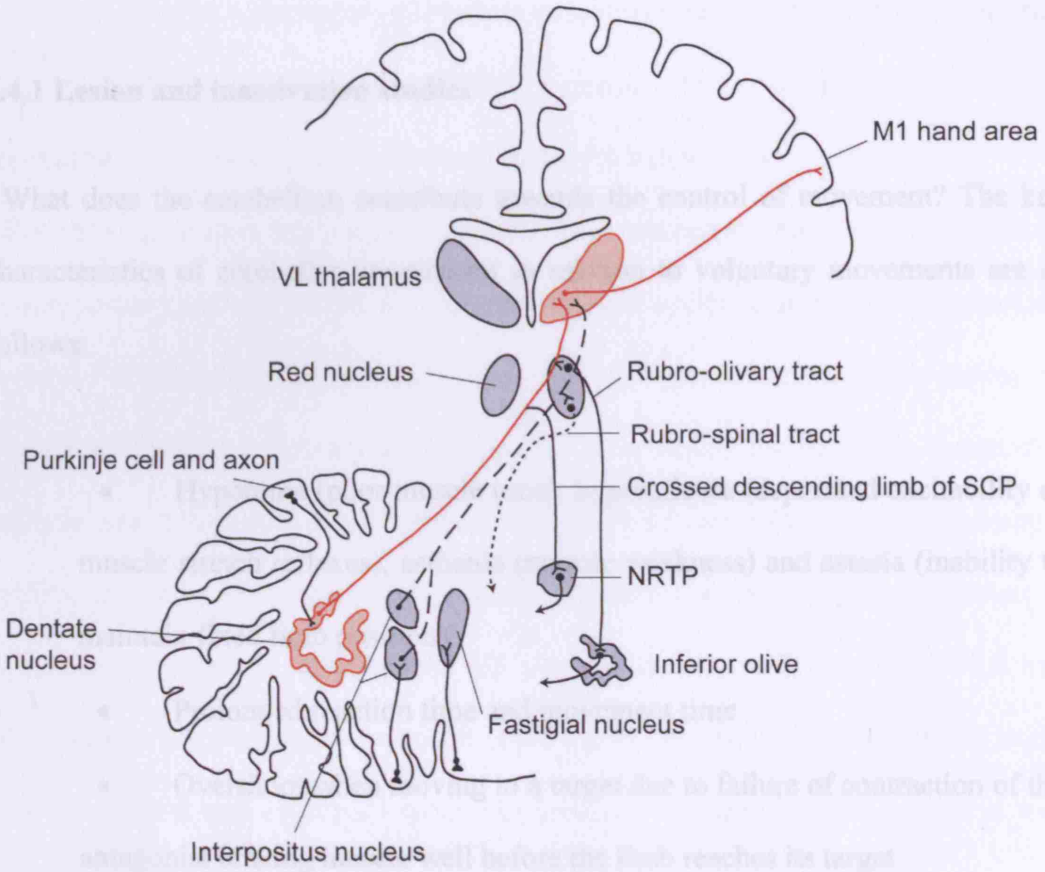

Figure 1.2. Cerebellar efferent connectivity
Simplified diagram of cerebellar efferent connectivity, adapted from Brodal (1981). Pathways and nuclei of interest are highlighted. Projections of fastigial nucleus are omitted for clarity. SCP = superior cerebellar peduncle. NRTP = nucleus reticularis tegmenti pontis.

1.4 Theories of cerebellar function

1.4.1 Lesion and inactivation studies

What does the cerebellum contribute towards the control of movement? The key characteristics of cerebellar impairment in relation to voluntary movements are as follows:

- Hypotonia (poor muscle tone), hyporeflexia (depressed excitability of muscle stretch reflexes), asthenia (muscle weakness) and astasia (inability to maintain fixed limb position)
- Prolonged reaction time and movement time
- Overshoot when moving to a target due to failure of contraction of the antagonist braking muscle well before the limb reaches its target
- Intention tremor, "hunting" for the target
- Impairments particularly to visually guided movements e.g pointing and tracking.
- Smooth, continuous movements become discontinuous ones
- Inability to perform rapid sequences of alternating movements (adiadochokinesia)
- Inability to produce periodic movements in response to an external signal

The general feature linking these deficits seems to be "coordination", as noted by Flourens in 1824 (Glickstein, 1997). Movements are not abolished but are poorly

timed and executed. It has been suggested that uncoordinated movements in these patients are due to a disruption of predictive control implemented by the cerebellum (Ito, 1984; Stein and Glickstein, 1992). Evidence from a variety of experimental approaches supporting this hypothesis is reviewed below.

Several studies have been able to replicate the impairments seen in human patients by temporarily inactivating dentate and interpositus nuclei in monkeys using cooling probes. For example, Conrad and Brooks (1974) observed errors in the timing of muscle contraction following dentate inactivation, during mechanically terminated ballistic arm movements. Inactivation of dentate and interpositus by cooling disrupts predictive muscle activation which normally counteracts perturbing torque pulses in an arm movement task, and reduces M1 activity related to this response (Vilis and Hore, 1980). Intention tremor was observed when dentate was cooled during rapid arm movements and especially when perturbation was applied while the arm was held in a target position (Vilis and Hore, 1977). Arm movements also become dysmetric (Flament and Hore, 1986). These findings suggest that the cerebellum makes an important contribution towards the timing and coordination of muscle activity in voluntary arm movements, including activity of a predictive nature (Stein and Glickstein, 1992).

As with human patients, cerebellar inactivation can also prolong reaction times: unilateral lesions to the dentate nucleus delay reaction time for ballistic arm movements in response to a cue (Spidalieri et al., 1983). These effects suggest that the cerebellum may be involved in movement initiation, which was investigated by way of electrophysiological recordings from dentate and interpositus nuclei. Consistent with these data, dentate units can fire in advance of the discharge of M1 units in wrist flexion/extension tasks by about 40-60 ms (Thach, 1975). Dentate

tends to lead M1 when arm movements are visually triggered (Thach, 1978), and Strick (1983) found preparatory dentate neuron activity related to a prior instruction. However, there can be much overlap in the timing of pre-movement activity between dentate and M1. Thus again the contribution of these cerebellar neurons in these tasks may be one of prediction in relation to a cue to move, which helps to speed up the reaction time (Stein and Glickstein, 1992).

1.4.2 Cerebellar motor learning

An influential theory of motor learning by the cerebellum (Marr, 1969; Albus, 1971) states that it acts as a pattern classification device which is taught to produce an appropriate output in response to an arbitrary input (Boyden et al., 2004). The focus here is the olivocerebellar system described above. According to the theory, mossy fibres – with their diverse projections to wide areas of cerebellar cortex – provide an opportunity for different combinations of sensory input to be associated with different motor outputs, through parallel fibre (PF) synapses onto Purkinje cells. Then, climbing fibres (CF) provide an instructive signal which regulates the strength of the PF – Purkinje cell synapse, forming new stimulus-response associations. Synaptic strength may be regulated by long term depression evoked by coincident activity of CFs and PFs (Ito, 2000).

Although undoubtedly a simplification, motor learning can be observed experimentally according to the principles of this theory, by studying eyeblink conditioning: classical conditioning of nictating membrane and eyeblink responses with airpuff as an unconditioned stimulus (US) and a tone as the conditioned

stimulus (CS). A large body of work suggests that this depends on the cerebellum (De Zeeuw and Yeo, 2005): inactivation of cerebellar cortex, nuclei and the inferior olive all prevent acquisition. In terms of the Marr-Albus hypothesis, the CS is conveyed to the cerebellum via activation of mossy fiber afferents from the pons while the US is signaled by climbing fiber afferents from the inferior olive. Output from the cerebellum, in the form of increased activity of particular neurons in the cerebellar interpositus nucleus, drives the efferent pathways responsible for the expression of the learned responses

A hallmark feature of this motor learning is the correct timing of the conditioned response – the nictating membrane or eyeblink response – which is elicited to avoid the air-puff signalled by the CS. Cerebellar involvement here is again consistent with its role as a predictor: the motor learning it implements is the learning of predictive control, through LTD or other types of plasticity in the cerebellar cortex (Stein and Glickstein, 1992; Boyden et al., 2004; De Zeeuw and Yeo, 2005; Ito, 2005).

1.4.3 Internal models

The processes within the cerebellum that might carry out this predictive control can be described using the concept of internal models: systems for mimicking the behaviour of natural processes, of which there are two types. Forward models generate up to date estimates of the state of the body and the external world using efference copy of the command to move (Wolpert et al., 1998; Davidson and Wolpert, 2005). They could be used when estimates of movement consequences through sensory feedback are too slow, for example during control of ballistic arm

movements or saccades (Ito, 1984), and so these movements are described as being under "feed-forward" or predictive control.

Complementary to these are inverse models which generate motor commands using sensory consequences as their input (Kawato et al., 2003). Multiple pairs of forward and inverse models could be used for accurate control of movements under a large variety of environmental conditions (Wolpert and Kawato, 1998).

Psychophysical evidence for the use of internal models by the motor system has been provided by experiments in which human subjects (Shadmehr and Mussa-Ivaldi, 1994) or monkeys (Krouchev and Kalaska, 2003) make arm movements in a novel mechanical system such as a velocity dependent force field. Formation of an internal model is inferred from the fact that arm trajectories in this novel field become similar to baseline, as if the motor system has learned to predict the mechanical dynamics of the task. More specifically, predictive control using forward models has been demonstrated experimentally by the predictive adjustment of grip force with load during object manipulation (Flanagan and Wing, 1997).

As argued above, the cerebellum is thought to be a prime candidate for predictive control and a recent fMRI study localised neural activity changes related to anticipatory grip force adjustment in the cerebellar cortex, suggesting that this could be a neural substrate for forward models (Kawato et al., 2003). However, evidence from neurophysiological cerebellar recordings in behaving monkeys is rather scant. Liu et al. (2003) observed a small proportion of lateral cerebellar cortical cells during a visually guided step tracking of a visual cursor with a manipulandum, whose responses were time locked to the direction of cursor movement. Since this could be dissociated from the direction of hand movement in a mirror task, these cells seemed intuitively to be encoding the visual consequences of the hand movement. This was

also observed by Ebner and Fu (1997) when they found Purkinje cell simple spike responses to be correlated with the gain of cursor movement in visually guided reaching.

1.5 Interactions between M1 and cerebellum

For a more complete understanding of the control of movement by the primary motor cortex and the cerebellum, we need to study how these structures interact and communicate with each other during movement. The need for them to cooperate closely in controlling hand function is a logical conclusion given three lines of evidence. Firstly, cerebellar dysfunction severely affects movement control, including skilled finger movements (Thach et al., 1992; Glickstein et al., 2005). Secondly, the enlargement of cerebral cortex, cerebellar hemispheres and the pontine nuclei in humans and the higher primates parallels the increased complexity of the corticospinal tract and the ability to make precise movements of the fingers. Thirdly, the dentate nucleus in particular lacks direct connections to the motoneurons of the cervical spinal cord that innervate the muscles of the hand (Brooks and Thach, 1981), but as described below is involved in the control of finger movements and grasp; this control must be implemented through M1-dentate interactions.

1.5.1 Cerebello-cortical connections

One of the principle pathways by which the cerebellum can influence activity in M1 is generally held to be a disynaptic excitatory pathway from the deep cerebellar nuclei, via the thalamus (Figure 2). Tracing by injections of horseradish peroxidase into these nuclei demonstrates substantial projections from dentate and interpositus to the ventrolateral (VL) nucleus of the thalamus (Asanuma et al., 1983a,b). Stimulation in VL thalamus elicits short latency excitation of M1 neurons, while stimulation in the superior cerebellar peduncle causes disynaptic effects (Na et al., 1997). Stimulation of dentate and interpositus also gives short latency facilitation of M1 unit discharge in cats (Jorntell and Ekerot, 1999) and monkeys (Holdefer et al., 2000). Finally, injections of transneuronal viral tracers in M1 causes retrograde labelling of neurons in VL thalamus and lateral dentate nucleus (Hoover and Strick, 1999).

1.5.2 Cortico-pontine pathway

As discussed in section 1.3.2, projections from motor and dorsal stream visual areas of the cortex reaches the cerebellum via the cortico-pontine pathway. Efferent fibres from the cerebral cortex course through the internal capsule and the crura cerebri, the massive fibre bundles at the base of the cerebral peduncles (Figure 1.1). In humans, there are an estimated 20 million fibres in the cerebral peduncles (Tomasch, 1969) but only approximately 1 million of these continue the medullary pyramid to eventually form the corticospinal tract. the most important targets of the remaining peduncular fibres are the pontine nuclei. A number of studies, using a

variety of methods, have demonstrated corticopontine projections arising from several areas of the cerebral cortex. Lesions of the cerebral cortex in monkeys produces degeneration of axons in the pontine nuclei (Kuypers and Lawrence, 1967; Dhanarajan et al., 1977; Brodal, 1978), and injections of autoradiographic tracers into precentral cortex results in labelling of the pontine grey (Hartmann-von Monakow et al., 1981). Injections of horseradish peroxidase (HRP) into the pontine nuclei result in retrograde labelling of extensive areas of the cerebral cortex in rat (Wiesendanger and Wiesendanger, 1982), cat (Kawamura and Chiba, 1979) and monkey (Glickstein et al., 1985). There is a degree of convergence of terminations in the pons. Populations of cortical cells with overlapping dendritic arbors show overlapping fields of labelling in the pontine nuclei. sites converge on single neurons (Ruegg et al., 1977), such as those from motor and somatosensory areas. There is a corresponding divergence of projections from single areas of the cortex to multiple clusters or lamellae in the PN at multiple sites over a number of rostro-caudal levels (Brodal and Bjaalie, 1997). Inputs from separate areas of cortex, for example different areas of the dorsal visual areas, remain largely segregated with some discrete overlap (Dhanarajan et al., 1977; Schmahmann et al., 2004). However, inputs from homeotopic representations in separate cortical areas (for example, parts of different cortical areas which refer to the same part of the visual field) show greater overlap of pontine terminations (Leergard et al 2004). The lamellar architecture provides a large interface for a highly specific integration of cortical inputs within the pontine nuclei (Hartmann-von Monakow et al., 1981; Brodal and Bjaalie, 1997). Pontine neurons then send efferent projections via the brachium pontis (middle cerebellar peduncle) to the cerebellar cortex where they terminate as

mossy fibres. As mentioned above, there is evidence that some pontocerebellar fibres send excitatory collaterals to the deep cerebellar nuclei (Shinoda et al., 1992).

Stimulation in the pyramid gives rise to mossy fibre responses in the cerebellum (Allen and Tsukahara, 1974), suggesting that collaterals of the corticospinal tract may synapse in the pons; this was subsequently confirmed by retrograde double labelling techniques (Ugolini and Kuypers, 1986). They concluded that nearly all corticospinal neurons send collaterals to the pontine nuclei, which would enable command signals from M1 to the motoneurons controlling hand muscles to be copied to the pontine nucleus (Porter et al., 1993). Thus the cerebellum could be informed of movements that are about to be initiated via efference copy, consistent with a proposed role of this structure in motor learning and feed-forward control (Wolpert et al., 1998). But in addition to CST collaterals, there exist direct cortico-pontine projections from layer V pyramidal neurons of the primary motor cortex, which do not collateralise to the spinal cord as CST fibres. These have been observed in the human brain by Cajal (Cajal 1952) and can also be inferred from the fact that since only a minority of M1's output gives rise to the CST (approximately 10-20% of layer V neurons in M1 – Humphrey and Corrie, 1978) the rest must be directed towards other subcortical targets, including the pontine nuclei. The cerebellum is therefore supplied with two parallel inputs from M1, one of which carries information from the corticospinal tract, and the other which is a dedicated "private line" to the cerebellum from the motor cortex via the pons.

1.5.3 Reciprocal connections

The extensive connectivity linking M1 and cerebellum in both directions is reciprocal. Using transneuronal viral tracers in monkeys, Kelly and Strick (2003) demonstrated that the same regions of cerebellar cortex which receive connections from the arm area of M1 (lobules IV-VI) also project to the arm area of M1. Injections in both these areas also resulted in labelling of lateral dentate nucleus (Dum and Strick, 2003). Transneuronal tracing techniques have provided a description of the functional topography of the dentate nucleus, in terms of its projections to different cerebral cortical areas. Regions that project to M1 and premotor areas of cortex are found mainly in dorsal parts of the nucleus, while projections to prefrontal (e.g Brodmann's area 46d and 9L) and posterior parietal areas (e.g. Brodmann's area 7b) arise from ventral parts of the nucleus. This functional topology can be plotted on an "unfolded" map of the nucleus (Fig 1.3). Note that this map was constructed using histology from Cebus monkeys (Cebus apella). Currently, a similar map has not yet been constructed for macaque dentate nucleus. The separate nature of these projections to different cortical areas has led to the suggestion that there are multiple, separate dentate "output channels" – or multiple cerebro-cerebellar loops (Kelly and Strick, 2003).

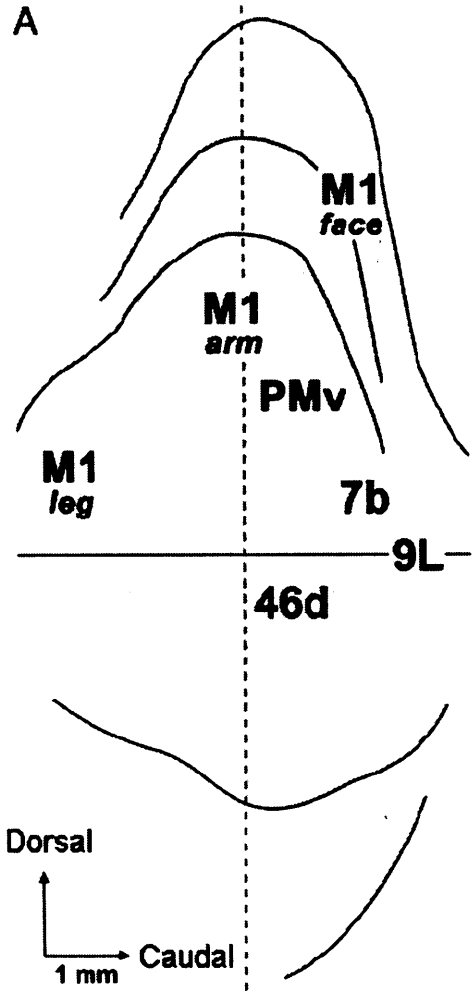

Figure 1.3 Map of dentate nucleus
"Unfolded map" of macaque dentate nucleus showing origin of peak projections to different cortical areas, assessed using transneuronal viral tracing techniques. Numbers represent Brodmann's areas (see text above). PMv = ventral premotor cortex. Adapted from Dum and Strick (2003).

The nature and possible functions of cerebro-cerebellar loops were reviewed by (Allen and Tsukahara, 1974), with a focus on motor control. A feature of these loops is that activity at various points within them is often observed to be similar: for example, the task related activity of neurons in ventral dentate and PMv (Mushiake

and Strick, 1993; Middleton and Strick, 2000), and activation of M1 and dentate during movement execution in humans (Jueptner et al., 1997). Concordant with this, evidence from lesion studies, stimulation and single unit recordings implicate dentate in the control of finger movements.

Thach et al., (1992) noted that lesions of the dentate nucleus disrupt coordinated finger movements of the ipsilateral hand in monkeys; and as noted above, patients and monkeys with damage to cerebellum show impaired finger movements (Glickstein et al., 2005). Stimulation of the most lateral parts of the dentate nucleus in baboons elicits a large variety of hand and finger movements: flexion/extension of the whole ipsilateral hand, opposition of finger and thumb, and flexion/extension of other digits (Rispal-Padel et al., 1982).

Recording from single cells, van Kan et al. (1993) observed neurons in the forelimb areas of interpositus and neighbouring dentate that discharged vigorously in relation to unrestrained, whole arm reaching, if it was combined with a grasping component. Focal injections of muscimol into anterior interpositus and dentate affects preshaping of grasp and object manipulation, in a similar task (Mason et al., 1998). Goodkin and Thach (2003b) also made single unit recordings from these nuclei and found neurons whose discharge correlated with compound and simple movements of the hand and digits, which were impaired during focal muscimol inactivation (Goodkin and Thach, 2003a). In contrast, Monzee et al. (2004) found little impact of muscimol on precise finger movements when making focal injections into the dentate nucleus, although a comparison of their inactivation sites with those illustrated in Goodkin and Thach (2003a) suggests that Monzee and collaborators may not have targeted lateral, arm/hand related dentate sites.

Thus it is reasonable to suggest that M1 and dentate nucleus are likely to cooperate extensively during the control of finger movements. Demonstrating connectivity, or recording from each area successively, does not address this issue directly. Activity must be monitored in the two structures simultaneously. Relative changes in activity between them could then be taken as evidence that they are interacting. For example, a recent PET imaging study in humans showed decreasing cerebellar activity coupled with increasing M1 activation during learning of a motor sequence task (Penhune and Doyon, 2005) – this can be interpreted as evidence that initial motor learning is implemented by the cortico-cerebellar system, but long term motor skills are ultimately stored in motor cortex. It is an interesting result, simply because it represents a more direct attempt to address cerebro-cerebellar communication underlying skilled motor control. But there are some difficulties in relating the findings of imaging studies to the interactions taking place between M1 and cerebellum at the neuronal level, since it is not quite clear at present how to intepret changes in the BOLD signal to underlying changes in neuronal plasticity (Kelly and Garavan, 2005). In addition, although M1-cerebellar interconnectivity is significant, it is highly specific at the neuronal level (Holdefer et al., 2000). Therefore it would seem that there is a strong motivation to investigate the issue of M1-cerebellar interactions more thoroughly, through simultaneous recordings of neurons in both structures during task performance. A key approach that is taken in this thesis to address this issue is the study of oscillatory neural activity in M1 and cerebellum.

1.5.4 M1 and cerebellar oscillations

Rhythmical activity in the human motor cortex between 15-30 Hz has been observed (Hari and Salenius, 1999; Mima et al., 1999; Salenius and Hari, 2003). These "β rhythms" are also found in local field potentials recorded from monkey motor cortex (Murthy and Fetz, 1996a; Baker et al., 1997). They appear during periods of steady contractions and during rest, and are suppressed during movements (Pfurtscheller et al., 1996a; Baker et al., 1997; Donoghue et al., 1998; Kilner et al., 1999) indicating that they are not involved in the direct programming of movements and might represent an "idling" rhythm. However, they are synchronised with similar 15-30 Hz oscillations in EMGs recorded from contralateral hand muscles (Conway et al., 1995; Hari and Salenius, 1999; Kilner et al., 1999) and the observation that this coherence is related to intrinsic movement parameters (Kilner et al., 2000) suggests that cortical oscillations might have greater functional significance in motor control. For example, it was speculated that beta activity might serve to bind sensory and motor information during the grip of compliant objects, similar to how related visual features might be bound together in the visual system (Singer, 1999).

β rhythms have also been observed in the cerebellar cortex of monkeys (Pellerin and Lamarre, 1997) and rats (Hartmann and Bower, 1998). While this activity was prominent during rest, it could be correlated with the expectation of reward following a stimulus (Courtemanche et al., 2002), so again does not represent simple "idling". A recent study (Aumann and Fetz, 2004) found β oscillatory activity in the dentate nucleus during the hold period of a wrist flexion/extension task, indicating that cerebellar rhythms are also associated with motor control. These oscillations

were coherent with β rhythms recorded in the ipsilateral hand and wrist muscle EMGs. Since the cerebellum lacks direct connections to the cervical levels of the spinal cord that innervate the hand, this coherence could be mediated by its extensive interconnectivity with M1 (Hoover and Strick, 1999; Kelly and Strick, 2003). Cerebellar oscillations should then be expected to show significant coherence with rhythms in M1, which is thought to underlie cortico-cerebellar communication (Courtemanche et al., 2002; O'Connor et al., 2002).

1.6 Thesis outline

The work described in this thesis utilizes simultaneous recordings of neural activity in primary motor cortex and cerebellar dentate nucleus of awake behaving monkeys, to address the issue of how groups of neurons in these two structures communicate and interact with each other to control finger movements during precision grip.

Chapter 2 describes the experimental methods. Chapter 3 addresses how individual neurons in both these structures encode finger movements, by correlating neural firing rates with both EMG activity in multiple hand muscles and the kinematics of precision grip finger movements. The results suggest that both areas encode muscle activity in a linear fashion, supporting the hypothesis that muscle control is the fundamental movement code in M1 and cerebellum. In addition, M1 activity is found to be more closely coupled to the spinal cord machinery for hand movements than cerebellar activity.

In chapter 4, two different outputs of M1 to the cerebellum are compared: collaterals of the corticospinal tract and direct cortico-pontine projections, by comparing the task-related firing of single neurons that project axons along these pathways. The comparison indicates that these pathways convey similar movement-related information in parallel to the cerebellum, although there are some subtle differences.

Interactions between these pathways are studied suggesting that they are partially segregated at the cortical level.

Chapter 5 presents a preliminary assessment of interactions between M1 and dentate nucleus. Application of ICMS to demonstrate functional connectivity is first described, followed by an analysis of the temporal coupling of spike and local field potential activity between areas. These results suggest that cerebro-cerebellar communication is unaltered by load condition.

In chapter 6 cerebro-cerebellar interactions are investigated in more detail. Firstly, an experimental condition comparing predictable and randomized load conditions is applied, to probe and compare feed-forward, predictive behaviour of single M1 and dentate neurons. Then, 15-30 Hz oscillatory activity is demonstrated in both these structures. The correlation of M1 rhythms with task parameters supports the hypothesis that these oscillations can encode features of movements. Furthermore, a clear dissociation of M1 and dentate rhythms in the predictable versus randomized task conditions is consistent with the proposed role of the cerebellum in predictive control. Nevertheless, analysis of the temporal coupling of these structures' oscillatory activity suggests that they cooperate closely in movement control across a range of conditions.

Finally, chapter 7 discusses the key findings of these experiments in the general context of current knowledge about movement control by M1 and cerebellum, and their interactions.

Chapter 2: Methods

2.1 Behavioural task

2.1.1 Training

The data presented here were recorded from three purpose-bred adult female *maccaca mulatta* monkeys: two females (M36 and M38) and one male (M41), weights 5.0 kg, 6.0 kg and 6.0 kg respectively. All monkeys were trained to perform the same basic precision grip task, detailed below. Before this training commenced, monkeys were taught to voluntarily move from their home cage to a smaller training cage and accept fruit from the experimenters. Then, they learned to perform a simple task such as reaching for fruit on a board, and the complexity of this task was slowly increased so that they learned to touch switches to receive a reward, before finally starting to use the precision grip manipulandum. At various stages, the monkeys were taught to accept increasing degrees of restraint including a metal neck collar, a loose sleeve to support the forearm and eventually head fixation. Whenever a new restraint was introduced, 1 – 2 mg/kg diazepam (APS Ltd.) was administered orally for the first few sessions to minimise stress to the animal. All procedures were carried out in accordance with appropriate UK Home Office regulations.

2.1.2 Precision grip task

This involved squeezing two levers between thumb and index finger. The levers were mounted onto the spindles of motors (Phantom, SensAble Technologies Inc.) which were computer controlled to produce a variety of position dependent forces. One complete trial involved moving both levers into a target displacement window (movement period) and maintaining this position for 1 second (hold period) before releasing. Three auditory cues were presented to the animal: the first indicated that both digits were in the target displacement window, the second that they had been held there for the required duration, and the third was accompanied with a fruit reward once the levers had been released and returned to baseline. For monkey M36, this target window was between 6mm and 8mm from baseline for both levers. Monkeys M38 and M41 were not as accurate in their performance of the task, so slightly larger windows between 5mm and 8mm were used.

Off-line, two time periods were defined for use in further analysis. The movement period was defined as the time during which either finger or thumb velocity was greater than 30 mm/s. The hold period began when both finger and thumb positions were within the target window and lasted for 1 s. Note that the hold period did not necessarily begin at the end of the movement period, as for the example shown in Figure 2.3 A.

2.1.3 Load conditions

A spring-like or compliant force was generated on each lever by the Phantom device. The resistive force F depended on the displacement of the lever d according

to the relationship $F(d) = sd + o$, where s represents the spring constant and o is the offset required to ensure the levers returned to baseline as they were released at the end of each trial. Monkeys M36 and M38 were presented with four load conditions: 0.02, 0.04, 0.06 and 0.08 N/mm, all with offset o = 0.015 N (Fig. 2.1 A). Monkey M41 was presented with three load conditions: 0.01, 0.04 and 0.07 N/mm, with offset 0.015N (Fig. 2.1 B).

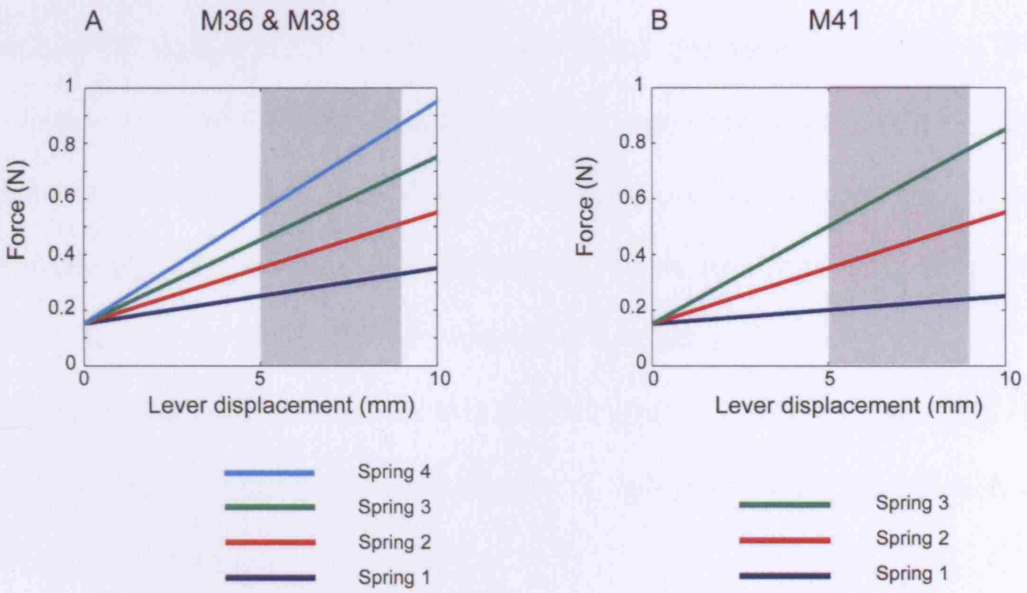

Figure 2.1 Load conditions
A, force-displacement plots for the load conditions used for monkeys M36 and M38. Shading indicates target displacement window. **B**, equivalent plot for load conditions presented to monkey M41.

In all experiments, trials were presented in blocks of 50-100 trials of the same type. In chapter 6, trials of the same type were presented in smaller blocks of 10 trials and

the order of block presentation was randomized. Further details about this condition can be found in chapter 6.

2.2 Surgical procedures

2.2.1 Anaesthesia and medication

Prior to any surgery involving craniotomy, animals received glucocorticoid premedication (25 mg/kg i.m., Solu-Medrone, Pharmacia & Upjohn Ltd.) to prevent cerebral oedema. General anaesthetic was induced with ketamine hydrochloride (10 mg/kg i.m., Ketaset, Fort Dodge Ltd.) administered concurrently with atropine sulphate (20 μg/kg i.m., Atrocare, Animalcare Ltd.), and maintained with 2 – 2.5% isoflurane in 50:50 O2:N2O inhaled through an endotracheal tube. Surgeries were performed in fully aseptic conditions with 0.9% sodium chloride administered intravenously to the animal (10 drops/min). Heart and respiration rate, body temperature and exhaled pCO2 were monitored throughout.

All surgical operations were followed by a full course of antibiotic (20 mg/kg i.m., Terramycin /LA, Pfizer Ltd.) and analgesic (10 μg/kg i.m., Vetergesic, Reckitt and Colman Products Ltd.).

Minor procedures such as removal of stitches and clearing of the dura mater were performed under sedation with ketamine and medetomidine (Dormitor, Pfizer Ltd.). 15 mg/kg i.m. Ketamine:Dormitor (mixed 80:1 by weight) was reversed with atipamezole hydrochloride (4 mg/kg i.m., Antisedan, Pfizer Ltd.).

2.2.2 MRI and skull mould

A magnetic resonance image (MRI) was taken of each animal to guide positioning of recording chambers and PT electrodes (Baker, Philbin et al., 1999). For monkey

M36, this procedure was combined with a mould of the cranial surface made using dental impression compound (Provil, Bayer Dental Co.). For M38 and M41, a plastic mould was made directly from the MRI scan. These moulds were used for shaping the headpiece for a better fit and planning the layout of recording chambers.

2.2.3 Chronic implants

In separate surgeries, each animal received the following chronic implants.

1. All three monkeys were implanted with subcutaneous EMG patch electrodes (Miller et al., 1993) sutured directly onto the surface of intrinsic hand and forearm muscles, in the hand used to perform the task. The electrode leads ran subcutaneously to a connector on the monkey's back. The muscles implanted in monkeys M36 and M38 are detailed in Table 2.1. The implant in monkey M41 was rejected early on during the recording period, therefore EMGs were sampled from a smaller number of muscles using custom-made electrodes attached to the overlying skin (1DI, AbPB, FDP and EDC).

2. Each animal was implanted with a headpiece for head restraint. This comprised a stainless steel ring secured to the skull with four bolts. Three threaded posts protruded from the upper surface of the ring and were used to fix the head during recording.

3. Each monkey underwent surgery to implant recording chambers and pyramidal tract electrodes. Chambers with an inner diameter of 12 mm were positioned around a craniotomy over M1, contralateral to the performing hand, and vertically above the ipsilateral cerebellum. The co-ordinates of chamber centres are shown in Table 2.2.

Monkeys M36 and M38 were also implanted with chambers over right M1 and left cerebellum; analysis of recordings from these structures is not presented here but can be found in Jackson (2002).Two varnish insulated tungsten stimulating electrodes (impedance ~ 20 kΩ at 1 kHz) were implanted in the pyramidal tract (PT) at the level of the medulla, contralateral to the performing hand (sterotaxic coordinates A2.0 L4.5 and P3.0 L5.0). Locations were confirmed by recording antidromic field potentials over motor cortex following stimulation. The thresholds for these potentials were 20 - 50 μA. The distribution of antidromic latencies for PTNs was in agreement with prior observations by Fromm and Evarts (1981). N.B In recordings from the pyramid during stimulation of ipsilateral M1 there is a relatively simple, short latency response known as a D wave, produced by direct activation of corticospinal neurons (Patton and Amassian 1954). This is then followed by later, more complex volleys known as I waves, resulting from indirect stimulation of corticospinal neurons (Patton and Amassian 1954).

4. In an additional surgery, monkeys M38 and M41 were implanted with chronic electrodes in the cerebral peduncle (CP) contralateral to the performing hand (A7.5 L4.5 and A9.0 L4.5). Locations were confirmed as for the PT electrodes, with stimulation thresholds of 30-100μA. Stimulation in the peduncle blocked antidromic activation of the cortex produced by pyramidal stimulation if the two were separated by a latency less than 1 ms, confirming localisation of the electrodes amongst axons of the same fibre tract at two rostro-caudal levels.

Post-mortem histology confirmed the location of all implanted electrodes within the pyramids for M36 and M38. M41 is still alive.

Table 2.1. Method of recording muscle EMG for each animal

Muscle	Abbreviation	M36	M38
Flexor digitorum profundus	FDP	Implanted	Implanted
Flexor digitorum sublimis	FDS	Implanted	-
Flexor carpi ulnaris	FCU	-	Implanted
Extensor digitorum communis	EDC	Implanted	Implanted
Extensor carpi radialis longus	ECR-L	Implanted	Implanted
Extensor carpi ulnaris	ECU	-	Implanted
Abductor pollicis longus	AbPL	Implanted	Implanted
Abductor pollicis brevis	AbPB	-	-
Thenar	-	Implanted	Implanted
First dorsal interosseous	1DI	Implanted	Implanted
Abductor digiti minimi	AbDM	-	Implanted

Table 2.2. Stereotaxic co-ordinates of chamber centres

Chamber	M36	M38	M41
Right M1	A10.5 L16.5	A9.0 L16.0	A10.0 L16.5
Left Cerebellum	-	P7.0 L6.5	P9.5 L6.5

2.2.4 Care of the dura mater and implants

Once exposed by craniotomy, the dura mater quickly becomes covered by scar tissue and penetration with electrodes becomes difficult. After some recording sessions, this tissue was stripped with a corneal hook after the area had first been covered with local anaesthetic cream (lignocaine/prilocaine; EMLA, Astra Pharmaceuticals Ltd.). Following this, it was treated with an antimitotic solution (25 mg/ml 5-fluorouracil, Sigma Chemicals Ltd.) for 5 min before thorough rinsing with a large volume of sterile saline. Topical antibiotic (0.3% Gentamicin; Genticin, Roche Products Ltd.) was added to each chamber before it was sealed with an airtight lid.

To prevent infection, exposed implants and skin edges were cleaned with 3% hydrogen peroxide and coated with neomycin powder (Cicatrin, Wellcome).

2.3 Experimental procedures

2.3.1 Cortical recording

All M1 data were recorded using a 16-channel Eckhorn multiple-electrode drive (Thomas Recording Ltd., Marburg, Germany). The complete system has been described in detail (Baker, Philbin et al., 1999). The drive allows a 4x4 grid of glass-insulated platinum electrodes (impedance 1-3 MΩ, interelectrode spacing 300 μm) to be independently lowered into the cortex to search for cells and record the LFP.

Before each penetration, the position of the guide tube tips was referenced to three triangulation points on the chamber wall, the stereotaxic locations of which had been measured during surgery. This allowed the position of the penetration site to be calculated in stereotaxic co-ordinates. Once the guide tubes were positioned close to the dura mater, the electrodes were driven through one at a time. To allow the tissue to recover from mechanical depression, electrodes were left for 10 mins before being advanced further into the cortex.

2.3.2 Cerebellar recording

During this period, in M38 and M41 up to 2 electrodes were inserted into the cerebellum ipsilateral to the performing hand, to make recordings from dentate nucleus simultaneously with M1. Electrodes were introduced using a smaller, 7-channel Eckhorn drive, equipped with fine sharpened guide tubes which were advanced through the cortical dura, up to 5 mm below it, before each electrode was advanced (stages 1 and 2 in figure 2.2). As the electrode approached the cerebellum, careful attention was paid to neural discharge. A sudden rush of rapidly firing neurons signalled penetration of the tentorium and entry into the cerebellar cortex (stage 3). Moving through the cortex, a period of intense simple spike discharge interposed between periods of reduced activity signalled transition of the electrode through molecular, Purkinje and granular layers of the cortex. This pattern was repeated several times as the electrode advanced, due to the highly folded cortical sheet (stage 4). After approximately 3-5mm, cerebellar cortex gave way to the cerebellar white matter, characterised by a lack of background neural discharge with

occasional spontaneous fibre activity (Stage 5). After another 3-5mm, another sudden rush of discharge indicated entry of the electrode into the dentate nucleus. The total depth of penetration from cerebral cortex to nucleus was usually around 30 mm. Electrodes were then controlled simultaneously within cerebellum and M1 to search for task-related units.

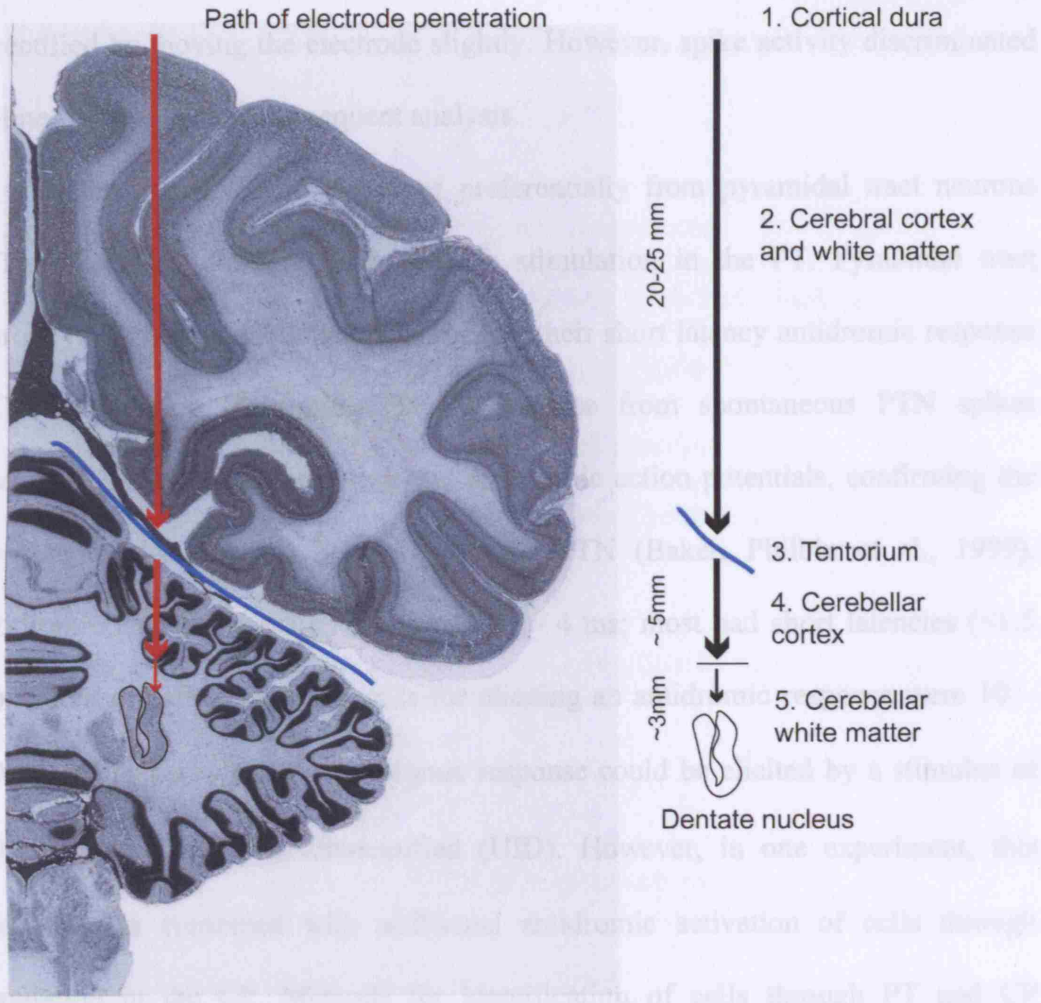

Figure 2.2. Cerebellar recording
Route of entry of electrodes into cerebellar dentate nucleus from vertically positioned recording chamber. See preceding text for details. Coronal section of macaque brain taken from Martin and Bowden (2000).

The signal from each recording electrode was pre-amplified then filtered for LFP (10-250 Hz) and spike activity (1-10 kHz). On-line, cells were discriminated using a double amplitude-time window algorithm allowing inter-spike interval (ISI) histograms to be compiled in real time. This is advantageous since a large number of

short ISIs (<2 ms) is a sign of poor discrimination of single-units and this can often be rectified by moving the electrode slightly. However, spike activity discriminated off-line was used for all subsequent analysis.

In M1, the objective was to record preferentially from pyramidal tract neurons (PTNs) identified antidromically through stimulation in the PT. Pyramidal tract neurons (PTNs) were identified according to their short latency antidromic response to PT stimulation. Triggering the PT impulse from spontaneous PTN spikes produced collision of orthodromic and antidromic action potentials, confirming the spontaneous discharge as belonging to the PTN (Baker, Philbin et al., 1999). Antidromic latencies were in the range 0.9 – 4 ms; most had short latencies (<1.5 ms). Threshold stimulating currents for eliciting an antidromic response were 10 – 200 μA. Cells for which no antidromic response could be elicited by a stimulus of 200 μA were classed as unidentified (UID). However, in one experiment, this approach was combined with additional antidromic activation of cells through stimulation in the CP. Methods for identification of cells through PT and CP stimulation are described in more detail in Chapter 4.

2.3.3 Stimulation

PT and CP stimuli consisted of biphasic constant current pulses (each phase 0.2 ms duration) delivered between the two PT electrodes. After each recording session, localisation of the recording electrodes within the hand area of M1 was confirmed using intra-cortical microstimulation (ICMS, 13 biphasic pulses of width 0.2 ms, at 300 Hz). Thresholds for eliciting an EMG response or movement of the hand or

digits were typically between 5-20 μA. ICMS was also applied to M1 and dentate at 10 Hz for ~3 minutes to activate single units; this is described further in Chapter 5.

2.3.4 Data capture

The following signals were recorded during each experiment:

- EMGs were recorded bipolarly with gains of 1000-5000, high-pass filtered at 30 Hz (NL824, Digitimer Ltd) and sampled at 5000 Hz. This was downsampled to 500 Hz for the purposes of analysis.
- Digital events (trial start and end times, end of hold period), together with lever position signals sampled at 500 Hz
- Spike activity recorded as the analog activity, filtered between 1 kHz and 10 kHz and sampled at 25 kHz.
- LFP sampled at 500 Hz.
- PT, CP and 10 Hz ICMS stimulus current waveform.

Data were recorded directly to hard disk via two A2D cards (PCI-6071E, National Instruments).

2.4 Data processing

2.4.1 Acceptance of trials

The analyses described in Chapter 5 were performed on continuous sections of recording. For all other chapters, analyses were based on successfully completed

trials only. Since investigating task-related activity in single neurons requires a large degree of averaging over successive trials, it was important to ensure that trials used in the analysis were as homogenous as possible. Therefore an additional trial selection procedure was applied offline. Trials were rejected if they did not meet the following two criteria:

1. The movement period (defined by finger or thumb velocity being greater than 30 mm/s) had to last less than 1 second. This criterion rejected trials where the finger or thumb levers did not move swiftly into the target displacement window on the first attempt.

2. The length of time that either finger or thumb levers were kept in their hold windows was greater than 0.5 s but less than 1.25 s. This criterion rejected trials where the hold was not achieved directly, and where the levers did not rapidly return to baseline at the end of the hold period. This latter point was important since although successful completion of the 1s hold was signalled by an auditory signal (see Methods), sometimes the monkey kept the levers within the target window for a short period after instead of immediately terminating the trial. An example of an accepted trial is illustrated in Figure 2.3A.

An example of a trial accepted by these criteria is illustrated in figure 2.3. Typically between 50-60% successful trials matched these requirements.

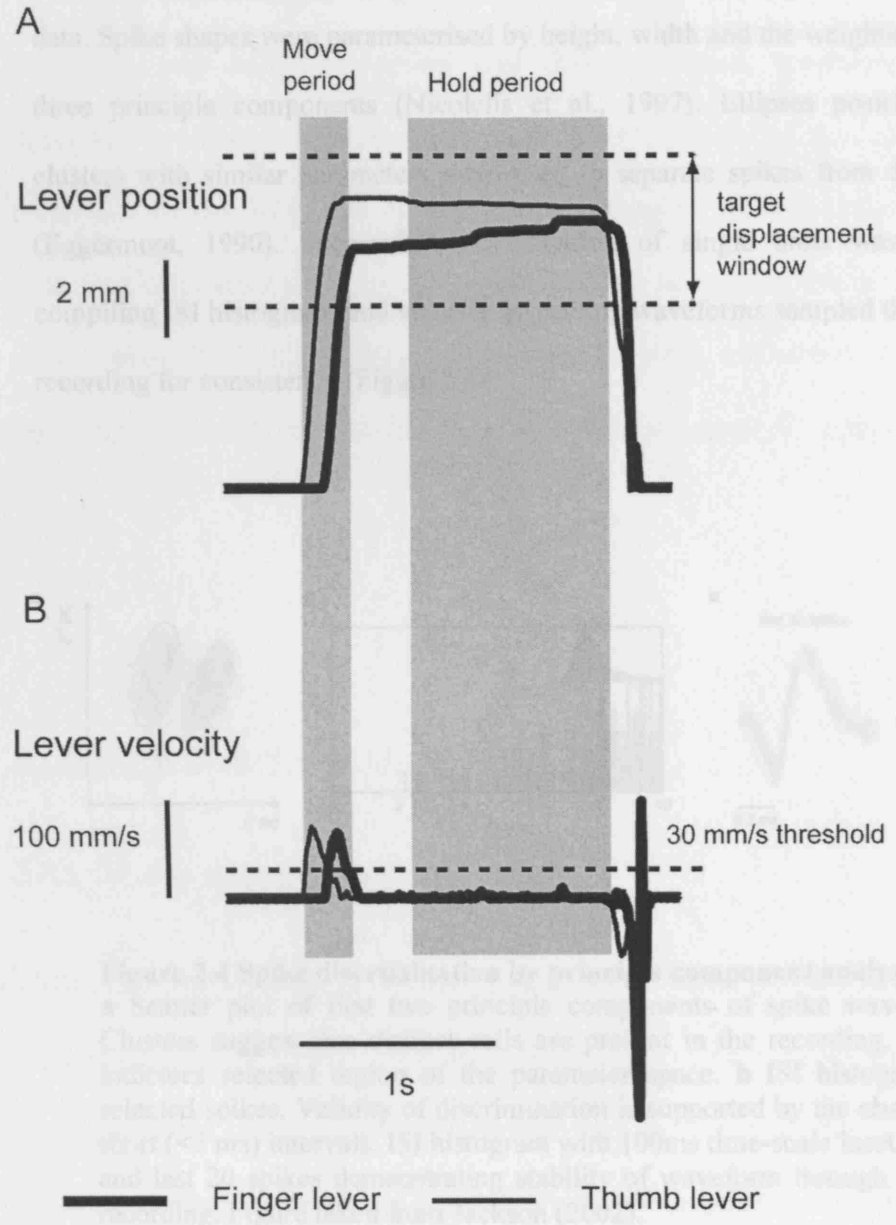

Figure 2.3 Trial selection
A, lever position traces for a trial accepted according to criteria 1 and 2. Dashed lines indicate target displacement window. **B**, lever velocity profiles. Dashed line indicates 30mm/s threshold for start of move period. Move and hold periods are shaded grey.

2.4.2 Spike discrimination

Off-line, spike events crossing a suitable threshold were extracted from the raw data. Spike shapes were parameterised by height, width and the weighting of the first three principle components (Nicolelis et al., 1997). Ellipses positioned around clusters with similar parameters were used to separate spikes from different cells (Eggermont, 1990). Successful discrimination of single units was verified by compiling ISI histograms and visually inspecting waveforms sampled throughout the recording for consistency (Figure 2.4).

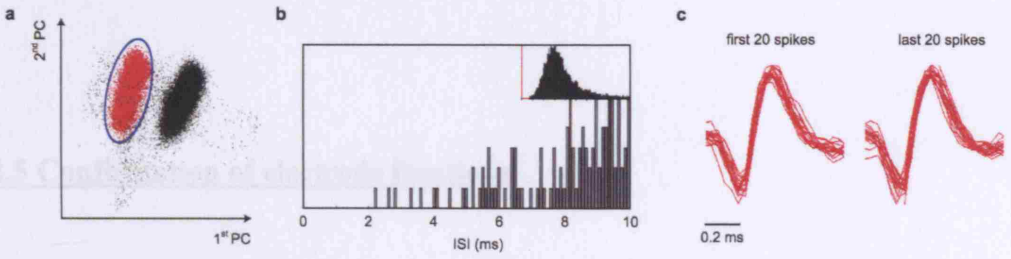

Figure 2.4 Spike discrimination by principle component analysis
a Scatter plot of first two principle components of spike waveforms. Clusters suggest two distinct cells are present in the recording. Ellipse indicates selected region of the parameter space. **b** ISI histogram for selected spikes. Validity of discrimination is supported by the absence of short (<2 ms) intervals. ISI histogram with 100ms time-scale inset. **c** First and last 20 spikes demonstrating stability of waveform through 30 min recording. Figure taken from Jackson (2002).

2.4.3 Instantaneous firing rate estimation

For each discriminated unit, an estimate of the instantaneous firing rate (IFR) throughout the recording period was first calculated, according to techniques described previously (Pauluis and Baker, 2000). Briefly, this method uses the reciprocal of the interspike interval as a first approximation to the IFR, explicitly detecting significant changes in firing rate while smoothing the periods in between these times. For this analysis, IFR profiles were calculated with a sampling resolution of 500 Hz and smoothed with a Gaussian kernel of width 10 ms.

2.5 Confirmation of electrode locations

2.5.1 Dentate nucleus maps

The stereotaxic locations of sites penetrated to make dentate nucleus recordings were mapped onto tracings of horizontal sections of the nucleus from a stereotaxic atlas, available online at www.brainmaps.org. No attempt was made to map the depth of penetration here: as described above, we targeted mainly dorsal portions of the dentate nucleus, and so horizontal sections of the cerebellum at more dorsal levels have been selected accordingly. According to these maps, recording locations should have target mainly lateral, rostral parts of the nucleus. Penetration sites in M38 were mapped onto a horizontal section taken at 5mm above the inter-aural line (IAL) (Fig 2.5A), while sites in M41 were mapped onto a section +3mm above IAL (Fig 2.5B). Each point represents the site of penetration through the cortical dura of

one of the guide tubes attached to the 7-electrode drive. In figure 2.5B, many of the sites target the dentate, although many fall off laterally and appear to miss the nucleus. However, inaccuracies in the stereotaxic measurements made from the recording chamber, as well as individual differences between these animals and the monkey used to construct the atlas, mean that these maps can only function as approximate guides to the locations of recordings within the dentate nucleus. They are intended to show that the two dimensional coordinates we used to insert cerebellar electrodes would be more likely to target the dentate nucleus, particularly lateral areas, as opposed to the interposed nuclei.

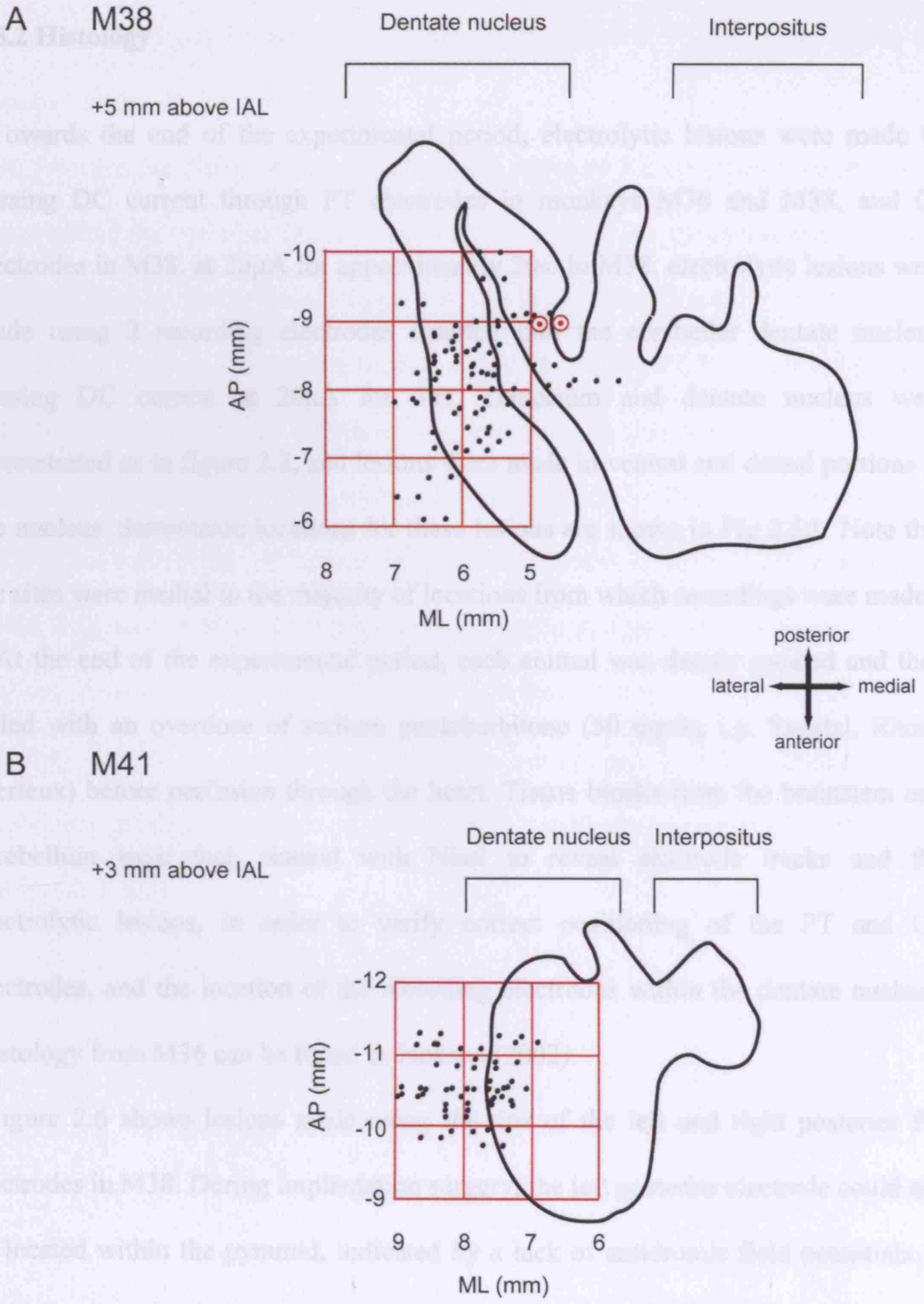

Figure 2.5. Dentate penetration maps
Maps of recording locations within dentate nucleus for monkeys M38 and M41. Red grid represents approximate stereotaxic location calculated from reference points in the atlas. See preceding text for further details. ⊙ indicates site of penetration for electrolytic lesion in dentate nucleus.

2.5.2 Histology

Towards the end of the experimental period, electrolytic lesions were made by passing DC current through PT electrodes in monkeys M36 and M38, and CP electrodes in M38, at 20μA for approximately 20s. In M38, electrolytic lesions were made using 2 recording electrodes inserted into the cerebellar dentate nucleus, passing DC current at 20μA for 30s. Tentorium and dentate nucleus were penetetrated as in figure 2.2, and lesions were made in ventral and dorsal portions of the nucleus. Stereotaxic locations for these lesions are shown in Fig 2.5A. Note that the sites were medial to the majority of locations from which recordings were made.

At the end of the experimental period, each animal was deeply sedated and then killed with an overdose of sodium pentobarbitone (50 mg/kg i.p. Sagatal, Rhone Merieux) before perfusion through the heart. Tissue blocks from the brainstem and cerebellum were then stained with Nissl to reveal electrode tracks and the electrolytic lesions, in order to verify correct positioning of the PT and CP electrodes, and the location of the recording electrodes within the dentate nucleus. Histology from M36 can be found in Jackson (2002).

Figure 2.6 shows lesions made using the tips of the left and right posterior PT electrodes in M38. During implantation surgery, the left posterior electrode could not be located within the pyramid, indicated by a lack of antidromic field potentials in M1 following stimulation. The lesion on this side in figure 2.6 is positioned lateral to the pyramid, confirming this observation. In contrast, the anterior electrode on the left hand side produced M1 antidromic field potentials with a threshold of 50μA. Therefore, during recording sessions, antidromic identification of cells within left

M1 was carried out by stimulating through the anterior PT electrode, using the posterior electrode as a reference.

On the right hand side of figure 2.6, the left posterior PT electrode is marked by a lesion within the pyramid. During implantation, stimulation using this electrode also produced M1 antidromic field potentials with a threshold of 50μA.

Figure 2.7 shows electrode tips located in the left and right CP. Figure 2.8A shows a small electrolytic lesion visible as a purple mark in the dorsal part of the right dentate nucleus in M38; a close up is provided in figure 2.8 B. An electrolytic lesion made in the ventral part of the same nucleus is indicated in figure 2.8 A and C. Each lesion is located in the medial portion of the nucleus, approximately 5mm from the midline, consistent with the stereotaxic positions plotted in figure 2.5A. Taken together, these data confirm that cerebellar recordings in M38 targeted mainly dorsolateral areas of the dentate nucleus, which send strong projections to M1 (Dum and Strick, 2003).

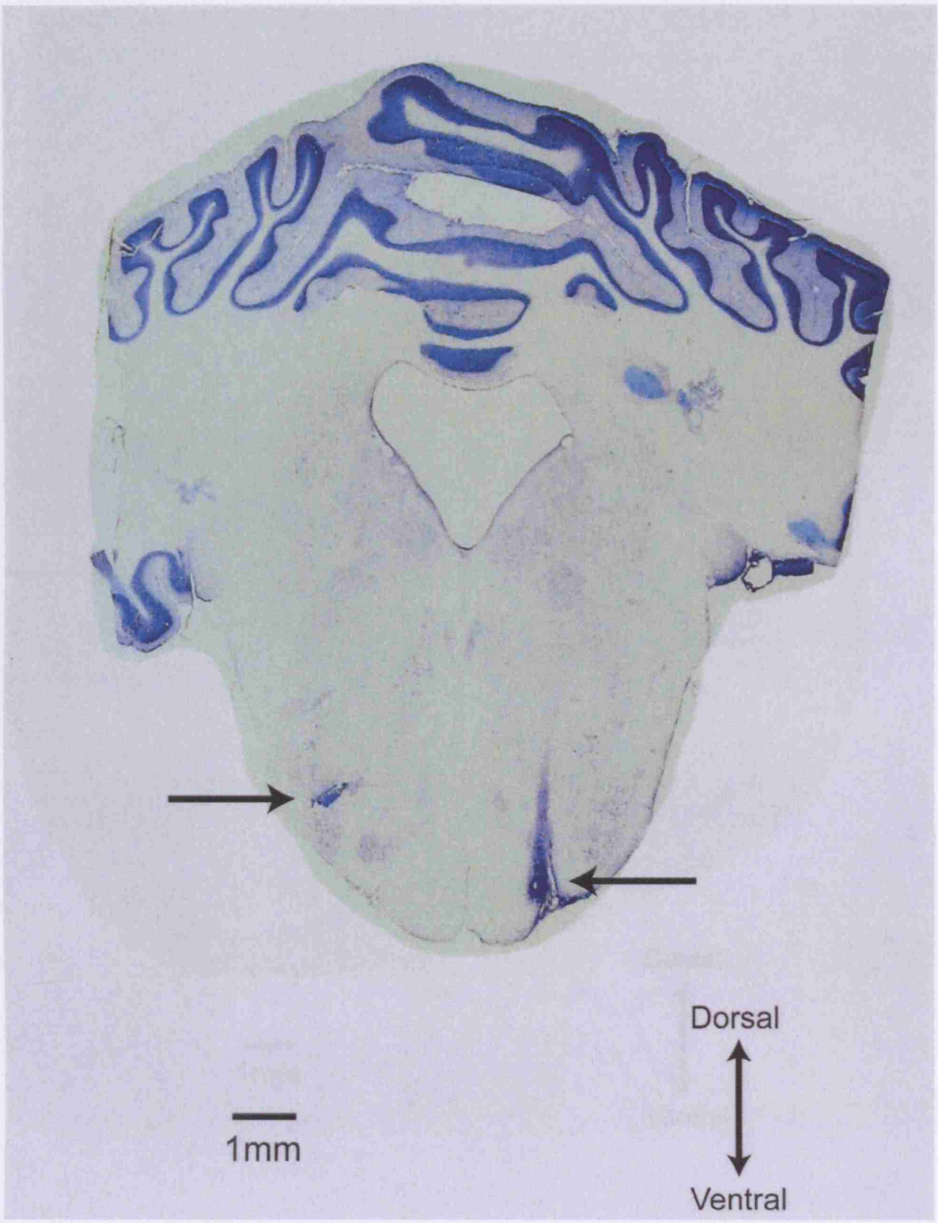

Figure 2.6. PT electrode lesions
Coronal section showing locations of PT electrodes in M38. Arrows indicate sites of electrolytic lesions.

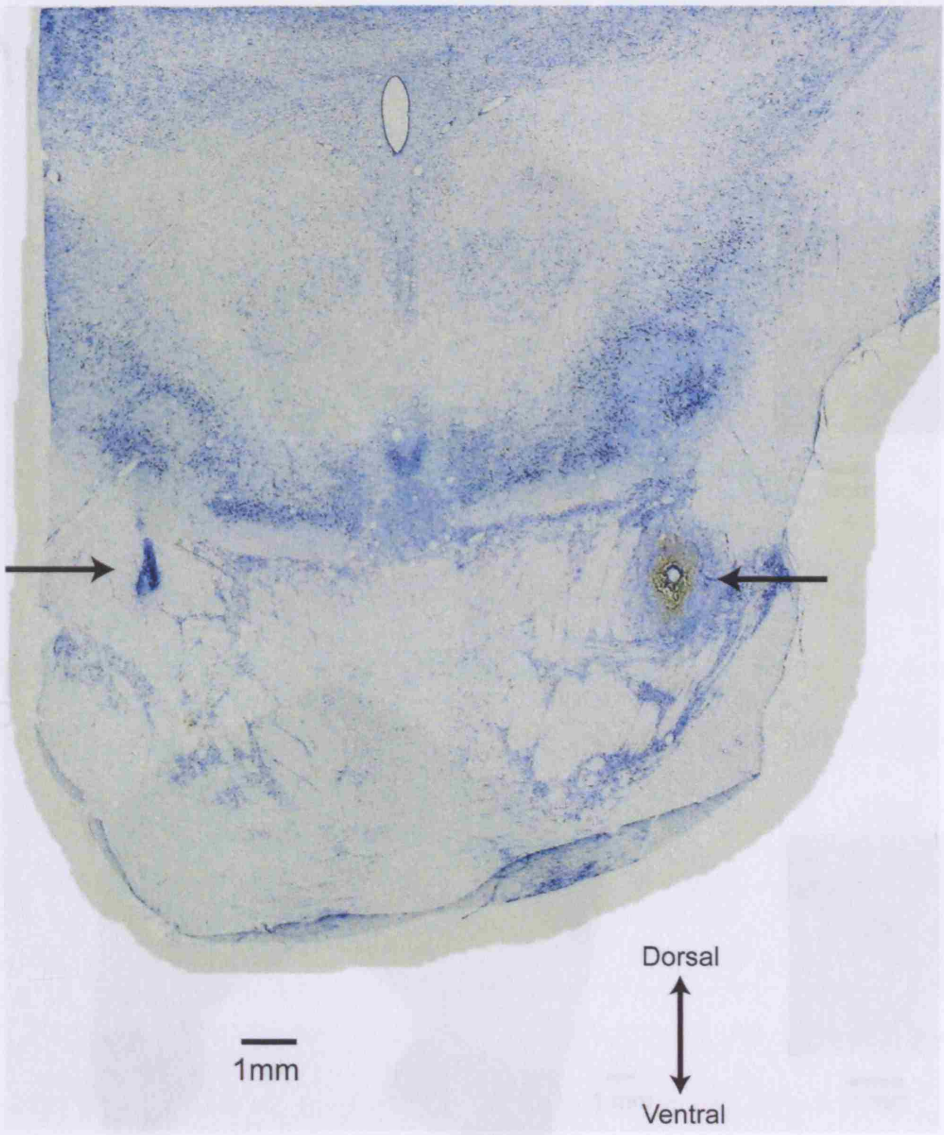

Figure 2.7. CP electrode lesions
Coronal section showing locations of CP electrodes in M38. Arrows mark lesion sites.

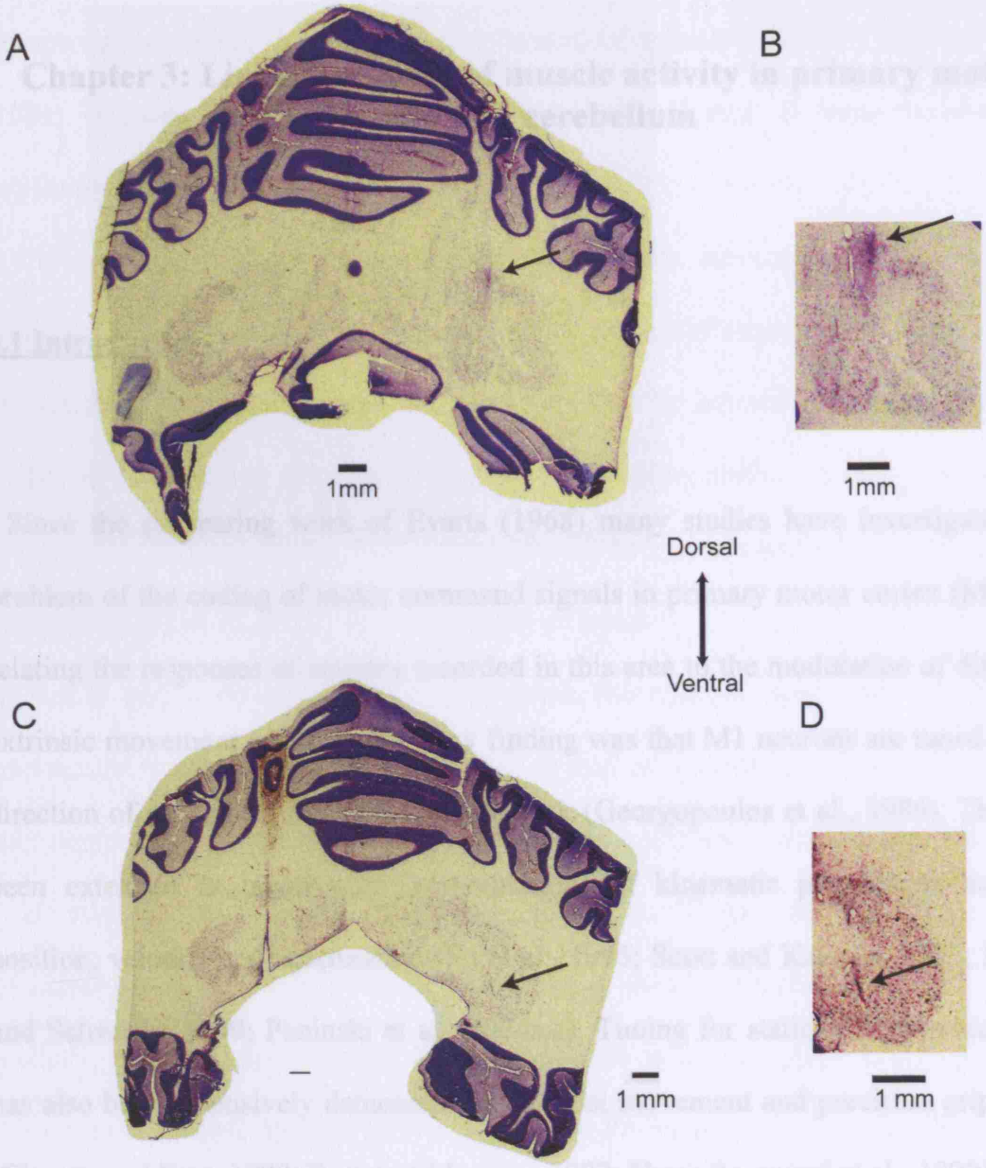

Figure 2.8. Dentate nucleus electrode lesions
A, C coronal sections showing locations of electrolytic lesions in dentate nucleus. Arrows mark lesion sites. **B, D** close up of nucleus to highlight lesion sites.

Chapter 3: Linear encoding of muscle activity in primary motor cortex and cerebellum

3.1 Introduction

Since the pioneering work of Evarts (1968) many studies have investigated the problem of the coding of motor command signals in primary motor cortex (M1), by relating the responses of neurons recorded in this area to the modulation of different extrinsic movement parameters. A key finding was that M1 neurons are tuned to the direction of movement during a reaching task (Georgopoulos et al., 1986). This has been extended to incorporate representations of kinematic parameters, such as position, velocity and acceleration (Fu et al., 1995; Scott and Kalaska, 1997; Moran and Schwartz, 1999; Paninski et al., 2004a,c). Tuning for static and dynamic force has also been extensively demonstrated, in wrist movement and precision grip tasks (Cheney and Fetz, 1980; Porter and Lemon, 1993; Hepp-Reymond et al., 1999).

Comparatively few studies have addressed the encoding of intrinsic movement parameters such as patterns of muscle activity (Kakei et al., 1999; Holdefer and Miller, 2002; Morrow and Miller, 2003). This is despite much evidence of functional modulation of connectivity between M1 cortico-motoneuronal (CM) cells and muscles used during task performance (Fetz and Cheney, 1980; Bennett and Lemon, 1996; Jackson et al., 2003). Furthermore, theoretical studies suggest that "muscle space" may be the fundamental coordinate system of M1, as apparent encoding of kinematic parameters might arise from position- and velocity-dependent

compensations made during the direct control of muscle activation (Mussa-Ivaldi, 1988; Todorov, 2000). It remains unclear which, if any, of these variables are explicitly encoded by M1.

The contribution made by the cerebellum towards movement control has been studied using similar methods. Just as for M1, tuning of cerebellar neurons, both in the cortex and the deep nuclei, has been observed for several parameters including direction of reaching (Fortier et al., 1989), position and/or velocity (Mano and Yamamoto, 1980; Fu et al., 1997), force (Smith and Bourbonnais, 1981) and muscle activity (Wetts et al., 1985) across a variety of tasks.

Thus it would be of interest to determine the relative importance of different parameters in the encoding of movement, as well as comparing this encoding in M1 and cerebellum. To try and tackle these issues, we applied a basic linear – nonlinear (LN) analysis (Chichilnisky, 2001; Simoncelli et al., 2004) to describe the encoding of muscle activity and kinematic parameters by single neurons in M1 and dentate nucleus, in the awake behaving macaque monkey performing a precision grip task. This type of analysis is ideal for relating neural discharge to the complex time course of the EMG signal and has already been applied to describe the encoding of hand position and velocity by neurons in macaque M1 (Paninski et al., 2004c). We demonstrate that the activity of single neurons in both regions can be accurately predicted using simultaneously recorded EMGs from up to nine hand and forearm muscles. This tuning of M1 and dentate neurons to muscle activity is linear in nature and contrasts with a more nonlinear tuning for kinematic information, while the relation of neuronal discharge to both types of parameters is on average weaker in the dentate nucleus compared to M1, in agreement with previous studies of the cerebellar nuclei and cortex (Thach, 1978; van Kan et al., 1993; Fu et al., 1997).

Overall, our results are consistent with a system that controls muscle activity in a linear fashion (Todorov 2000, Ethier et al. 2006), and thus linear methods are sufficient to describe this encoding, in M1 and cerebellar dentate nucleus.

3.2 Methods

3.2.1 Experimental procedures

Behavioural task The monkeys were presented with a variety of load conditions (0.02, 0.04, 0.06 and 0.08 N/mm, all with offset o = 0.015 N). However, the analysis in this chapter was not aimed at addressing the influence of spring constant on the encoding of muscle activity, thus we only selected data from the 0.04 N/mm condition. This was chosen as it represented the middle of the range of forces produced by the animals, and could be performed with relative ease thus resulting in a good number of trials for the analysis. Only successfully completed trials were included giving an average of 72 trials (standard deviation +/- 37) per session.

Off-line, two time periods were defined (Fig. 2.3A) as described in Section 2.x.x. These periods were used for offline trial selection criteria applied to data sets that were used for the comparison of fits by the model to EMG and kinematic data. Here it was important to ensure that trial performance was as homogenous as possible since greater variability in task performance could weaken the correlation of kinematic parameters with neural discharge. In all animals, around 40% of trials performed passed these criteria and were available for analysis.

EMG recordings Monkeys M36 and M38 were implanted with subcutaneous EMG patch electrodes (Miller et al. 1993) sutured directly onto the surface of intrinsic hand and forearm muscles, in the hand used to perform the task. The electrode leads ran subcutaneously to a connector on the monkey's back. The muscles implanted and their abbreviations are detailed in Table 2.1. EMGs were recorded bipolarly with gains of 1000-5000, high-pass filtered at 30Hz (NL824, Digitimer Ltd) and were

sampled at 5000Hz. This was downsampled to 500Hz for the purposes of the analysis described below.

The criteria used for selecting muscles for EMG implants were as follows. Firstly, no proximal muscles were implanted, since only distal muscles act on the thumb and index finger during precision grip (Maier and Hepp-Reymond 1995). Furthermore, the monkey's arm was supported by a loose sleeve that was securely fixed to the side of the experimental chair just above the elbow joint, so proximal muscles were uninvolved in task performance.

The intrinsic hand muscles are particularly important for the control of skilled finger movements, including the generation of finely graded force during precision grip in humans and monkeys (Maier and Hepp-Reymond 1995; Porter and Lemon 1993). We therefore recorded EMGs from the intrinsic hand muscles 1DI, and two muscles of the thenar eminence (flexor pollicis brevis and adductor pollicis brevis) which due to their close proximity and the small size of the macaque thumb were sampled by a single implanted electrode, and are referred to as the "thenar" EMG. The long flexors of the fingers (FDP and FDS) were recorded from since they too are primarily involved in the generation of pinch force by the index finger. The extensors of the wrist (ECU, ECR-L), extensors of the fingers (EDC) and flexors of the wrist (FCU) were implanted as these would be active during the removal and insertion of the hand and digits from/into the manipulandum. These muscles also act to stabilise joint torques and maintain equilibrium during precision grip (Maier and Hepp-Reymond 1995; Schieber and Santanello 2004). Coordinated activity in all these muscles is required to perform the precision grip, and thus we recorded EMGs from multiple muscles simultaneously rather than one at a time.

To assess the extent of correlation between EMG signals we calculated the mean absolute correlation coefficient between each possible pair-wise combination of EMGs, across all data sets in monkey M38 (9 EMGs = 36 possible pairs) and M36 (7 EMGs = 21 possible pairs). The mean level of correlation was 0.31, standard deviation 0.10 for M38 and mean 0.54, standard deviation 0.03 for M36, indicating quite low background levels of correlated activity. However, in both animals particular pairs of EMGs showed strong correlations, for example ECU x 1DI in M38 (0.67) and thenar x 1DI in M36 (0.85), consistent with the similar actions that these muscles exert upon the hand. In contrast, other pairs showed particularly weak correlations, for example AbPL x FDP in M38 (0.05) and EDC x FDS in M36 (0.3), in agreement with the different actions that these muscles exert on the hand. Overall there was a mixture of correlation strengths between pairs of muscles, with no clear tendency towards very strong or weak correlations across all pairs. Please note that the level of physical crosstalk in these EMG recordings was very low (see Brochier et al., 2004).

3.2.2 Analysis

Instantaneous firing rate estimation. For each discriminated unit, an estimate of the instantaneous firing rate (IFR) throughout the recording period was first calculated, according to techniques described in Pauluis and Baker (2000). Briefly, this method uses the reciprocal of the interspike interval as a first approximation to the IFR, explicitly detecting significant changes in firing rate while smoothing the periods in between these times. For this analysis, IFR profiles were calculated with a sampling resolution of 500 Hz and smoothed with a Gaussian kernel of width 10 ms.

Encoding model. To study how cells in M1 and dentate encode muscle activity, we described the dependence of cell firing rate on EMG activity from multiple muscles using a linear – nonlinear (LN) model (Fig. 3.1). This analysis used standard techniques based on spike-triggered regression. Full descriptions of these procedures can be found in previous work (Chichilnisky 2001; Paninski et al. 2004c; Simoncelli et al. 2004; Shoham et al. 2005). The application of these methods to EMG data is outlined as follows.

The input vector $\vec{w}$ was formed by concatenating the full-wave rectified EMG signals from each of the nine hand and forearm muscles (seven in monkey M36) at a particular lag τ after each spike bin (Fig. 3.1 A).

Regression was used to estimate the cell's weighting of the EMG activity from each muscle $\vec{k}$, as $\vec{k} = (E(\vec{w}^t \vec{w}))^{-1} E_{\vec{w}|spike}(\vec{w})$. The first term is the inverse of the correlation matrix of w, which is computed in order to remove any correlations of the EMG input vector with itself. This is a key requirement of spike triggered

regression techniques (the probability distribution for values of the input vector is assumed to be radially symmetric or 'white'; Chichilnisky 2001). The second term is the cross-correlation of the EMG input vector with the spike train, which reduces to a conditional expectation (E) because of the binary nature of the spike train.

$\vec{k}$, as the spike triggered average (STA), gives the average value of the normalized EMG activity in each muscle at τ = 40 ms after the spike. $\vec{k}$ can be conceptualized as describing how the cell weights activity in each of the muscles at this lag (Fig. 3.1 B, top panel).

The relationship between spiking of the cell and EMG activity in the set of muscles is then captured by the term $(\vec{k} \cdot \vec{w})$, which is a linearly filtered version of the concatenated muscle activity in $\vec{w}$ carried out by the cell using its weight vector $\vec{k}$ (Fig. 3.1 B, bottom panel). To determine the vale of the filtered signal at time *t*, the EMG level in each muscle at lag τ after time *t* is weighted according to entries of the fixed vector $\vec{k}$. These values are then summed to give the filtered signal. Thus a muscle with a positive weight will increase the amplitude of the filtered signal at time $t+\tau$; a muscle with zero weight will make no contribution; and a muscle with a negative weight will decrease the amplitude of the filtered signal at time $t+\tau$.

Cells in M1 can show nonlinearity in the relation of their discharge to movement parameters such as hand position and velocity (Paninski et al. 2004c). Therefore we included a nonlinear term *f* in the description of muscle encoding given above. In the LN model, the filtered signal $(\vec{k} \cdot \vec{w})$ controls cell firing rate through this nonlinearity *f*, which is written $f(\vec{k} \cdot \vec{w})$. We did not assume a particular type of nonlinearity beforehand, but instead estimated *f* separately for each cell from $(\vec{k} \cdot \vec{w})$ using an intuitive, non-parametric binning process. This procedure consists of finding, for any

possible value u of the filtered signal $\vec{k} \cdot \vec{w}$, all times $\{t\}_u$ at which $\vec{k} \cdot \vec{w}$ was found to be approximately equal to u. The conditional firing rate $f(u)$ is then given by the fraction of time bins $\{t\}_u$ that contained a spike. In this procedure, $f(u)$ has an underdetermined scale factor [because a scale factor in the argument u-axis can always be absorbed by rescaling f itself (Chichilnisky 2001)]. Therefore we standardized u by linearly mapping the 1st and 99th quantiles of the observed distributions of u to -1 and +1, respectively, in all plots.

In figure 3.1 C it can be seen that $f(\vec{k} \cdot \vec{w})$ gives the estimated firing rate of the cell for each value of $(\vec{k} \cdot \vec{w})$. Mapping the signal $(\vec{k} \cdot \vec{w})$ through the nonlinearity f therefore provided an estimate of the instantaneous firing rate of the cell during the experiment. This relationship is encapsulated in formula 1, including terms for the current time bin of width dt (here this was 2 ms, small enough so that only one spike was observed per bin) centered at time t.

(1) $$p[spike \text{ in } (t, t+dt)] = f(\vec{k} \cdot \vec{w}(t))\, dt$$

Cross validation. We used the following cross-validation procedure to test the accuracy of the cascade model at predicting cell IFR from EMG activity. The analysis was performed on sections of data from successfully performed trials only, and periods of inactivity between the end of each trial and the start of the next one were omitted. For the dataset from each recording session, 60% of the trials were designated training data, and 40% of trials as test data. We selected trials for each of the two sets in an interleaved fashion running through the total period of time analysed from a given recording session (i.e. trials 1, 3 and 5 = train, trials 2 and 4 =

test) to ensure that no order effects were introduced. These data sets were separate and non-overlapping: each trial was allocated only to one set.

For each neuron, the training set was used to fit $\vec{k}$ and the nonlinearity $f(\vec{k}\cdot\vec{w})$. First, the signal $\vec{k}\cdot\vec{w}$ was computed using $\vec{k}$ from the train set and $\vec{w}$ from the test set. As described above, this signal captures the relationship between cell discharge and muscle activity. In effect, it is a linear prediction of cell discharge made from the EMG (although scaled between -1 and +1 as detailed above). This prediction was then compared to the cell's observed IFR for the test set simply by computing the correlation coefficient of the two signals. This provided a measure of how accurate the linear stage of the model was at predicting cell activity from a non-overlapping data segment.

Following this, $f(\vec{k}\cdot\vec{w})$ was used to generate the non-linear prediction of cell IFR using f and $\vec{k}$ fitted from the training set, and $\vec{w}$ from the test set. Again, this non-linear prediction was compared to the observed IFR for the test set by means of the correlation coefficient, to give a measure of how accurate the non-linear stage of the model was at predicting cell activity. In addition, all example encoding functions shown in *Results* and figure 3.1 were also cross validated by fitting $\vec{k}$ to the training subset and $f(\vec{k}\cdot\vec{w})$ to the test subset.

This cross-validation procedure provided a measure of how accurate our analyses were in predicting the cell's activity rather than simply reproducing observed data. In the analysis, steps were taken to minimise overfitting, whereby predictions of the test data decrease in accuracy when too many regressors are fitted to the training data. These steps are detailed where relevant.

We also carried out the same analysis on kinematic instead of EMG data, forming the input signal $\vec{w}$ from the finger position and velocity signals, at the same lags that were used for the EMG.

Although the analysis studied the combined activity of several concurrent EMGs, it was possible that a small subset of these muscles could dominate the predictions of cell discharge made from the total combined EMG signal. To address this, we first calculated the frequency at which each muscle was allocated the strongest absolute weight by $\vec{k}$. In M38 all muscles were not weighted equally: instead, two muscles in particular tended to be allocated the strongest weights (EDC and FDP). This may in part be due to the strong task-dependent activity of these muscles: EDC showed strong activity during the release phase at the end of each trial, since it acted to extend the digits as they were removed from the manipulandum, while FDP would be critically involved in generating and maintaining force during the grip (Maier and Hepp-Reymond 1995). In M36, the thenar muscles and FDP tended to show the strongest weighting across the population. Thus, some muscles were weighted more strongly across the population than others.

Secondly, for each cell, nonlinear predictions of IFR were generated separately for each of the 9 EMGs from M38, and each of the 7 EMGs in M36. These were compared to the observed IFR by calculating the correlation coefficient between the two signals. We then found the frequency at which each muscle provided the best prediction of cell IFR across the population. In M38, thenar, 1DI and ECU tended to give the best predictions when EMGs were fitted one at a time; in M36, it was 1DI and EDC. Thus for a given cell, it was not possible to determine in advance the best set of EMGs for making the IFR prediction from looking at the pattern of weighting

in $\vec{k}$. For example, a cell which allocated a strong regression weight to muscle 1DI might lead to a poor prediction when cell discharge was fitted to EMG from that muscle alone, because the cell's activity was dependent upon the difference in activity between 1DI and other muscles with different weights.

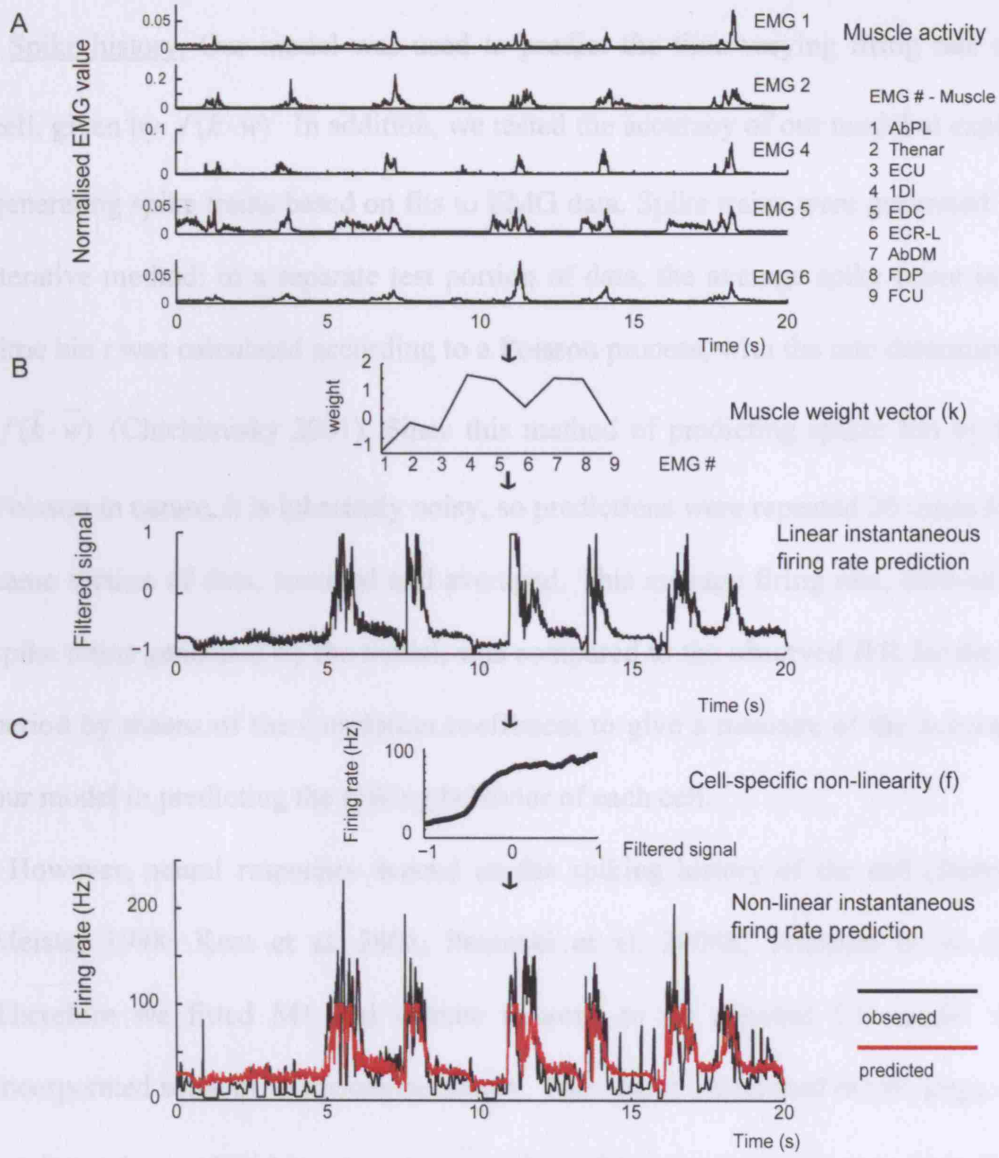

Figure 3.1. Predicting M1 and dentate instantaneous firing rate (IFR) from muscle activity. A, sample rectified EMG signals from five hand and forearm muscles. **B**, muscle activity is linearly filtered by the muscle weight vector $\vec{k}$ to give the filtered signal $\vec{k} \cdot \vec{w}$. C, $\vec{k} \cdot \vec{w}$ is transformed by the nonlinearity f to produce a nonlinear prediction of the IFR for that neuron. Observed IFR shown for comparison. Figure displays a randomly chosen section of the data. Analysis is for a single M1 PTN.

Spike history. Our model was used to predict the time-varying firing rate of the cell, given by $f(\vec{k} \cdot \vec{w})$ In addition, we tested the accuracy of our model at explicitly generating spike trains based on fits to EMG data. Spike trains were generated by an iterative method: in a separate test portion of data, the average spike count in each time bin *t* was calculated according to a Poisson process, with the rate determined by $f(\vec{k} \cdot \vec{w})$ (Chichilnisky 2001). Since this method of predicting spikes bin by bin is Poisson in nature, it is inherently noisy, so predictions were repeated 20 times for the same section of data, summed and averaged. This average firing rate, derived from spike trains generated by the model, was compared to the observed IFR for the same period by means of the correlation coefficient to give a measure of the accuracy of our model in predicting the spiking behavior of each cell.

However, neural responses depend on the spiking history of the cell (Berry and Meister 1998; Keat et al. 2001, Paninski et al. 2004b, Truccolo et al. 2005). Therefore we fitted M1 and dentate neurons to an adjusted LN model which incorporated some of this response history. This was implemented in two steps. First, we formed a modified input vector $\vec{w}_H$, formed by concatenating the original input vector $\vec{w}$ and the spike count of the neuron in the previous five bins.

(2) $$\vec{w}_H = \{w_1, w_2, \ldots, w_{end}, r_{\{-1\}}, r_{\{-2\}}, \ldots, r_{\{-5\}}\}$$

Where w_1 is the first element of the original $\vec{w}$ and w_{end} is the last, and $r_{\{i\}}$ denotes the observed spike count i time bins ago. The linear filter $\vec{k}$ fitted to this modified input vector is referred to as $\vec{k}_H$. A single lag was chosen here in contrast to the full filter length (see "Multiple Filter Delays" section below) to minimise overfitting.

Second, in a separate test set of data, a spike train was again generated iteratively,using $\vec{k}_H$ and $\vec{w}_H$.

(3) $$p[spike \text{ in } (t, t+dt)] = f(\vec{k}_H \cdot \vec{w}_H(t))\, dt$$

Here each element $r_{\{i\}}$ of $\vec{w}_H$ was the model's *prediction* of the neuronal spike count *i* time bins ago, instead of the observed spike count used in equation 2. Simulating response history in this way, by "feeding back" the model's output rather than using the cell's real spike history, ensured that we did not contaminate our model's predictions with spike trains that had already been observed. Again, predictions of the spike count were repeated 20 times, averaged and compared to the IFR, which enabled us to compare the prediction accuracies of the spike history and basic LN models.

3.3 Results

3.3.1 Data set

51 data sets from three monkeys were analysed, comprising a total of 216 neurons. We divided these data up as follows. For fits of the encoding model to both EMG and kinematic signals, data from M36 and M38 were used. Cells recorded from these animals were split into 3 groups: M1 pyramidal tract neurons or PTNs, unidentified M1 neurons or UIDs, and cells from cerebellar dentate nucleus. This gave 22 PTNs and 14 UIDs from monkey M36, together with 29 PTNs, 32 UIDs and 33 dentate cells from monkey M38. 16/22 PTNs in M36 exhibited significant postspike facilitation or suppression effects in EMG of one or more hand muscles, which is evidence that they were cortico-motoneuronal (CM) cells. Additional data for the analysis of fits to kinematic information came from recordings in monkey M41 (no EMGs were recorded in this animal). This comprised 63 M1 neurons and 23 dentate neurons.

We first describe linearity of muscle activity encoding by these neurons, and the temporal properties of this encoding. Next, we compare this encoding to tuning for kinematic parameters. Finally, the results of an attempt to model precise spiking behavior in a subset of this population are discussed.

3.3.2 Nonlinear encoding

We computed the EMG encoding functions $f(\vec{k}\cdot\vec{w})$ for a total of 130 cells from M1 and dentate nucleus. The majority were nonlinear in nature: therefore it was of interest to determine whether predictions of each cell's instantaneous firing rate were more or less accurate when incorporating this nonlinearity in the model. This was tested by comparing the correlation coefficient of each cell's observed IFR with the linearly filtered signal $\vec{k}\cdot\vec{w}$, versus the coefficient between observed IFR and the nonlinear predicted activity given by transforming $\vec{k}\cdot\vec{w}$ through f (Fig. 3.2 A,B). The mean difference between nonlinear and linear prediction accuracies for monkey M38 was small (0.003) and not significantly larger than zero (one-tailed t-test, $P<0.05$). For monkey M36, the mean difference was also small (0.01) but significant (one-tailed t-test, $P<0.05$) (Fig 3.2, C,D).

Dividing the population into the 3 cell classes, predictions of the activity of PTNs were significantly more accurate than those for dentate units and M1 UIDs, and M1 UIDs were significantly more accurate than dentate (all comparisons made using one-tailed t-tests, $P<0.05$).

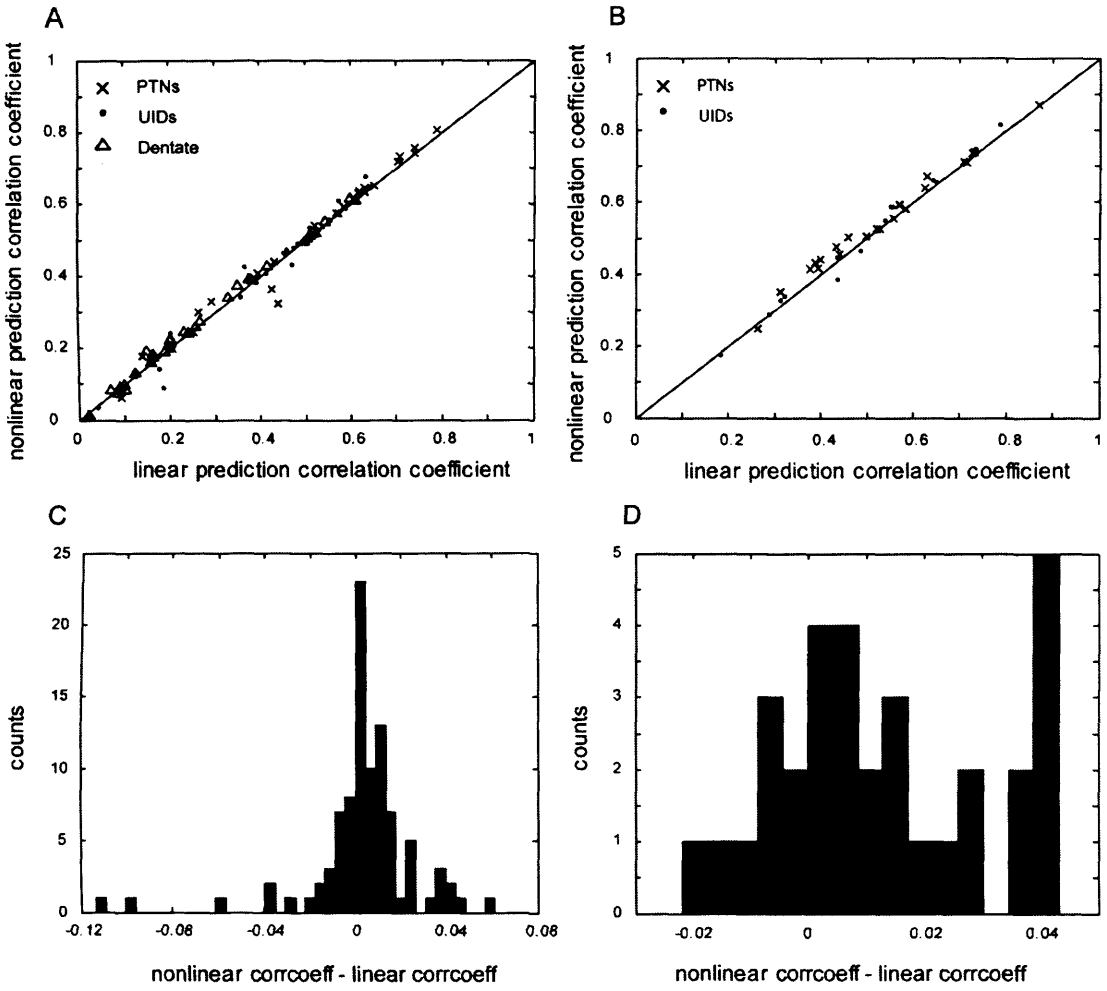

Figure 3.2. A, Scatter plot of nonlinear versus linear prediction accuracies for cells from monkey M38. Each point represents the correlation coefficient for a single cell between the observed and predicted IFR, for the two types of predictions. Diagonal line indicates unity: cells fall close to this line, indicating that incorporating the nonlinearity f did not significantly increase the prediction accuracy. Point types correspond to the three cell types sampled. Predictions were made using maximum filter $\vec{k}$ length (see section titled Multiple Filter Delays). **C**, histogram of differences between nonlinear and linear prediction accuracies. Mean difference is very small (0.003). **B, D**: same analyses for M1 neurons recorded in monkey M36. Mean difference = 0.01.

Figure 3.3 A compares the encoding function $f(\vec{k}\cdot\vec{w})$ with the distribution of values of $\vec{k}\cdot\vec{w}$ (Fig 3.3 B) for a PTN from M1. The small improvement offered by incorporating the nonlinearity into our model of the cell, despite the fact that the shape of the encoding function is clearly nonlinear, can be explained by the restricted range of $\vec{k}\cdot\vec{w}$. Most values of $\vec{k}\cdot\vec{w}$ are confined to the linear portion of the full encoding function and thus the behavior of the cell in relation to muscle activity is effectively linear.

It should be noted that we compared predictions of IFR made using the linear filter $\vec{k}$ obtained through spike triggered averaging (STA), to predictions made with $\vec{k}$ estimates computed through an "information maximisation" technique based on a probabilistic distance measure between spike-triggered and 'no-spike'-triggered distributions (Paninski 2003). The conventional STA estimates were at least as accurate in predicting cell activity.

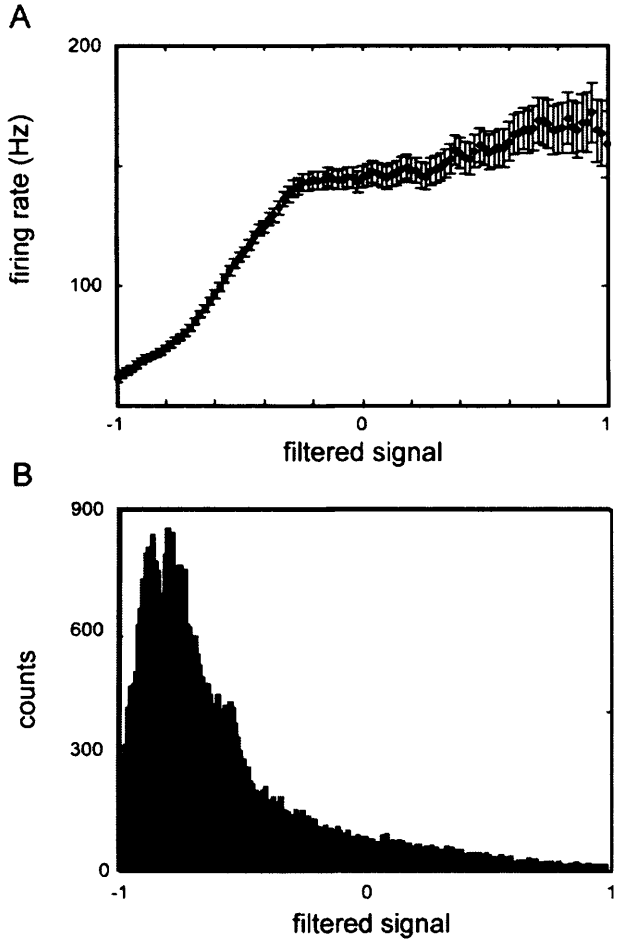

Figure 3.3. A, Example nonlinear encoding function $f(\vec{k}\cdot\vec{w}) = p(spike \mid \vec{k}\cdot\vec{w})$ **for a PTN from M1.** This function gives the conditional firing rate (y-axis) for each value of the filtered signal $\vec{k}\cdot\vec{w}$ (x-axis), after applying the non-parametric binning process outlined in *Analysis*. **B**, although the form of $f(\vec{k}\cdot\vec{w})$ is nonlinear, examining the distribution of values of $\vec{k}\cdot\vec{w}$ observed for this neuron indicates that most of the signal was restricted to a narrow range corresponding to the linear portion of the encoding function. Therefore the dependence of the firing rate of this cell on the EMG signal $\vec{w}$ filtered by its weight vector $\vec{k}$ was effectively linear.

3.3.3 Comparison with cortico-motoneuronal cells

The greater accuracy of fits to PTNs versus UIDs could be due to the fact that these cells are more directly involved in the control of muscle activity. To test this hypothesis further we analysed fits made to 9 of the subset of 16 PTNs recorded in monkey M36 that were shown to be CM cells, using the maximum filter $\vec{k}$ length for highest fit accuracy (see section below entitled *Multiple Filter Delays*). This group of 9 cells showed only postspike *facilitation* (not suppression) of one or more of the 7 EMGs recorded in this monkey. Methods for identification of genuine post-spike effects are described in Jackson et al. (2003). Nonlinear prediction accuracies were compared to those from a separate collection of 9 PTNs from M36 which showed no significant postspike effects in any of the EMGs. Of this group, 4 PTNs came from the original group of 22 PTNs in M36, and an additional 5 PTNs from extra data sets were included purely for this comparison and are not analysed elsewhere. For all cells, models were fitted at a single τ = 40ms using all 7 EMGs recorded in this monkey.

Mean prediction accuracies for the two cell types were as follows. For the 9 PTNs with no postspike effects, mean accuracy was 0.26, standard deviation 0.24. Mean prediction accuracy for the nine PTNs showing postspike facilitation was 0.61, standard deviation 0.17. This difference was significant (1-tailed t-test, $P<0.01$). Also for the 9 CM cells showing postspike facilitation there was a weak positive relationship between the size of the muscle field and prediction accuracy for the cascade model, which was not significant ($R^2 = 0.41$). The more accurate fits of CM cells to EMG in our model is consistent with the fact that the discharge of these cells directly influences the activity of one or more of the muscles analysed, through the precise time locking of a proportion of CM cell spikes to motoneuron discharge.

Similarly, CM cells showing postspike effects in a larger proportion of the muscles analysed (i.e. cells with larger muscle fields), would be expected to be fitted more accurately.

Furthermore, we looked at the relationship between the pattern of muscle weighting given by $\vec{k}$ and the pattern of post spike effects in the same muscles, for a subset of 7/16 CM cells from M36. Three of these cells showed a good degree of correspondence between the two, so that muscles with large positive weights in $\vec{k}$ also showed significant post-spike facilitation from the cell, and muscles with negative weights showed significant post-spike suppression. These neurons are akin to a group of CM cells ('set A') reported by Bennett and Lemon (1996) in which the pattern of postspike effects and cell-muscle covariation would act together to promote a fractionated pattern of muscle activity important for the performance of precision grip.

In contrast, four cells showed a poor overlap between $\vec{k}$ and the pattern of postspike effects. While the post spike effects of these CM cells would also tend to fractionate activity, this was not reinforced by the weighting of muscle activity in $\vec{k}$, and so these cells are similar to the 'set B' neurons described by Bennett and Lemon (1996).

3.3.4 Spike triggered covariance

In the analysis section, it was assumed that the spike rate depends upon a single dimension of the input signal $\vec{w}$: namely, the amplitude of this signal. The relationship of cell discharge to the level of EMG activity in multiple muscles depended upon a weight vector or "linear filter", $\vec{k}$. However, the spike rate of many neurons (e.g. cells in primary visual cortex, V1) is best related to not one, but multiple dimensions of the input signal. To account fully for the dimensionality of the signal to which these cells respond therefore requires multiple linear filters, $\vec{k_1}, \vec{k_2} ... \vec{k_n}$ (Adelson & Bergen 1985; Rust et al. 2005). Here, we examined whether single neurons in M1 and dentate nucleus encode multiple dimensions of the EMG signal, by testing whether the relationship of cell spiking to EMG was better described by multiple filters instead of only one. To do so, we applied the following analysis.

The different dimensions along which $\vec{w}$ varies can be thought of as dimensions in a vector space, and each possible value of $\vec{w}$ as a vector in this space. Returning to the basic LN model, firing rate depended only on the projection of this EMG vector $\vec{w}$ along a single direction in this space, $\vec{k}$.

However, if in reality the cell responds to multiple dimensions of the signal, then firing rate would depend not on one but on multiple vectors in the stimulus space, corresponding to the multiple linear filters $\vec{k_1}, \vec{k_2} ... \vec{k_n}$. These multiple vectors can be estimated using spike triggered covariance (STC) techniques: full details can be found in previous studies (Brenner et al. 2000; Simoncelli et al. 2004).

For each cell this involved computing the covariance matrix C_{spike}, by taking all stimulus vectors s (i.e., values of $\vec{w}$) that were conditional on the occurrence of a spike (at time t_{spike}) (equation 4).

(4) $$C_{spike} = \langle s(t_{spike} - \tau) \cdot s(t_{spike} - \tau') \rangle - \langle s(t_{spike} - \tau) \rangle \cdot \langle s(t_{spike} - \tau') \rangle$$

We next computed C_{prior} , the covariance matrix formed from all stimulus vectors s at all times t. C_{prior} is the covariation matrix of the EMG input $\vec{w}$ with itself (5)

(5) $$C_{prior} = \langle s \cdot s' \rangle - \langle s \rangle \cdot \langle s' \rangle$$

We then calculated $\Delta C = C_{prior} - C_{spike}$ .The eigenvectors E of the matrix ΔC correspond to linear combinations of the STC vectors or linear filters: the STC vectors were then extracted by computing $(C_{prior}^{-1})E$. We selected two STC vectors giving two linear filters $\vec{k_1}, \vec{k_2}$, by taking the two eigenvectors that were most different from zero. The LN model was then applied in the usual manner except that now the response of the cell modelled in equation 1 was given by the filtering of the EMG input $\vec{w}$ by 2 filters.

(6) $$p[spike \text{ in } (t, t+dt)] = f(\vec{k}_1 \cdot \vec{w}(t), \vec{k}_2 \cdot \vec{w}(t))\, dt$$

According to equation 5, cell firing rate is dependent on a two-dimensional nonlinear encoding function $f(\vec{k}_1 \cdot \vec{w}, \vec{k}_2 \cdot \vec{w})$ applied to the two filtered signals $\vec{k}_1 \cdot \vec{w}$

and $\vec{k}_2 \cdot \vec{w}$. We computed two dimensional encoding functions for each cell from M38. Fig. 3.4 A shows an example for a representative cell in M1: contours of firing rate modulation are approximately linear in the region where most stimulus vectors conditional on spiking were distributed (grey points in fig 3.4 B), suggesting that the relationship of cell firing to muscle activity is sufficiently captured by the application of a single filter. To test the accuracy of this new model in predicting cell activity we mapped the filtered input signal $(\vec{k}_1 \cdot \vec{w}, \vec{k}_2 \cdot \vec{w})$ through the corresponding 2D encoding function and compared the predicted firing rate to the observed IFR by means of the correlation coefficient as above. For all cells, these predictions were less accurate due to overfitting; computing two filters and the resulting two-dimensional encoding functions for each cell involved fitting a greater number of regressors to the training data, which decreased the accuracy of predictions of the test data. This suggests that a single linear filter $\vec{k}$ (i.e., the spike-triggered average) is sufficient to describe the encoding of muscle activity by M1 and dentate neurons.

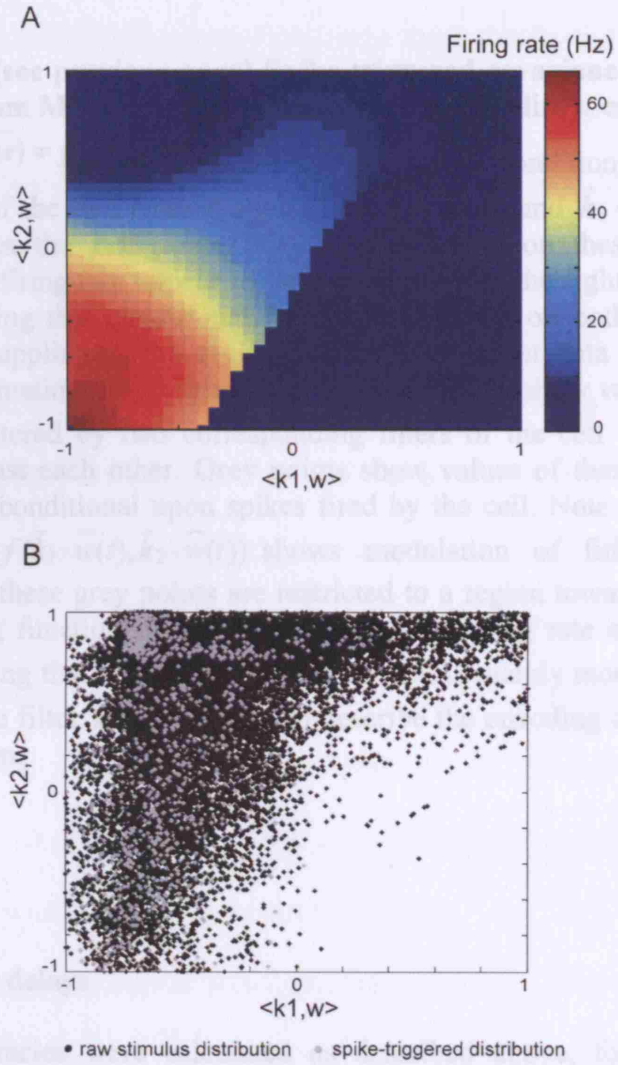
A
Firing rate (Hz)
60
40
20
0
1
0
-1
<k2,w>
-1
0
1
<k1,w>
B
1
0
-1
<k2,w>
-1
0
1
<k1,w>
raw stimulus distribution
spike-triggered distribution

Figure 3.4. (see previous page) Spike-triggered covariance (STC) analysis of a PTN from M1. A, example two-dimensional nonlinear encoding function $f(\vec{k}_1 \cdot \vec{w}, \vec{k}_2 \cdot \vec{w}) = p(spike \mid \vec{k}_1 \cdot \vec{w}, \vec{k}_2 \cdot \vec{w})$ giving the conditional firing rate for each value of the two filtered signals $\vec{k}_1 \cdot \vec{w}$ (x axis) and $\vec{k}_2 \cdot \vec{w}$ (y axis). Color axis indicates the firing rate (in Hz) conditional on these two variables. Contours of firing rate appear to be curved towards the right hand side of the plot suggesting that conditional firing rate depends on both filtered signals. Masking is applied to the regions where insufficient data are observed for accurate estimation of the firing rate. **B**, black points show values of the EMG signal $\vec{w}$ filtered by two corresponding filters of the cell $\vec{k}_1 \cdot \vec{w}$ and $\vec{k}_2 \cdot \vec{w}$ plotted against each other. Grey points show values of these filtered signals which were conditional upon spikes fired by the cell. Note that although the form of $f(\vec{k}_1 \cdot \vec{w}(t), \vec{k}_2 \cdot \vec{w}(t))$ shows modulation of firing rate in two dimensions, these grey points are restricted to a region towards the left of the 2D encoding function in A where contours of firing rate are approximately linear, showing that spiking activity of the cell is mainly modulated by $\vec{k}_2 \cdot \vec{w}$. Thus a single filter $\vec{k}$ is sufficient to describe the encoding of muscle activity by this neuron.

3.3.5 Single filter delays

Prediction accuracies were calculated as described above, for different single delays τ between spike and EMG (ranging from -160 ms to +320 ms in 10 ms increments) to assess the temporal evolution of tuning for muscle activity in these neurons. Since linear and nonlinear predictions were found to be equivalent, we refer to firing rate predictions made using $f(\vec{k} \cdot \vec{w})$ unless otherwise stated. Different cells had a different value of τ which gave the best fit (Fig. 3.5 A). For example, the tuning of the cell given by the uppermost curve reaches peak prediction accuracy at close to $\tau = 0$ s, while the curve below peaks at approximately $\tau = 0.18$. There was no consistent optimum τ across cells.

When the model was fitted to one EMG at a time, the level of heterogeneity in optimum lags across cells showed some dependence on the muscle that was fitted. To quantify this, the top 50% of neurons from each cell group in M38 were fitted at a range of lags τ, one muscle at a time, which gave a total of 47 individual temporal tuning curves for each muscle. The optimal lag τ corresponding to peak prediction accuracy was found from each curve. We then used Levene's test for homogeneity of variance (Miller 1986) to determine whether the levels of variation in optimal lag values for fits to each muscle were the same: this was significant ($P<0.05$), indicating that they were not. In line with this, fits to thenar EMG showed more variance in the optimal lag across cells (standard deviation 0.03), while fits to 1DI showed less variance in the distribution of optimal lags (standard deviation 0.02). This suggests that cells showed more variation in the temporal profiles of their spike-EMG correlations with some muscles than with others.

Overall, temporal tuning curves were broad (Fig. 3.5 A). These broad curves were not an artefact of the filtering and smoothing that we applied to the EMG data. The total filter length (as measured by applying the same pre-processing to a signal comprising a spike in a single bin) was 78 ms, shorter than the time-scale of the correlations we observed. We also confirmed that this broadness was not simply a result of combining multiple EMGs that were acting at different times relative to each other during task performance, as the same broad tuning curves were found for correlations with single muscles.

Next, we analysed the shapes of these temporal tuning curves in more detail. All cells from monkey M36 were included. In monkey M38 less accurate task performance may have resulted in greater trial-trial variability of cell firing rates and EMG, reducing the strength of correlation between cell discharge and muscle

activity (mean nonlinear prediction accuracy at 40 ms lag for M1 cells from M38 was 0.38, compared to 0.48 for neurons sampled in M36). To reduce the effect of noise on the shapes of temporal tuning curves we therefore selected the most accurate 50% of the cells in each group from M38.

Dividing cells up into three groups – PTNs, UIDs and dentate – revealed that there were no significant differences either in the peak lag distributions between the three groups (two-tailed Kolmogorov-Smirnov test between each distribution pair, $P<0.05$), or in the mean peak lag (two-tailed t-tests, $P<0.05$). Figure 3.5 B plots the mean change in prediction accuracy with lag for the population. PTNs and dentate units reached maximum prediction accuracy at 10 ms lag, while the peak lag for UIDs was 30 ms. The peak lag for PTNs corresponds to values obtained from previous regression analyses (Morrow and Miller, 2003) and spike-triggered averaging work (Fetz and Cheney, 1980). At all values of τ, PTNs were on average more strongly correlated with EMG than UIDs, which showed stronger correlations than dentate units.

Finally, we looked at temporal tuning curves for 16 PTNs from M36 identified as CM cells, once again using the concatenated activity of all 7 EMGs recorded from this monkey. Here also, the shapes of temporal tuning curves for single cells were broadly curved. Optimal lags were measured from these curves, which again were heterogeneous in their distribution. The level of heterogeneity for CM cells was not significantly different from other cells. For a fair comparison against cells showing no CM connections, we compared the variance in optimal lags measured for CM cells with those for the top 50% of dentate cells in M38, using Levene's test for homogeneity of variance. This was not significant ($P>0.05$). Thus CM cells showed

similar temporal profiles of tuning for muscle activity as for the other cell types in our model.

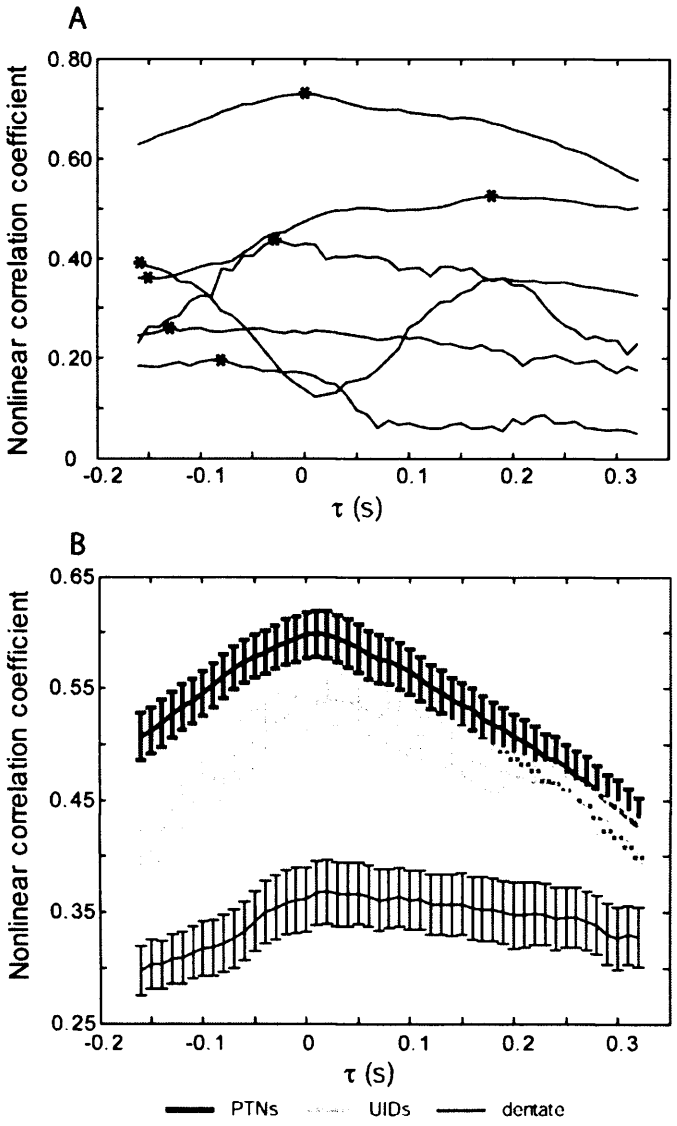

Figure 3.5. Temporal tuning functions for the encoding of muscle activity. A, tuning curves for single cells. Each curve corresponds to the nonlinear prediction accuracy as a function of τ for a single cell. Asterisk indicates optimal lag. Only a randomly chosen subsample of the population is shown to avoid overcrowding. **B**, average temporal tuning functions for the population, divided into 3 cell types (see legend). Each trace represents the mean change in nonlinear prediction accuracy as a function of τ for each cell group. Error bars indicate standard error.

3.3.6 Multiple filter delays

Prediction accuracies were compared for different lengths of the linear filter $\vec{k}$ using 40 ms increments from 40 ms to 360 ms after each spike. Again, there was some heterogeneity in the optimal filter length (Fig 3.6 A). Fig. 3.6 B shows the mean change in prediction accuracy with increasing filter length for all cells, once again taking all cells from M36 and the top 50% of each subpopulation of neurons from M38. For all three cell types, the mean correlation coefficient increased smoothly with increasing length but the range of this increase was small. PTNs showed a larger range of increase in correlation coefficient values than dentate units. Looking at the total population (without selecting the most accurate cells), at all filter lengths the highest prediction accuracies were achieved using PTNs, followed by UIDs and then by dentate units. At the maximum filter length, M1 neurons together were approximately twice as accurate as dentate cells.

The analysis was repeated using nine lag increments of 10 ms to test whether much of the growth in accuracy occurred over a narrower region closer to the spike, which resulted in more linear increases in accuracy over a smaller range. Thus the accuracy of our model continued to grow even when fitting EMG data at long delays of 200-300 ms after each spike. Therefore the maximum filter length was used for subsequent analyses, with the exception of the spike history analysis described above.

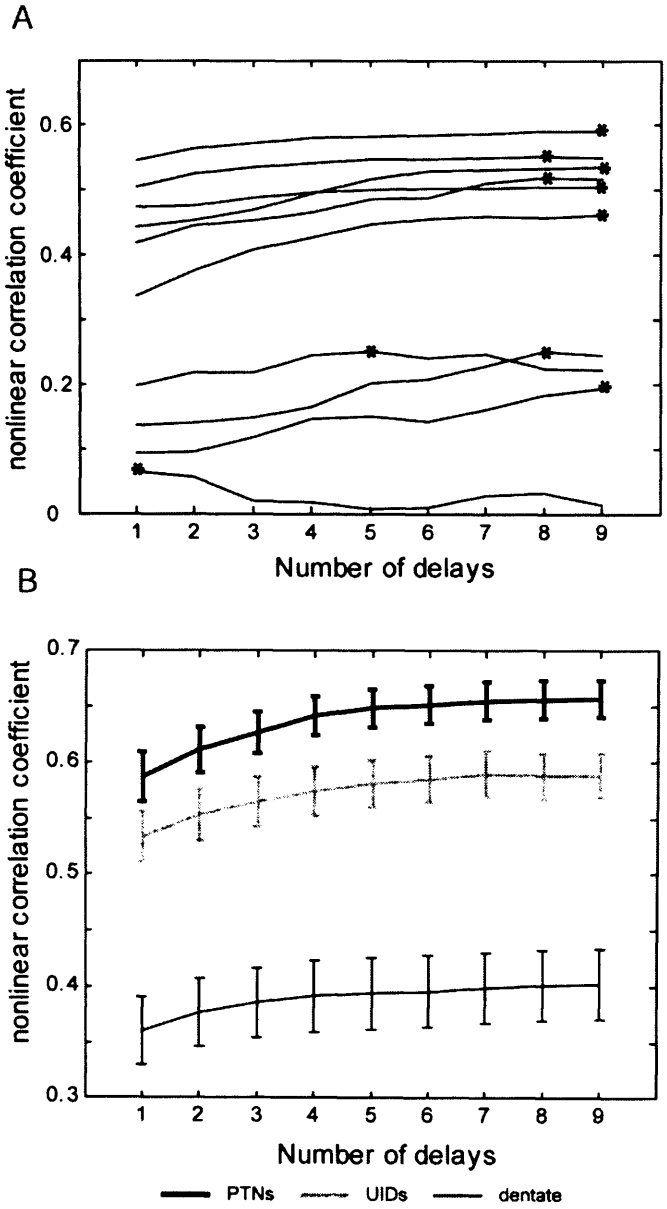

Figure 3.6. Prediction accuracy as a function of number of delay samples. **A**, modulation for single cells. Each trace corresponds to the nonlinear prediction accuracy versus number of delays for a single cell, where the delay increment is 40 ms. Asterisk indicates optimal number of delays. A random subsample of cells is shown to avoid overcrowding. **B**, population mean prediction accuracy as a function of number of delay samples, divided into 3 cell types (see legend). Each trace represents the mean change in nonlinear prediction accuracy versus number of delays. Error bars indicate standard error.

3.3.7 Kinematic information

LN models were fitted to neurons from M36 and M38 using finger position and velocity information recorded during task performance, for the same single lag and multiple lag increments described above. We compared these fits to correlations of cell discharge with muscle activity. Before making this comparison of fits to different movement parameters, trials were selected for analysis using the criteria described in Methods to ensure that trial performance was as homogenous as possible. In monkey M38, three PTNs were subsequently excluded from analysis as they fired mainly during trials that were rejected.

Correlation coefficients for nonlinear versus linear predictions were compared (Fig. 3.7 A). In contrast to the analysis conducted with EMG data, cascade models using finger position and velocity information showed an increase in the strength of the nonlinearity: more cells were above unity (M38: 76% for kinematic fit, compared to 69% for EMG fit; M36: 95% for kinematic fit compared to 70% for EMG). The mean difference in prediction accuracy between nonlinear and linear predictions was greater for fits to kinematic data: in M38 it was 0.03 for kinematic fits compared to 0.003 for EMG; in M36 it was 0.03 for kinematic fits compared to 0.01 for EMG. However, in both monkeys this difference did not reach significance (1-tailed t-test, $P>0.05$). The increased effect of the nonlinearity for fits to kinematic variables is consistent with a previous study of M1 neurons during an arm reaching task, where kinematic encoding was found to be significantly nonlinear, but the effect of this nonlinearity was also small (Paninski et al. 2004c).

Prediction accuracy was compared for M1 and dentate neurons fitted using kinematic data in M38. Since no cerebellar recordings were included from M36, data from a third monkey (M41) were incorporated here to make a comparison across two

animals. In both cases, mean prediction accuracy for M1 neurons was approximately twice as accurate as for dentate cells. This difference was significant (paired one-tailed t-test, $P<0.001$).

Finally, fits made using kinematic and EMG information in M36 and M38 were compared across all neurons. There was no significant difference in mean prediction accuracy between kinematic and EMG information (paired t-test, $P>0.05$) (Fig. 3.7 B). Combining both kinematic and EMG information increased prediction accuracy above what was observed with either EMG or kinematic data alone (Fig. 3.7 C). In all of these instances, PTNs were always modelled with greater accuracy compared to UIDs and dentate neurons.

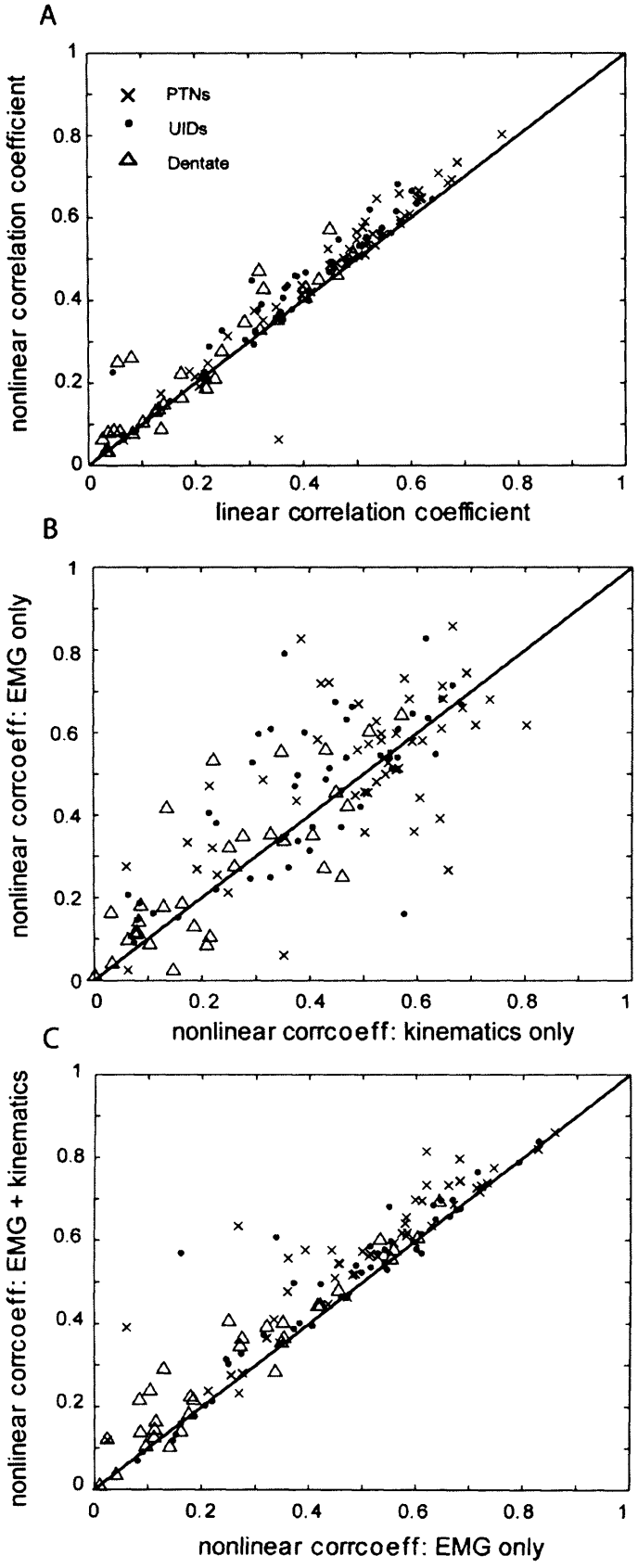
A
PTNs
UIDs
Dentate
nonlinear correlation coefficient
linear correlation coefficient
B
nonlinear corrcoeff: EMG only
nonlinear corrcoeff: kinematics only
C
nonlinear corrcoeff: EMG + kinematics
nonlinear corrcoeff: EMG only

Figure 3.7. (see previous page) Comparing the encoding of muscle activity versus kinematic information. **A**, scatter plot of nonlinear versus linear prediction accuracies using finger position and velocity information. Conventions are the same as for figure 3.2: note that points fall further above the diagonal in the current figure suggesting a greater increase in prediction accuracy for encoding of kinematic information when incorporating the nonlinearity, *f*. **B**, scatter plot comparing prediction accuracies for muscle activity (Y axis) versus kinematic information (X axis). Each dot represents the correlation coefficient for a single cell between the observed and predicted IFR, obtained using the two types of information. Diagonal line indicates unity. Correlation coefficients do not fall significantly either side of diagonal indicating equal accuracy of the model when fitted to muscle activity or kinematic information. **C**, scatter plot of prediction accuracies for a combination of muscle activity and kinematic information (Y axis) versus muscle activity alone (X axis). Correlation coefficients fall significantly above diagonal indicating greatest accuracy of the model accuracy when fitted to both types of information. All plots show data from M36 and M38.

3.3.8 Predictions of spiking activity

We compared the ability of the Poisson and spike history (SH) models described above to predict novel spike trains, in the population of cells from monkey M38. Fitting $\vec{k}$ and f to training data which incorporated the spiking history of the neuron, improved the dynamic range of the encoding function (Fig. 3.8 A). For all 94 cells, both the absolute and percentage modulation of firing rate measured from the function were significantly higher when cells were fitted with the SH terms compared to EMG alone (1 tailed t-test, $P<0.05$). However, despite this apparent improvement, cross-validated predictions of the observed IFR made by mapping the filtered signal $\vec{k} \cdot \vec{w}$ through the encoding function f were significantly less accurate for the SH model, compared to when cells were fitted with the EMG alone (1 tailed t-test, $P<0.05$). The increase in dynamic range captured by incorporating the SH terms failed to improve fit quality due to the fact that, as with the basic LN model,

the rising part of the curve still corresponded to the tail of the distribution of the filtered signal, where there was little data (fig 3.8 B). In turn, fits made using SH terms did not lead to improved performance of the model when predicting the spike count in a novel, cross-validated section of the data (Fig 3.9). As the iterative spike generation process was fairly time consuming, a subset made up of the 10 cells which gave the most accurate nonlinear predictions of the IFR were tested. For each cell, the cross-validated average firing rate computed from 20 repeats of the spike generation process was compared to the observed IFR by means of the correlation coefficient, for the LN and the SH models. The SH model was not significantly more accurate at predicting the spike count (1-tailed t test, $P>0.05$).

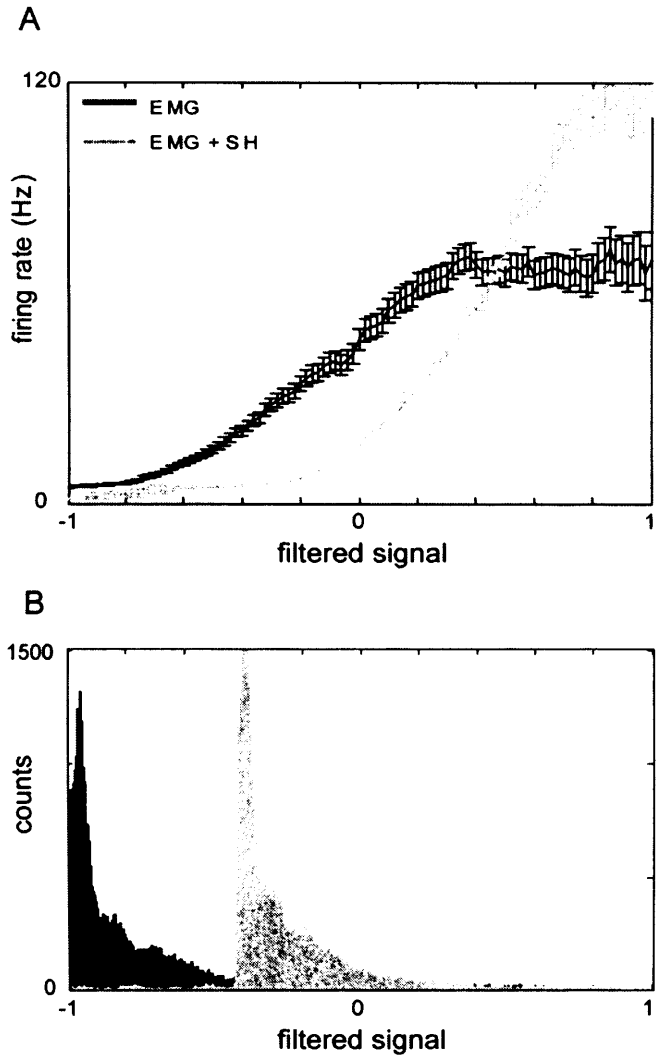

Figure 3.8. Incorporating spike history (SH) effects. A, effect of including SH terms on dynamic range of cell encoding function. Black trace, example encoding function *f*, for a PTN from M1, for LN model fitted to muscle activity as in Fig. 4. Grey trace, encoding function for same cell fitted to both muscle activity and the previous response history of the cell up to 10 ms previously. Note that although the dynamic range of modulation increases, the curve shifts right to higher values of the filtered signal $\vec{k} \cdot \vec{w}$. Error bars indicate standard error. **B**, effect of SH on filtered signal. Black histogram shows distribution of filtered signal values for fit to muscle activity as in Fig. 3.3. Grey histogram shows distribution of filtered signal values for fit incorporating SH, this shifts to the right. Thus for both fits, much of the change in the firing rate of the cell takes place at the tail of the corresponding distribution, where there is little data. Filtered signal values have been scaled to –1 and +1 as described in *Methods*.

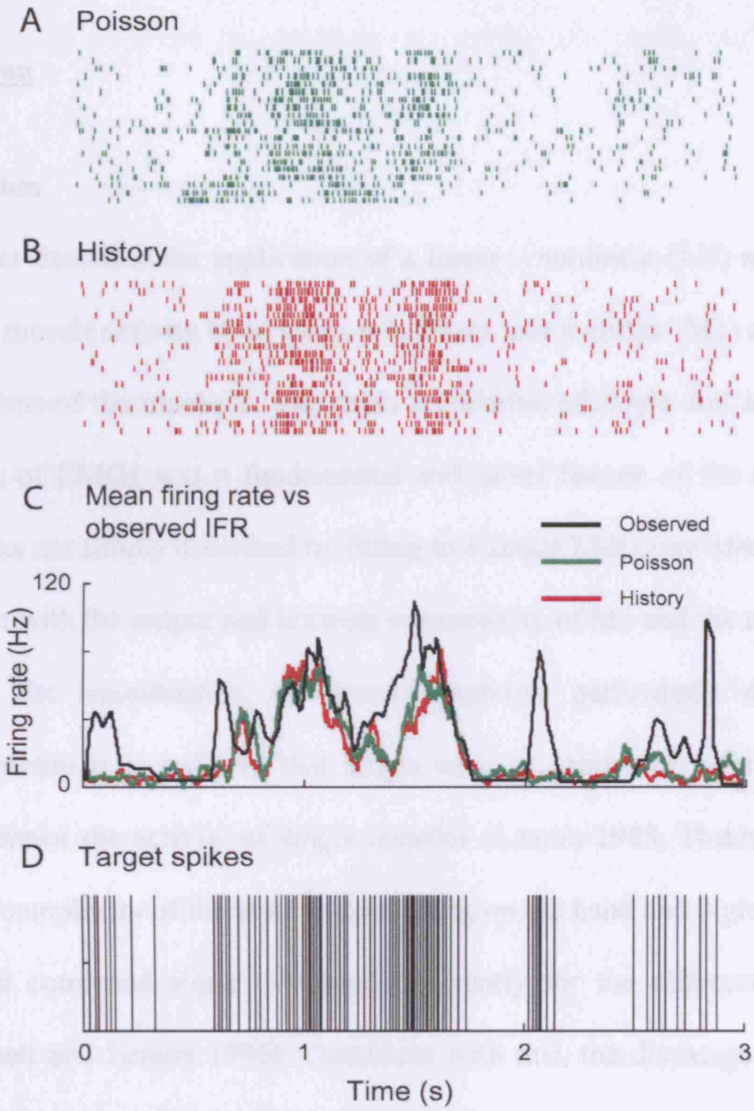

Figure 3.9. Predicting spikes from muscle activity. Figure shows same cell as Fig. 3.8. A, raster display showing 20 iterations of predictions of spiking activity for a M1 neuron using the basic LN model. **B**, equivalent raster display for predictions made using the spike history model described in *Analysis*. C, averages of the above rasters (green and red traces, respectively) compared to observed IFR. Both types of predictions do about as well as each other at predicting the periods of spiking activity. D, observed spikes shown for comparison. Predictions are illustrated for a small, randomly chosen portion (3 seconds long) of the total data recorded from this neuron.

3.4 Discussion

3.4.1 Overview

This chapter describes the application of a linear – nonlinear (LN) analysis to the encoding of muscle activity by neurons in primary motor cortex (M1) and cerebellar dentate nucleus of the macaque. The cross correlation of single unit activity with a combination of EMGs was a fundamental and novel feature of the analysis. Cell discharge was not simply described by fitting to a single EMG (see *Methods*). This is in agreement with the output and intrinsic connectivity of M1 and the role of dentate nucleus in the coordination of muscle activity, particularly during finger movements,where it is unlikely that single cells or groups of cells within these structures control the activity of single muscles (Lemon 1988, Thach et al. 1992). Instead, the complexity of the musculature acting on the hand and digits may require a distributed command signal weighted differently for the different motoneuron pools (Bennett and Lemon 1996). Consistent with this, the discharge properties of single neurons within M1 have been described within a "muscle space" coordinate system wherein cell firing can be related to the activity of a set of muscles, for example by cross correlating cell activity with each EMG one at a time (Holdefer and Miller 2002). The aim of the current study was to extend this previous work by investigating how single cells encode the full time-varying concurrent activity of multiple muscles. The key result we have demonstrated is that the control of movements by these neurons within a muscle parameter space is linear in nature. The results of two important comparisons are described: neurons in M1 are on average two times more strongly correlated with movement parameters than those in dentate, and a combination of EMG signals from multiple muscles provides predictions of

neural discharge that are as accurate as predictions made using kinematic information.

3.4.2 Linearity of encoding

The linear nature of muscle encoding reported here contrasts with the encoding of kinematic parameters in the same task, and during an arm reaching task where encoding was significantly nonlinear in about 1/3 of the cells analysed (Paninski et al. 2004c). However, it was suggested in the latter study that the full strength of the nonlinearity in kinematic encoding was masked, and that the inclusion of other behaviorally relevant parameters in the analysis (such as EMG) could expose additional, and possibly stronger nonlinearity. We have demonstrated that the inclusion of muscle activity does not have this effect, at least under these task conditions.

Our work complements previous spike-triggered averaging studies (Cheney and Fetz 1980; Jackson et al. 2003; Morrow and Miller 2003). It is also consistent with results from a recent intra-cortical microstimulation study which found linear summation of corticospinal outputs in cat M1 measured using a combination of eight forelimb EMG signals (Ethier et al. 2006). Furthermore, it is interesting to compare our findings with certain features of a model put forward by Todorov (2000): assuming that M1 PTNs contribute additively towards the activation of muscles, apparent encoding of kinematic parameters then emerges due to compensations made by the M1 output for each muscle's state dependence. Linear encoding of muscle activity by single neurons represents the inverse of this model: neuronal discharge rates are a linear sum of the activity in multiple muscles. Of the three cell types

(PTNs, UIDs and dentate neurons) the activity of PTNs was predicted with greatest accuracy by the LN analysis. Since most M1 hand area PTNs have axons that terminate within the spinal cord segments controlling arm and hand muscles, and therefore directly influence activity in these muscles, this finding is not unexpected. However, Todorov's framework only considers cortico-motoneuronal neurons (which make direct connections with motoneurons). In monkey M36 a total of 16/22 PTNs sampled were also identified by spike-triggered averaging to be CM cells, but it is difficult to incorporate the unidentified M1 cortical neurons (UIDs) and cerebellar dentate cells that we analysed within this scheme.

Furthermore, there was no nonlinearity in the encoding surfaces $f(\vec{k}_1 \cdot \vec{w}, \vec{k}_2 \cdot \vec{w})$ computed from two orthogonal filters $\vec{k}_1$ and $\vec{k}_2$ (Fig. 3.4), indicating that a single filter was sufficient to capture firing rate modulation with muscle activity in these neurons, and further validating the linear model. This is in agreement with neurons sensitive to hand position and velocity in M1, which are also sufficiently described by a single filter (Paninski et al. 2004c). However, it is possible that additional nonlinearity might be exposed after including information about other movement parameters (such as joint angles and torques) that were not analysed here.

3.4.3 Temporal dynamics of encoding

The temporal (that is, τ- or lag-dependent) properties of muscle encoding have been addressed previously using correlative methods, in M1 and red nucleus. Initial studies addressed single neuron – muscle pairs (Miller et al. 1993); more recently, the correlation of ensembles of neurons with individual muscles has been

investigated (Morrow and Miller 2003). Our study complements this work by looking at the encoding of activity in multiple muscles by single neurons.

The resulting "temporal tuning curves" were heterogenous (Fig. 3.5). There was no consistent optimum τ for all neurons, and the shapes of the tuning curves varied considerably from cell to cell. Similar heterogeneity was observed for the tuning of M1 neurons to hand position and velocity in a pursuit tracking task (Paninski et al. 2004a). Tuning curves also tended to be broad, for both single-cells and population means, with no sharp tuning to a particular τ, and cells remained relatively well correlated with muscles even at long positive and negative lags. Interestingly, our analysis uncovered the same broad tuning functions for identified CM cells from monkey M36.

This broad range of tuning properties is consistent with previous descriptions of the diversity of the correlation strength between neural activity and various behavioral parameters (Kakei et al. 1999; Porter and Lemon 1993). However, it conflicts with rapid latencies of 5-10ms for the onset of postspike facilitation (PSF) estimated in previous spike-triggered averaging studies (Fetz and Cheney 1980; McKiernan et al. 1998, 2000)..There was also a disparity between the pattern of muscle weighting given by $\vec{k}$ and the pattern of postspike effects in some CM cells. Why might these discrepancies exist?

As detailed above, these findings are not simply due to the nature of the filtering we applied, nor are they a result of combining activity from multiple muscles: firing rate was correlated with single EMGs in a similar fashion. Broad temporal tuning has been observed previously for neurons in the magnocellular red nucleus (Miller and Sinkjaer 1998) and interpositus (Soechting et al. 1978) and it has been argued that it

represents a non-specific modulation of α-motoneuron activity by these cells; this could certainly be the case for the broad lag functions we observed among dentate neurons and UIDs.

But why did PTNs, some of which were CM cells directly controlling α-motoneuron activity, behave in the same way? PSF effects for cortico-motoneuronal (CM) cells represent an increased probability of motoneuron discharge that is time locked to CM cell spiking, at latencies close to the conduction delay between cell and muscle (Porter and Lemon 1993). However, the synaptic input to a motoneuron from a single CM cell is very small when compared with the total synaptic drive to the motoneuron; and as a result the probability that the discharge of a single CM cell will cause a motoneuron to fire is very low (Porter and Lemon 1993; Baker and Lemon 1998). Thus only a few percent of a CM cell's total spike activity are exactly time-locked to discharges of motoneurons in the cell's target muscle, and therefore to its EMG activity. Of course, the vast majority of spikes that do not cause motoneurons to discharge are nevertheless still contributing to the overall excitatory synaptic drive to the same motoneurons, and this is reflected in a broader co-activation of cell and muscle activity. This in turn accounts for the more general correlation between the envelopes of cell and muscle activity that can often be observed over longer time scales of several hundred milliseconds. These broad correlations are more common, as cells and muscles tend to co-vary during the task for the reasons given above. However, both sources of correlation are thought to be of importance in understanding the encoding of movements in terms of muscles. For example, the interaction between the pattern of postspike effects and the pattern of CM cell – muscle coactivation might enhance the fractionation of hand muscle activity during precision grip (Bennett and Lemon 1996). The overall strength of

correlations between CM cell spike trains and target muscle EMG will be enhanced by the fact that CM cells with common target muscles are synchronised together at the cortical level (Jackson et al. 2003).

Our findings bear a noticeable similarity to results presented by Morrow and Miller (2003; see their Fig. 3A) who fitted EMG in single muscles to activity in ensembles of up to 15 M1 neurons – essentially the converse of our analysis – during reach-to-grasp movements. Importantly, the task studied differed from ours in that arm movements were unrestrained, and grip was exerted against a static rather than compliant load. Yet good fits (Rsquare values around 0.6) could be obtained for long negative and positive delays (–400 ms and +500 ms respectively). Their observation of similarly broad neuron-muscle correlations during a different task would tend to suggest that the tuning curves shown above are not just a by-product of task-related coactivation.

Furthermore, we examined how best to combine the EMG information at multiple lags in addition to computing single lag tuning curves. The ability of our model to predict novel cell discharge improved as more of the EMG waveform was included even at very long positive lags (+360 ms) (Fig. 3.6), consistent with broad temporal tuning. But the improvement was only slight, suggesting that much of the modulation in cell firing could be explained by incorporating muscle activity at only a single time point relative to each spike.

3.4.4 Kinematics

In this study we were able to make a direct comparison via LN analysis between the encoding of time varying muscle activity and the encoding of basic kinematic

parameters (finger position and velocity), in the same population of neurons. Such a comparison was aimed at assessing the relative importance of these two signals in describing M1 and cerebellar activity, and was of interest given the long-standing debate about the precise nature of the neural "code" for movement (Scott 2000). The finding that neural discharge in both structures was correlated with muscle activity and kinematic information to a similar extent is consistent with previous reports suggesting an intermixing of neurons encoding both types of parameters in M1 (Thach 1978; Kakei, Hoffman et al. 1999). It also adds to work from several studies which have addressed kinematic encoding in M1 and cerebellum during arm reaching movements (Fu et al. 1995; Fu et al. 1997; Serruya et al. 2002; Paninski et al. 2004a,c) by studying this encoding during execution of precision grip. These two types of task involve fundmentally different control strategies (Porter and Lemon 1993; Scott and Kalaska 1997). Interestingly, the encoding of digit position and velocity by these cells was more nonlinear in nature compared to the encoding of EMG (Fig. 3.7 A), supporting the results of previous work on the representation of kinematics in M1 (Paninski et al. 2004c).

3.4.5 Spike history model

We evaluated the effects of incorporating neuronal response history in our model. Including spike history (SH) increased the apparent dynamic range of the encoding function (Fig. 3.8 A). This result would seem to be consistent with previous studies measuring likelihood and tuning curve modulation (Berry and Meister 1998; Paninski et al. 2004b). However, despite this increase in dynamic range, the SH model actually resulted in significantly decreased accuracy of predictions of observed IFR. The reason for this decrease is that much of the dynamic behavior of

the cell captured by the SH terms took place at the tail of the distribution of the filtered signal $\vec{k} \cdot \vec{w}$, where there was little data (Fig. 3.8 B). This effect is similar to the weak influence of the nonlinearity described above (Fig. 3.3), where much of the filtered signal distribution was confined to the linear portion of the curve. Consequently, fits made using SH terms did not lead to improved *predictive* performance: our spike history model failed to give more accurate predictions of the neuron's spiking activity on novel, cross-validated data (Fig. 3.9). This conflicts with findings from the aforementioned studies, but is consistent with the overall picture we present here, of linear encoding of muscle activity. The activity of the cells was sufficiently described by a linear combination of the EMG signals from multiple hand muscles, without needing to incorporate the response history of the cell up to 10ms previously. In turn, this could be interpreted as support for weakly time-locked spike generation in models of muscle encoding by these neurons, under these particular task conditions.

3.4.6 Comparison of different cell types

Finally, another important finding of this study was the consistent trend of greater correlation strengths with movement parameters for PTNs than UIDs, which were on average two times greater than dentate neurons. This result is in agreement with the extent to which these different cell types control the intrinsic hand and forearm muscles. Dentate neurons should be expected to show the weakest relationships to specific movement parameters, given that this structure lacks any direct projections to the cervical levels of the spinal cord (Brooks and Thach 1981). Since the major projections from the dentate nucleus involve the motor thalamus and motor cortex, it

is likely that this is the main pathway that mediates cerebellar influence over muscle activity. In line with this theory, functionally related regions of M1 and dentate are interconnected (Holdefer and Miller 2000; Dum and Strick 2003) and dysfunction of the cerebellar hemispheres and dentate nucleus disrupts skilled finger movements in monkeys and humans (Thach et al. 1992; Glickstein et al. 2005), indicating that these two structures work in close cooperation during precision grip. This may explain why, despite differences in the relative strength of their correlations with EMG and kinematic parameters, neurons from both structures showed the same basic features of movement encoding.

3.5 Summary

The activity of neurons in primary motor cortex (M1) and cerebellum is known to correlate with extrinsic movement parameters, including hand position and velocity. Relatively few studies have addressed the encoding of intrinsic parameters, such as muscle activity. Here we applied a generalized regression analysis in order to describe the relationship of neurons in M1 and cerebellar dentate nucleus to electromyographic (EMG) activity from hand and forearm muscles, during performance of precision grip by macaque monkeys. We showed that cells in both M1 and dentate encode muscle activity in a linear fashion, and that EMG signals provide predictions of neural discharge that are equally accurate to those from kinematic information under these task conditions. Neural activity in M1 was significantly more correlated with both EMG and kinematic signals than was activity in dentate nucleus. Furthermore, the analysis enabled us to look at the temporal properties of muscle encoding. Cells were broadly tuned to muscle activity as a function of the lag between spiking and EMG and there was much heterogeneity in the optimal delay among individual neurons. However, a single lag (40 ms) was generally sufficient to provide good fits. Finally, incorporating spike history effects in our model offered no advantage in predicting novel spike trains, reinforcing the simple nature of the muscle encoding that we observed here.

Chapter 4: M1 output pathways

4.1 Introduction

As described in Chapter 1, there are two parallel pathways by which information from M1 can reach the cerebellum through the pontine nuclei: via collaterals of the corticospinal tract, and through a direct cortico-pontine projection. Therefore the cerebellum could receive information from M1 in the form of efference copy of movement commands, as well as communication through a dedicated "private line" respectively. The goal of the experiments described in this chapter was to compare the activity of neurons in M1 that belong to each of these pathways.

Much of the previous single unit work in M1 has focussed on its output, due to the bias of electrophysiological recordings towards the large layer V pyramidal output neurons (Humphrey and Corrie, 1978). Combining these recordings with antidromic stimulation enables the target structures of these outputs to be identified, so the functional significance of neurons within the M1 network that project to a particular location can be interpreted. Previous studies have focussed on the activity of cells identified as PTNs which send information through the corticospinal tract. The experiments described below extend this by comparing these neurons to a separate class of cells identified as potentially projecting to the pontine nuclei and not the pyramids: so called cortico-pontine neurons (CPNs). This facilitates an understanding of how M1 communicates with spinal cord motoneurons and the cerebellum during hand movements, since corticopontine projections are relayed to the cerebellum.

The experiments described in this chapter used simultaneous recordings from the two types of neuron to answer two basic questions. Firstly, do CPNs show the same task-related activity as PTNs? The discharge patterns of the latter during precision grip have been described at length (Porter et al., 1993; Baker et al., 2001) and so serve as a useful standard against which to measure the activity of M1 CPNs. Given that the cerebellum receives information about the features of corticospinal output via CST collaterals to the pons, CPNs might be expected to communicate different information and might therefore demonstrate different responses to the parameters of the task. As simultaneous recordings were made from the two cell types, comparisons of task related activity were less confounded by the effects of inter-session variation in task performance. The second question was, do these CPNs show significant synchronization with each other or with other PTNs? This is relevant as synchronization provides a means of establishing the degree and type of connectivity between different networks of neurons within the motor cortex, classified according to their corticomotoneuronal connectivity (Baker et al., 2003; Jackson et al., 2003). We applied similar techniques to these studies to look at the interactions between corticospinal and corticopontine networks in M1.

4.2 Methods

4.2.1 Cell identification

Cells were identified by antidromic stimulation of their axons using chronically implanted, varnish insulated tungsten stimulating electrodes in the pyramidal tract and the cerebral peduncle (see Chapter 2). Classification of pyramidal tract and cortico-pontine neurons was carried out as follows. Pyramidal tract neurons (PTNs) were identified according to their short latency antidromic response to PT stimulation. Triggering the PT impulse from spontaneous PTN spikes produced collision of orthodromic and antidromic action potentials, confirming the spontaneous discharge as belonging to the PTN (Baker, Philbin et al., 1999); see figure 4.1 A. Since PTN axons course through the peduncles before reaching the pyramid, the identity of these cells was doubly confirmed by similar antidromic activation and collision from peduncular stimulation (Fig. 4.1 B).

The axons of cortico-pontine neurons (CPNs) on the other hand terminate in the pontine nuclei and so do not pass through the pyramid. Thus M1 neurons were identified as CPNs if they could be antidromically activated and collided using the peduncular electrodes (Fig. 4.1 C) but were not activated by the pyramidal electrodes (Fig. 4.1 D). Strictly these cells were "cortico-peduncular neurons" as they were not backfired from the pons. However, stimulation in the pontine nuclei would theoretically activate both the axons of direct cortico-pontine neurons as well as PTN collaterals and fibres of passage (Ugolini and Kuypers, 1986), and so it would be impossible to differentiate between the two neuronal varieties using this approach. Therefore pontine projections of CPNs were inferred from the fact that the vast majority of non-corticospinal axons in the peduncle probably terminate in the

pontine nuclei (Tomasch, 1969; Glickstein, 2000). The distribution of latencies of antidromic activation of PTNs was similar to that reported by Fromm and Evarts (1981), and over the periods of recordings in both monkeys there were no clear differences in antidromic latencies between PTNs and CPNs.

Those cells which we could not identify by stimulation in either location were termed unidentified neurons (UIDs). Table 4.1 summarises the cell classification procedure.

Table 4.1. Summary of response to stimulation of different cell types identified in M1.

	PTN	CPN	UID
Pyramid	✔	✘	✘
Cerebral Peduncle	✔	✔	✘

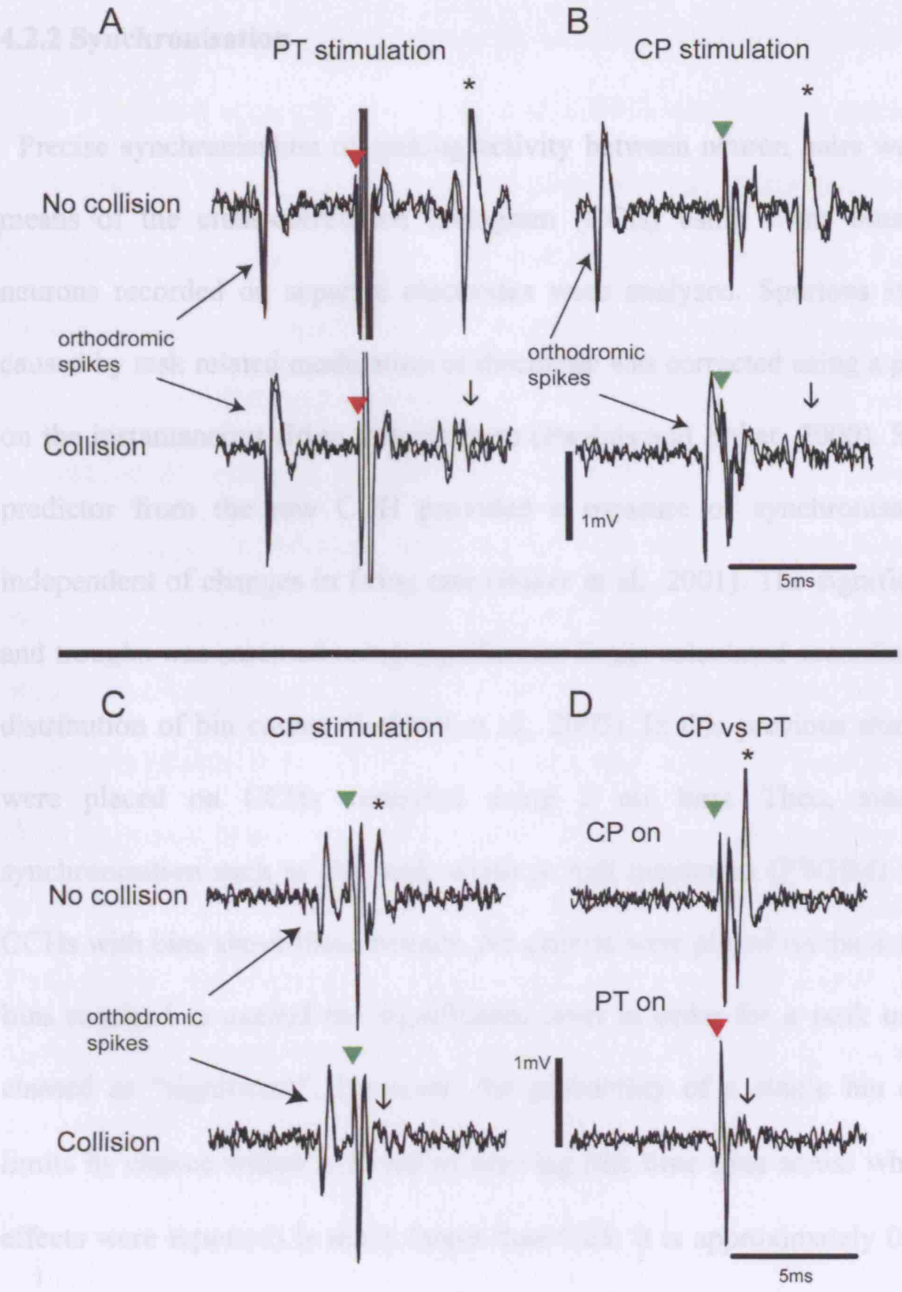

Figure 4.1 Identification of M1 neurons from stimulating electrodes in the pyramidal tract (PT) and cerebral peduncle (CP). **A**, collision of PTN antidromic response (*) by PT stimulation (red triangle). Collision occurred (↓) when stimulation was delivered at a shorter latency than the cell's antidromic latency. **B**, collision of same PTN by CP stimulation (green triangle). Antidromic spike occured at shorter latency than during PT stimulation. **C**, collision of CPN antidromic response by CP stimulation. **D**, CPN failed to respond to PT stimulation indicating that CPN axon did not run through the pyramidal tract. Different cell illustrated from that in C. 2 traces overlaid for each plot.

4.2.2 Synchronisation

Precise synchronisation of spiking activity between neuron pairs was assessed by means of the cross-correlation histogram (CCH) using 1 ms bins. Only single neurons recorded on separate electrodes were analysed. Spurious synchronisation caused by task related modulation of discharge was corrected using a predictor based on the instantaneous firing rate estimate (Pauluis and Baker, 2000). Subtracting the predictor from the raw CCH provided a measure of synchronisation that was independent of changes in firing rate (Baker et al., 2001). The significance of peaks and troughs was assessed using significance limits calculated according to a Poisson distribution of bin counts (Jackson et al., 2003). In this previous study, 95% limits were placed on CCHs compiled using 2 ms bins. Then, measurements of synchronisation such as the peak width at half maximum (PWHM) were made on CCHs with bins above these bounds. No criteria were placed on the actual number of bins required to exceed the significance level in order for a peak or trough to be classed as "significant". However, the probability of a single bin crossing these limits by chance within ± 10 ms of zero lag (the time span across which synchrony effects were reported) is much larger than 0.05: it is approximately 0.43, according to the binomial cumulative distribution function. Thus a peak or trough must comprise a total of three or more bins which all cross these 95% limits, for it to be classed as genuine.

For CCHs presented below, 99% limits were placed with a 1 ms bin width , thus requiring 2 or more bins above this limit for a peak or trough to be accepted as genuine. As described in *Results*, this dramatically lowered the number of significant correlations, making it difficult to determine the overall level of synchronisation

between the different types of neurons by measuring features from each correlogram. Thus a different approach to Jackson et al. (2003) was taken to assess synchrony at the population level. This involved compiling average cross-correlation histograms from the summed raw CCHs for each pair, regardless of whether that pair showed significant synchrony itself. The IFR predictor CCHs were also summed in the same way. Then, an IFR-corrected cross correlogram was computed on this data, by subtracting the summed predictor from the summed raw CCH. This resulted in a "grand average" correlogram across all the pairs within a group, which represented the mean percentage excess of observed bins above those expected, for the population. Averaging of cross correlograms across neuron pairs has been described previously (Baker et al., 2001). Adding together individual histograms in this way gave increased sample sizes from which to assess synchrony between cell types, rather than taking measurements of correlogram features from isolated examples. Furthermore, the summed histograms still comprised bin counts, permitting the application of poisson statistics to generate theoretical significance limits on the IFR corrected CCH at the 99% level, as outlined above.

4.3 Results

4.3.1 Dataset

A total of 93 cells from 2 monkeys (25 PTNs, 36 CPNs and 32 UIDs) were analysed. This total comprised 15 PTNs, 15 CPNs and 22 UIDs recorded over 9 sessions from M41, and 10 PTNs, 21 CPNs and 10 UIDs recorded over 14 sessions from M38.

4.3.2 Basic task relationship

Figure 4.2 shows the activity of three simultaneously recorded M1 neurons (PTN, CPN and UID) during the performance of a precision grip task. The task-relationship of the PTN and CPN was highly similar (Fig. 4.2 B, C), characterised by a phasic increase in discharge during the movement phases of the task, and a lower level of firing during the hold period (Bennett and Lemon, 1996; Baker et al., 2001). These two cells appeared to be related to activity in the flexor and extensor muscles during movement of the levers into the hold period and their release at the end of the trial, respectively. In contrast, the UID shown here shows tonic firing during the hold period as well as phasic activity at the end of the trial, and so its activity could be related to that of the long flexors required to produce pinch force (e.g. FDP and FDS). The discharge pattern of this latter cell resembles the phasic-tonic neurons described by Cheney and Fetz (1980). In fact, this was the most common response pattern for each type of cell (52% of all PTNs, 69% of all CPNs and 72% of all UIDs recorded in M38 and M41). Other response patterns such as the purely phasic type

shown in figure 4.2, purely tonic, and phasic-ramp patterns were also observed across the population, but these were much less numerous. This is in agreement with the findings of Cheney and Fetz (1980). Furthermore, no systematic differences in the proportions of cells with different response patterns were found between PTNs, CPNs and UIDs.

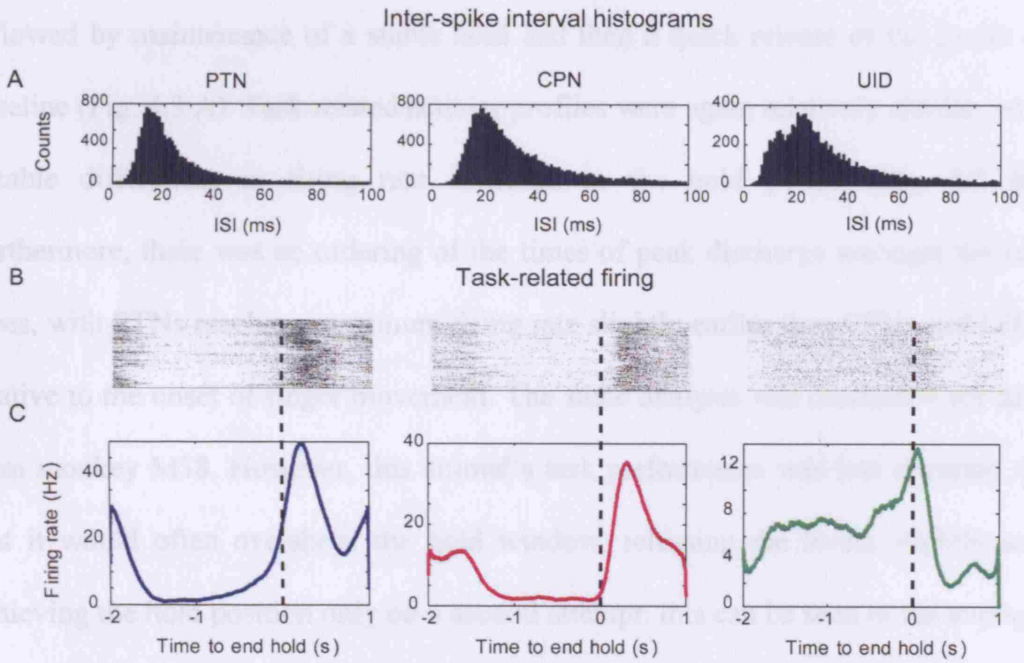

Figure 4.2. Task relationships of single units. A, Inter-spike interval histograms for three different cell types recorded in M1. **B**, Dot raster display of spiking activity for each cell over 200 trials of the task, for 2s before and 1s after the end hold marker. **C**, firing rate profiles for each cell calculated by averaging each respective raster display, smoothed with a 100ms moving average window. Abscissa for B and C show time relative to the end hold marker, which is superimposed as a dotted line in C.

4.3.3 Timing of discharge

Next, average firing rates were computed for a 3s time window aligned this time to the initial movement phase: specifically, the point of maximum finger lever velocity during movement into the hold at the start of the trial. Task performance in M41 was homogenous across sessions, characterised by a smooth ramp into the hold period followed by maintenance of a stable hold and then a quick release of the levers to baseline (Fig. 4.3 A). Task related activity profiles were again relatively similar, with notable differences in firing rate confined to the hold period (Fig. 4.3 B). Furthermore, there was an ordering of the times of peak discharge amongst the cell types, with PTNs reaching maximum firing rate slightly earlier than CPNs and UIDs relative to the onset of finger movement. The same analysis was conducted for data from monkey M38. However, this animal's task performance was less accurate, so that it would often overshoot the hold window, releasing the levers slightly and achieving the hold position only on a second attempt: this can be seen in the average finger position profiles (Fig. 4.3 C). Aligning data to the first movement period thus resulted in bimodal peaks in the average firing rate profiles for all three cell types, corresponding to the two periods of lever movement at the start of the trial (Fig. 4.3D). This made it difficult to establish a clear pattern in the timing of discharge relative to movement amongst the cells in order to corroborate the pattern that was observed in M41. A more thorough analysis was therefore conducted on a select group of cells from both animals that showed clear peaks in discharge.

A sample of 12 PTNs, 14 CPNs and 19 UIDs were selected from M41 which showed a peak in their average firing rates before movement onset at the start of the trial. For each cell the time of this peak was measured relative to the time of

maximum finger velocity, defining that cell's timing of discharge relative to finger movement onset.

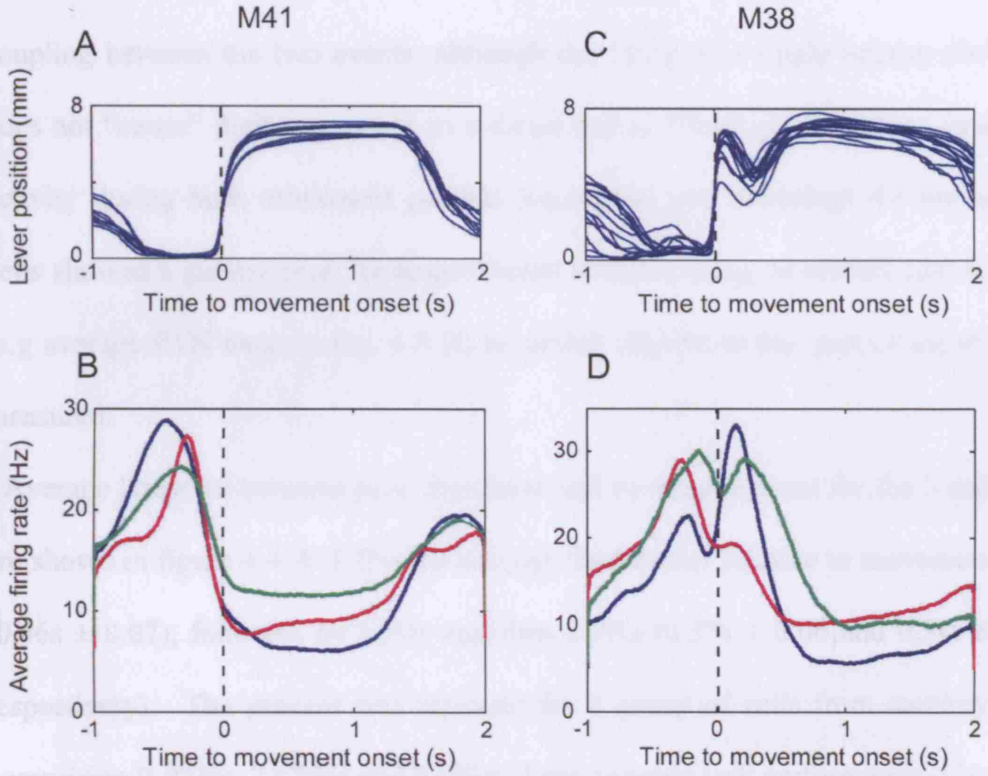

Figure 4.3. Alignment of discharge to movement onset. A, average finger position trace for M41 during 3 second window aligned to movement onset, indicated by dotted line. Each trace represents mean finger position over all trials recorded from each of 9 recording sessions analysed in this monkey. **B**, average task-related firing rates for all neurons recorded in M41, aligned to movement onset. **C**, **D**, equivalent analyses for M38. Note that consistent error in trial performance leads to bimodal average firing rate peaks.

The time of peak firing was chosen for latency measurements for two reasons. Firstly, it was not possible to measure the onset of firing above a particular baseline as the task was self paced, and did not have a specified rest period during which

background firing rate could be assessed. Secondly, M1 PTNs and UIDs are known to peak in activity during or slightly before digit movement in this type of task (Bennett and Lemon, 1996; Baker et al., 2001) so it is natural to assume a temporal coupling between the two events, although the firing of a single neuron obviously does not "cause" digit movement in a direct sense. While many neurons peaked in activity during both movement periods (squeezing and releasing) the majority of cells showed a greater peak for finger/thumb flexion during movement into the hold (e.g average PTN trace in Fig. 4.3 B) so timing relative to this part of the trial was measured.

Average latencies between peak discharge and movement onset for the 3 cell types are shown in figure 4.4 A: PTNs on average fired earlier relative to movement onset (0.46s ± 0.07), followed by UIDs and then CPNs (0.37s ± 0.06 and 0.34s ± 0.06, respectively). The process was repeated for a group of cells from monkey M38, comprising 9 PTNs, 7 CPNs and 7 UIDs. Less accurate task performance (Fig 4.3 C) again introduced greater trial-trial variability so the resulting average firing rate profiles were slightly noisier, and the two initial movement periods described above resulted in double peaks at the start of the analysis window for most cells. Therefore two latencies were measured for this subpopulation of cells, giving the time difference between the first and second peak in finger velocity at the trial start, and the first and second peak in cell discharge. Average latencies for the first peaks showed a similar trend as in monkey M41 with PTNs again firing earliest (Fig 4.4 B) suggesting a consistent trend in timing of activity for the different cell types. However, UID and CPN discharge timing was more similar in this data set. Furthermore, combining the data from M38 and M41, there were no significant differences between these mean latencies (comparisons by 1 tailed t tests, $P>0.05$),

indicating that there was much overlap in timing of discharge relative to movement onset among the groups.

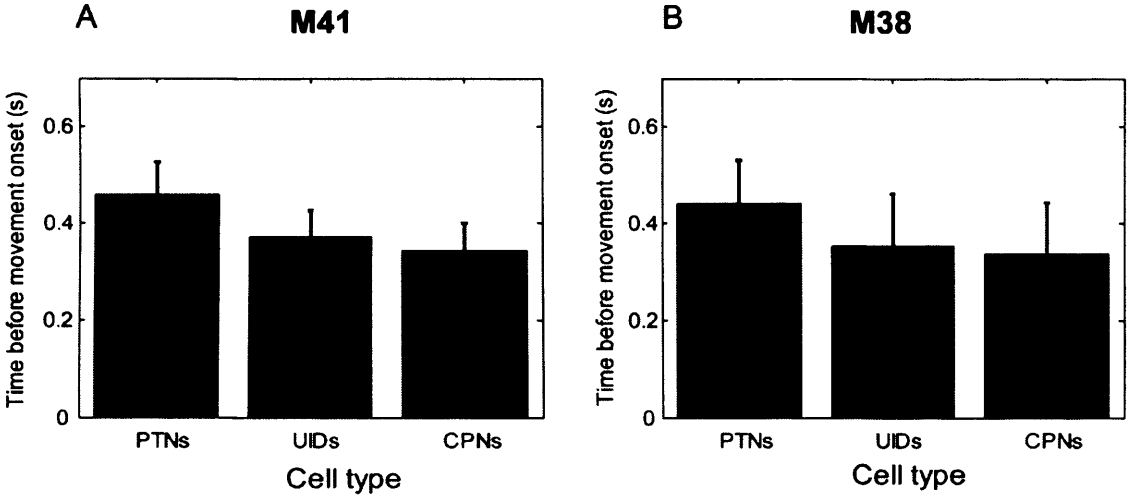

Figure 4.4. Timing of discharge relative to movement onset. A, average latency between peak discharge and onset of finger movement for sample of cells recorded from M41. **B**, average latencies for sample of cells from M38. Error bars indicate standard error.

4.3.4 Relationship to force

For recordings in monkey M41, the animal performed the precision grip task against three different compliant load conditions (see Chapter 2), allowing a comparison of force-related activity amongst PTNs, CPNs and UIDs. Figure 4.5 A illustrates scaling of activity level for average EMG traces from the forearm muscle FDP: at larger spring constants, this activity level is higher as more effort is required to squeeze the levers. Averaging activity in four 250 ms epochs aligned to the onset of finger movement (-250→ 0 ms, 0→250 ms, 250→500 ms and 500→750 ms,

movement onset defined as the point of maximum finger or thumb velocity during movement into the hold, whichever occurred earliest) highlights this relationship (Fig. 4.5 D). Note that scaling of EMG level begins before movement onset in the first epoch, consistent with prediction of load condition by the motor system.

Motor cortex neurons are known to scale their firing rates with force level in this type of task. This scaling was observed to an extent in the task related firing rate profiles for a PTN and CPN (Fig. 4.5 B,C) but again was more clear when activity was averaged across the four epochs (Fig. 4.5 E,F). In particular, each type of neuron demonstrated the same predictive behaviour seen in the EMG traces for the first epoch.

Force scaling was assessed for a total of 56 neurons. Of these, 17 cells were rejected due to firing rate drift across the recording session which contaminated force dependence, leaving 13 PTNs, 10 CPNs and 16 UIDs. For each cell, scaling of neuronal firing rates with spring constant was determined by averaging discharge over 4 behavioural epochs relative to movement onset. The rates for each epoch were then normalized (by dividing by the maximum) to allow comparisons across cells and task sequences. Many neurons showed inverse relationships so that their firing rates decreased with increasing force consistent with previous work (Maier et al., 1993). For example, the PTN illustrated in figure 4.5 E showed positive force scaling in the first epoch and negative scaling in the other three epochs.

Data from single cells were combined to give an average measure of force scaling. A regression line was fitted for each epoch and normalized firing rates for each spring force were obtained from this line (e.g. Fig 4.5 F). This gave the force-rate relationship for a single cell.

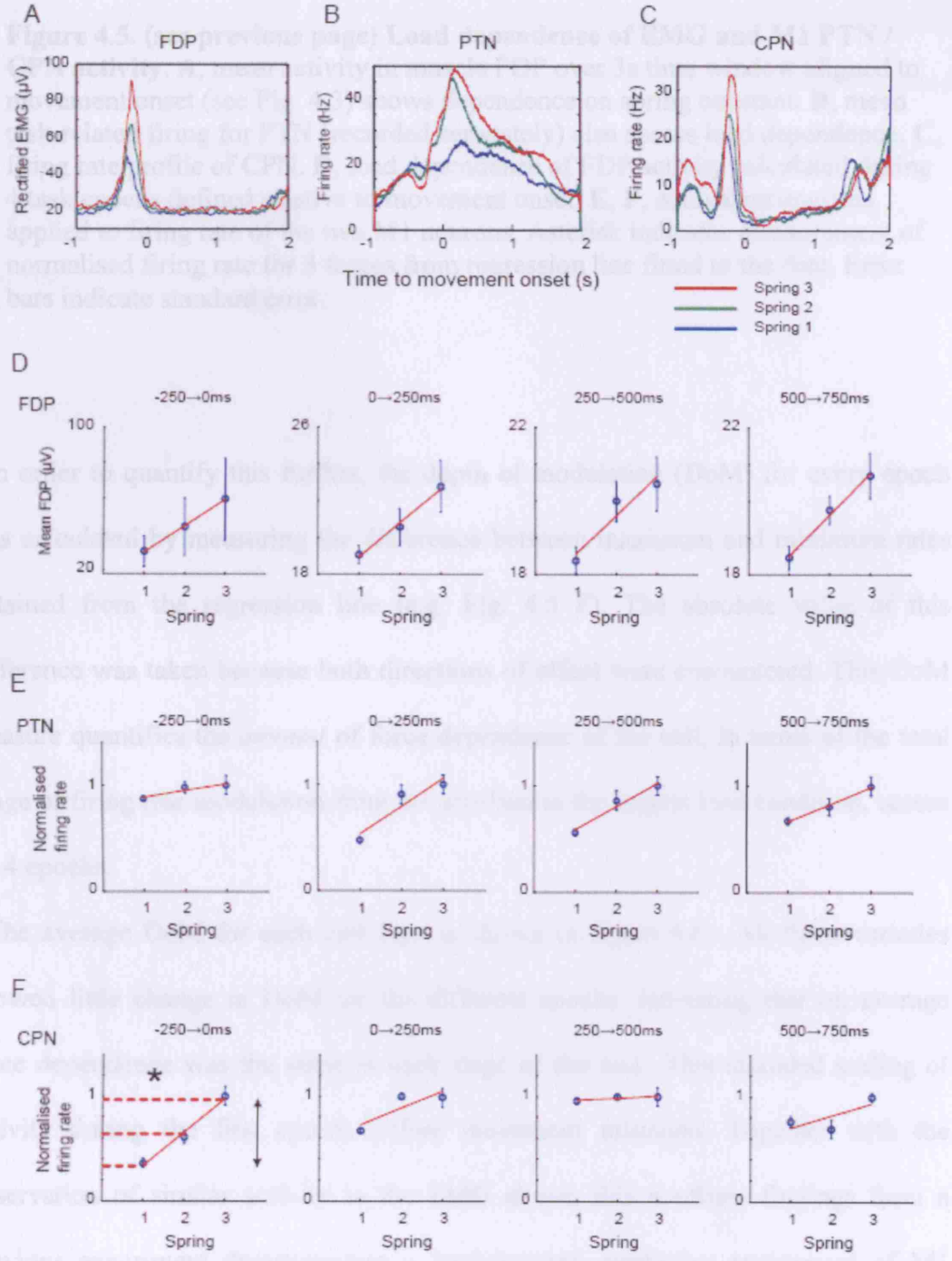
A
FDP
Rectified EMG (μV)
B
PTN
Firing rate (Hz)
C
CPN
Firing rate (Hz)
Time to movement onset (s)
Spring 3
Spring 2
Spring 1
D
FDP
-250→0ms
0→250ms
250→500ms
500→750ms
Mean FDP (μV)
Spring
E
PTN
Normalised firing rate
F
CPN
*

Figure 4.5. (see previous page) Load dependence of EMG and M1 PTN / CPN activity. **A**, mean activity in muscle FDP over 3s time window aligned to movement onset (see Fig. 4.3) shows dependence on spring constant. **B**, mean task-related firing for PTN (recorded separately) also shows load dependence. **C**, firing rate profile of CPN. **D**, load dependence of FDP activity calculated during 4 task epochs defined relative to movement onset. **E**, **F**, equivalent analysis applied to firing rate of the two M1 neurons. Asterisk indicates measurement of normalised firing rate for 3 forces from regression line fitted to the data. Error bars indicate standard error.

In order to quantify this further, the depth of modulation (DoM) for every epoch was calculated by measuring the difference between maximum and minimum rates obtained from the regression line (e.g. Fig. 4.5 F). The absolute value of this difference was taken because both directions of effect were encountered. This DoM measure quantifies the *amount* of force dependence of the cell, in terms of the total range of firing rate modulation from the smallest to the largest load condition, across all 4 epochs.

The average DoM for each cell type is shown in figure 4.6. All three varieties showed little change in DoM for the different epochs, indicating that on average force dependence was the same at each stage of the task. This included scaling of activity during the first epoch, before movement initiation. Together with the observation of similar activity in the EMG above, this confirms findings from a previous experiment demonstrating a feed-forward, predictive component of M1 discharge (Jackson, 2002).

PTNs on average showed a larger DoM compared to CPNs and UIDs. A two-way univariate ANOVA found no interaction between cell type and epoch, indicating that all three types of unit showed similar levels of modulation in firing rate across the four stages of the task. However, there was a main effect of cell type: post-hoc t tests

found that the average DoM for PTNs was significantly greater than both CPNs and UIDs [PTNs 0.3 ± 0.02; CPNs 0.2 ± 0.02; UIDs 0.2 ± 0.02; mean ± standard deviation] (1 tailed t-test, $P<0.05$). This suggests that PTNs tended to show a greater range of firing rate modulation for the different spring loads compared to the other two neuron types.

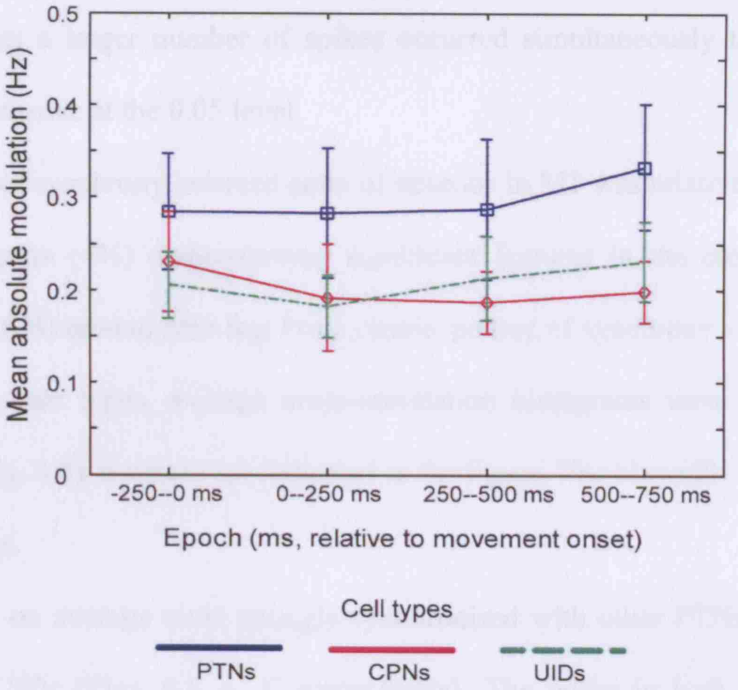

Figure 4.6. Spring force depth of modulation. Mean absolute depth of modulation (DoM) for PTNs, CPNs and UIDs as a function of task epoch. Mean DoM averaged across all four epochs was significantly higher for PTNs compared to CPNs ($P<0.05$). Error bars indicate standard error.

4.3.5 Synchrony

Synchronisation of neural discharge was assessed for a total of 158 pairs of simultaneously recorded neurons from M38 and M41. Fig 4.7 shows examples of cross correlation histograms (CCHs) between these pairs, calculated with a 1 ms bin width. For each pair an instantaneous firing rate (IFR) predictor was computed which gave a measure of the level of synchrony due to changes in firing rate alone (Baker et al 2001). Subtracting this from the raw CCH resulted in a third histogram showing the percentage excess of observed CCH counts above the predictor. In each case, two or more bins around zero lag rose above the 99% significance limits,

indicating that a larger number of spikes occurred simultaneously than would be expected by chance at the 0.05 level.

The extent of synchrony between pairs of neurons in M1 was relatively small, with only 6/158 pairs (4%) demonstrating significant features in the cross correlation histogram (CCH) around zero lag. For a clearer picture of synchrony values amongst the different pair types, average cross-correlation histograms were computed for each type (Fig. 4.8): n values are indicated in the figure. The binwidth of these CCHs was also 1 ms.

PTNs were on average most strongly synchronised with other PTNs, followed by PTNs with UIDs (Figs. 4.8 A, C respectively). The peaks in both these average histograms are comprised of two bins that exceed the significance limits, indicating statistically significant synchrony at the $P<0.05$ level; these are shaded in the figure. The strength of this synchrony was relatively weak: the largest bin gave a percentage excess of only 5% and 4% for A and C respectively, in part due to dilution of the contribution of pairs with strong effects by pairs showing no synchrony, during the averaging process. The single large bin rising above the significance limit near 0 ms, in the mean CCH between pairs of CPNs (Fig. 4.8B) might have been due to the inclusion in the average of an artefact – a rapid latency non-spike event recorded simultaneously on both electrodes. However, this peak was not present when the CCH was recompiled using smaller 0.5 ms bins, suggesting that it was in fact due to incorporation in the average of CPN-PTN pairs showing genuine synchrony, rather than an artefact. Yet across this sample of PTN-CPN pairs, synchrony was not statistically significant, in contrast to figures 4.8 A and C. Figures 4.8 D, E and F did not show clear peaks around zero lag that crossed the significance threshold.

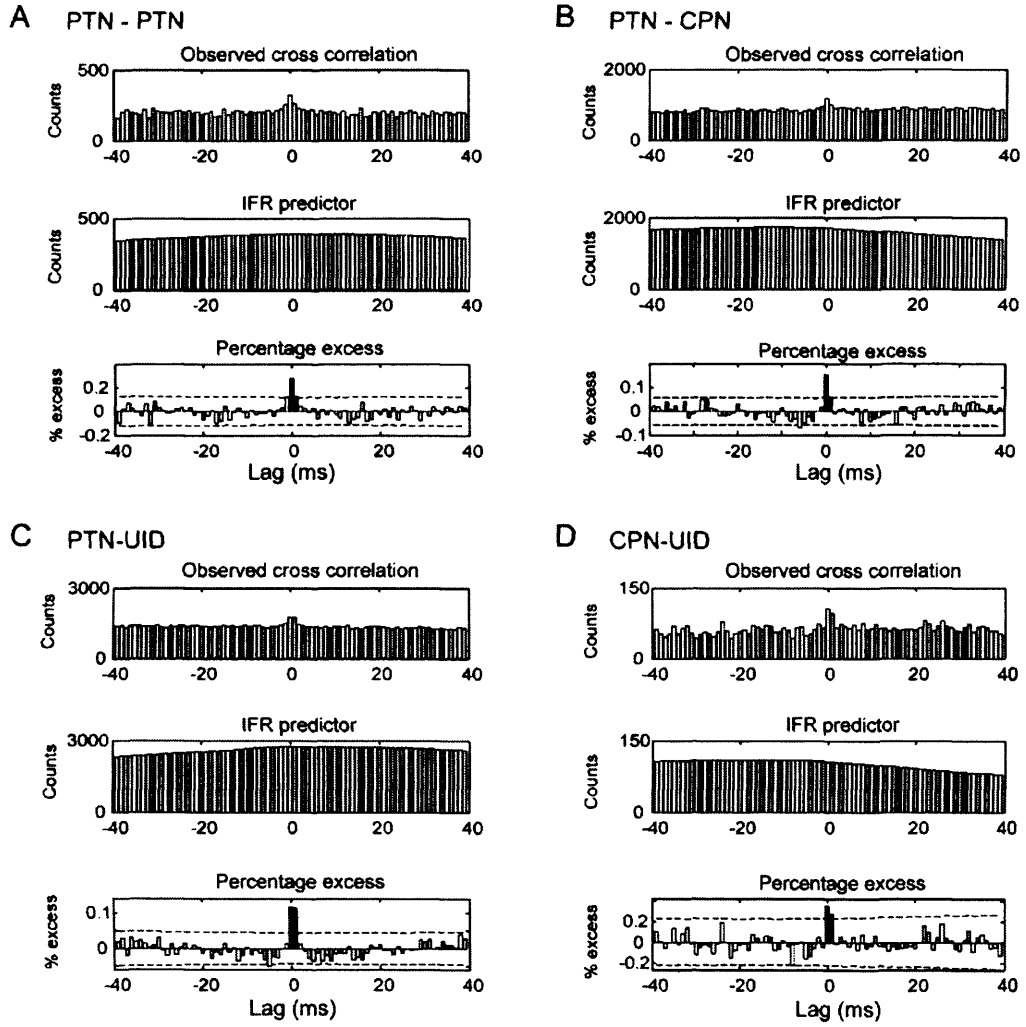

Figure 4.7. Cross correlations for pairs of different cell types. A, top panel: observed cross correlation histogram for a synchronous pair of PTNs. Middle panel: instantaneous firing rate predictor. Bottom panel: % excess of observed counts over expected. Dotted line indicates theoretical 99% significance limits based on the Poisson distribution. Pairs of bins crossing these limits are highlighted in black as they represent significant synchrony at $P<0.05$ level. PTN 1: 17552 spikes, PTN 2: 7760 spikes. **B**, equivalent analysis for a PTN-CPN pair. PTN: 52457 spikes, CPN: 16698 spikes. **C**, PTN: 52608 spikes, UID: 30028 spikes. **D**, CPN: 14553 spikes, UID: 6399 spikes.

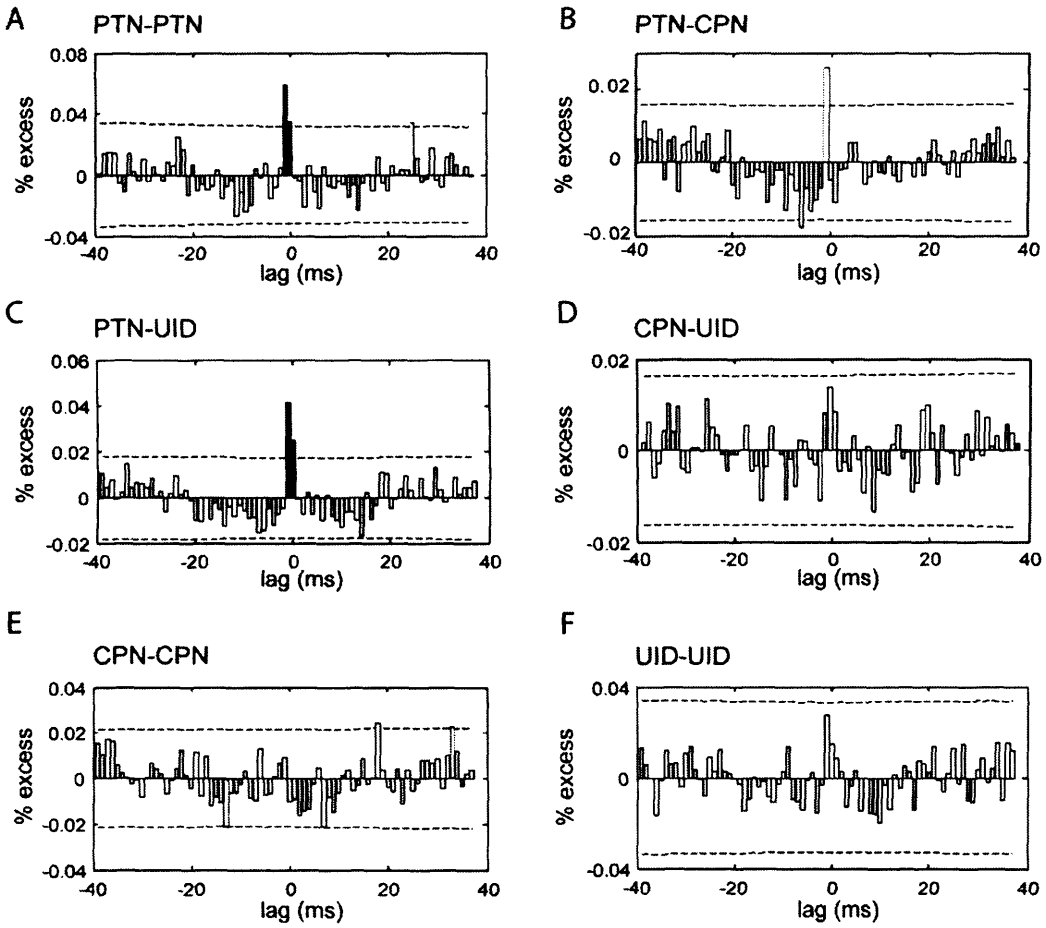

Figure 4.8. Average cross correlograms. Average cross correlation histograms for each pair type, calculated by summing together individual CCHs. Dotted lines indicate 99% significance limits. Pairs of bins crossing significance are highlighted in black. N values: **A**=12 pairs, **B**=31 pairs, **C**=28 pairs, **D**=33 pairs, **E**=19 pairs, **F**=15 pairs.

4.4 Discussion

4.4.1 Similar activity of different cell types

The results presented here show that M1 communicates relatively similar information in parallel through two output pathways to the spinal cord and other brain stem nuclei such as the pontine grey matter. Equivalent numbers of task related PTNs and CPNs were encountered during recording and their firing rate profiles were fundamentally alike. This basic similarity makes sense within the context of the extrinsic connectivity of M1. Both sets of cells project to the pontine nucleus forming part of an overall cortico-cerebellar loop (Allen and Tsukahara, 1974; Kelly and Strick, 2003). Neural activity at various points within this loop, such as areas of the motor thalamus, cerebellar cortex and deep cerebellar nuclei that connect to M1, is often similar (Thach, 1978; Jueptner et al., 1997; Middleton and Strick, 2000; Kurata, 2005). Thus it is perhaps not surprising that groups of neurons within M1, which form part of the same circuit, should show similar types of activity. This is in contrast to the discharge properties of M1 cortico-striatal neurons, which differ significantly from those of the spinal cord/brain stem output neurons studied here in that they exhibit low spontaneous rates, and their discharge is poorly correlated with parameters of movement such as force (Bauswein et al., 1989; Turner and DeLong, 2000).

Furthermore, all cells were recorded from the same "hand" area of M1. Neurons in regions of M1 representing the same digits have common synaptic inputs and are extensively and reciprocally interconnected by means of horizontal axon collaterals

(Porter et al., 1993). Being part of the same network means again that these cells are likely to show similar task-related patterns of activity.

However, it was still possible to expose some subtle differences in the response properties of PTNs and CPNs during task performance, indicating that within the context of M1- spinal and cerebellar connectivity, information output is somewhat modified according to its target destination. In addition, synchronisation among these different cell types was found to vary, suggesting that there are relative differences in the level of interaction between these output networks. These findings will now be discussed in more detail.

4.4.2 Order of timing of discharge

While hold-related activity was found to vary, the timing of cell discharge in relation to movement onset did not differ significantly among PTNs, CPNs and UIDs: these cells tended to become active at approximately the same time. Such overlap and variation in the relative timing of neuronal discharge has been observed for cells recorded in different cortical and subcortical motor structures e.g. within the M1-cerebellar loop (Thach, 1975, 1978). It suggests that neural activity in these areas occurs in parallel rather than proceeding in a simple serial fashion.

4.4.3 Scaling of neural activity with force

All three types of neurons in M1 showed a linear relationship of their activity to force level during precision grip, consistent with previous work in the motor cortex (Smith et al., 1975; Wannier et al., 1991; Maier et al., 1993; Hepp-Reymond et al., 1999). This relationship was the same across the four task epochs studied, and was

also seen in EMGs from intrinsic hand muscles. PTNs showed slightly but significantly stronger scaling of their activity compared to the other cell types, consistent with their influence on hand muscle motoneurons: a previous study of force-related activity found it to be more prevalent amongst corticomotoneuronal (CM) cells (Cheney and Fetz, 1980). The observation of similar activity in CPNs indicates that force-related information is conveyed from M1 through an output pathway other than the corticospinal tract, to reach a potentially wide range of targets. It is consistent with findings of force-dependent activity at multiple loci in the motor system such as the cerebellar cortex (Smith and Bourbonnais, 1981), premotor cortex (Werner et al., 1991), and basal ganglia (Pope et al., 2005).

The observation of scaling in the first epoch before movement initiation is suggestive of a predictive, feed-forward signal in the motor cortex which has been observed before under the same task conditions (Jackson, 2002). As all three types of neuron exhibited this predictive behaviour, it indicates that it might not be generated by specific local circuitry within M1 but is a common feature of movement coding throughout this area of cortex. This in turn suggests that external input to M1 might have an influence: a suitable candidate would be the cerebellum since this structure is strongly implicated in the feed-forward control of movements (Wolpert et al., 1998).

4.4.4 Functional significance of task-relationships

Feed-forward control by the cerebellum uses efference copy of the command to move. In the case of hand movements this signal would be transmitted through

collaterals of corticospinal axons that terminate in the pontine nucleus. The observation of similar task-related activity in CPNs is significant as it implies that similar movement related information reaches the cerebellum through an alternative corticopontine pathway. But as this information is not an exact copy of the corticospinal output, it suggests that it may have a different function for cerebellar processing. It could, for example, be used to calibrate or modify feed-forward predictions based on the efference copy signal.

However, the functional significance of these similarities and differences must be interpreted in terms of the influence of PTNs and CPNs on neurons further "downstream". For example, there is evidence for a segregation of input connectivity in the pontine nuclei. Corticospinal inputs terminate mainly distally on the dendrites of pontine neurons, whereas other inputs (such as those from CPNs) synapse more proximally (Mihailoff and McArdle, 1981). Thus signals transmitted from M1 might be modified somewhat in the pontine nucleus before reaching the cerebellar cortex.

It should be noted that in some of the comparisons made in this chapter, CPNs seemed more similar to UIDs than PTNs (e.g. Fig. 4.6). It is possible that a proportion of unidentified cells were in fact CPNs. As the cerebral peduncle is a much more massive structure compared to the pyramid, it is harder to activate the same number of fibres through stimulation, so the probability of a failed identification is higher compared to PTNs which can also be activated at the pyramid. If a CPN fails to be activated from peduncular stimulation, the only alternative is to class it as a UID. Thus one might expect a larger proportion of the unidentified population to be real CPNs as opposed to PTNs, and the task relationships of CPNs and UIDs would consequently be more similar. However, more emphasis has been placed on the functional consequences of differences

between CPNs and PTNs, as these groups represent two separate sources of M1 corticofugal output.

4.4.5 Weak synchrony between pairs of neurons

Individual examples of significant synchrony were observed between all pair types except for CPN-CPN and UID-UID. Since cross correlations were corrected for task-dependent modulations in synchrony, this suggests that significant features in these CCHs were due to genuine synaptic connectivity between cells. The observation of a significant peak around zero lag between a PTN and a CPN is of particular importance, as it indicates that these neurons may have reciprocal excitatory connections or a common excitatory input (Kirkwood, 1979), rather than remaining completely segregated according to their output pathways.

While synchrony defined quantitatively was relatively weak in extent (only 4% of pairs showed significant features) it should be noted that some CCHs had convincing central peaks as judged by eye, but these did not comprise the minimum two bins above the 99% limits, so were strictly "unsynchronised". Thus the high significance threshold by which effects were assessed here may have underestimated the overall extent of synchronisation between single units in M1. Thus to extract a clearer measurement of synchrony, average cross correlograms were constructed for each of the possible pair types.

When cross correlograms between PTN-PTNs and between PTN-UIDs were averaged across pairs, they showed clear synchrony on average that was significant at the $P<0.05$ level (Fig. 4.8 A,C). All the other pairs including PTN-CPNs did not

contain significant peaks or troughs. Focussing on the PTN-CPN pairs, the lack of significant features in the average correlogram does *not* mean that these types of cells do not interact in M1. The observation of significant synchrony between a single pair (Fig. 4.7 B) shows otherwise. It also cannot represent cancellation of single correlograms containing peaks and troughs, as no convincing examples of negative synchrony were observed in the individual pairs. Instead, the average CCH in figure 4.8 B indicates that amongst the sample of neurons analysed, synchrony was present between PTNs and CPNs – hence there was a peak around zero lag – but it was weaker than synchrony between other pairs, and so failed to reach significance. In turn, this could be interpreted as evidence for relative but not total segregation of these two output pathways within the motor cortex.

The average correlograms for UID pairs and CPN-UID pairs also indicate weaker synchrony on average between these neurons. However, to the eye these CCHs seem to contain central peaks, which remained below the significance threshold – suggesting that synchrony was present between these neurons but remained obscured by noise even after averaging. Given a larger sample of neuron pairs and longer spike trains used to compile the cross correlations, a more widespread level of interaction might be observed. However, the average strength of this synchronisation would be expected to be quite weak as observed in Fig 4.8 A,C and in a previous study (Baker et al., 2001).

4.5 Chapter summary

The results presented in this chapter demonstrate that there are parallel output pathways from M1 conveying similar but also subtly different information about movement to the spinal cord and cerebellum. Interactions between these pathways have been studied within the cortex. The next chapter will address in more detail the communication between M1 and cerebellum by utilising recordings made from the two structures simultaneously.

Chapter 5: Interactions between M1 and cerebellum

I – Functional Connectivity

5.1 Introduction

In the previous chapter the routes of efferent connectivity from primary motor cortex to cerebellum were described in some detail. Likewise, in order for the cerebellum to cooperate closely with M1 during movement control, it requires a pathway by which it can output information to the motor cortex and modify the processing of motor commands. The most direct path by which cerebellum can influence M1 is a disynaptic, excitatory pathway from the deep cerebellar nuclei via the ventrolateral thalamus, which has been demonstrated anatomically and electrophysiologically in cat and monkey (Steriade, 1995; Na et al., 1997; Jorntell and Ekerot, 1999; Holdefer et al., 2000). The existence of bi-directional connectivity has led to theories of "cerebro-cerebellar loops", whereby movement-related processing is fulfilled by reciprocal connections between M1 and cerebellum (Allen and Tsukahara, 1974) and this has recently been confirmed for M1-cerebellar cortex by transneuronal viral tracing methods (Kelly and Strick, 2003).

To prove that these loops are used during motor control, their activation needs to be observed in an awake animal as it performs movements, as this represents a physiologically relevant state where multi-synaptic pathways are operating near or above threshold (Holdefer et al., 2000). In other words, the connectivity must be shown to be "functional" in nature. This can be accomplished first of all by focal microstimulation, in one area coupled with simultaneous recording of neuronal

discharge in the other. Deep cerebellar nuclei (dentate and interpositus) – M1 connectivity has already been studied this way during a reaching and button-pushing task (Holdefer et al., 2000). The first aim of the experiments in this chapter was to confirm these microstimulation findings, and extend them by recording dentate neurons while stimulating in M1.

A disadvantage of this technique, however, is that it does not accurately represent the underlying task-dependent activation of these pathways and structures. A more intuitive approach is to study the correlation of single unit discharge in M1 with that in the cerebellum. Yet, in line with the work of Holdefer et al., simultaneous recordings from three monkeys in this laboratory have consistently failed to observe significant single unit cross correlations between M1 and cerebellar neurons, suggesting that this interconnectivity is either very weak or highly specific, or both. A way around this problem is to cross-correlate single unit discharge in one area with local field potentials (LFPs) recorded simultaneously in the other, by means of spike triggered averaging. This technique has been widely applied to demonstrate connectivity of single cells with populations of neurons at remote locations in the CNS (Porter et al., 1993), see also Chapter 3. Since it utilises the spontaneous discharge of these neurons, this approach allows an analysis of whether and how inter-area coupling is modified during task performance, which in turn would provide evidence for movement related cerebro-cerebellar communication. Thus the second part of this chapter presents findings from spike triggered averaging of M1 LFP from single dentate neurons, and of dentate LFP from single M1 neurons, and investigates whether these averages show any clear relationship to a parameter of the precision grip task, namely the force upon a compliant, spring-like load.

5.2 Methods

Paired recordings and stimulus triggered averages were made from sites within contralateral M1 and ipsilateral dentate nucleus of two monkeys (M38 and M41) trained to perform a precision grip task with the right hand. For focal microstimulation, biphasic current pulses (width 0.2 ms, amplitude ~25μA) were delivered continuously at 10 Hz for around 3 minutes (i.e. ~1800 stimuli), through recording electrodes inserted into M1 or dentate. At the same time, action potentials of single units in the other area were recorded and the times of these spikes were discriminated as described in Chapter 2. Offline, the characteristic waveform of the stimulus artefact was readily distinguished from recorded action potentials by the principle component analysis. However, facilitation of unit discharge was confirmed by examining the raw spike file (see below).

5.3 Results

5.3.1 Stimulus-triggered effects

Post-stimulus time histograms (PSTHs) were compiled for the discharge of M1 units during focal dentate stimulation and dentate units during focal M1 stimulation, with a 1 ms binwidth, for the period 20 ms before and 20 ms after stimulation. Facilitation of unit activity was classed as significant if 2 or more contiguous bins post-stimulus crossed the 99% significance limit calculated from the mean bin height pre-stimulus. The probability of 2 bins exceeding these limits is given by the binomial cumulative distribution function as less than 0.05, as described in chapter 4. Using these criteria, the number of significant unit facilitation effects observed was small. For monkey M38 and M41, out of 58 and 73 dentate stimulations respectively, only 2 significant M1 activations were observed, both in monkey M38 (Fig. 5.1). Likewise, for 24 and 17 M1 stimulations in M38 and M41, only one significant dentate unit activation was found in both monkeys.

Figure 5.1 A illustrates significant facilitation of an unidentified M1 unit during dentate stimulation. The effect of stimulation is weak, with a small peak comprising two bins which just exceeded 99% significance, indicating an increased likelihood of unit discharge –i.e. excitation – at a latency of approximately 6-9 ms. Facilitation of this unit was confirmed by superimposing 100 sweeps from the raw spike recording made during stimulation, aligned to the peak in the PSTH (Fig. 5.1 B). Spontaneously occurring spikes appeared to cluster around the same latency after the stimulus artefact as the histogram peaks. The waveforms of the discriminated spikes (see Chapter 2), whose times were used to compile the PSTH, matched those of the

spikes in the superimposed traces, confirming that the PSTH peak resulted from activation of this discriminated unit by CN stimulation (Fig. 5.1 C,D). Another M1 unit was activated at a shorter latency of 2-3 ms (Fig. 5.2). Superimposition of raw spike recording sweeps confirmed that these significant bins were not simply a result of discriminating the stimulus artefact (Fig. 5.2 B,C).

Figure 5.3 shows activation of dentate units during M1 stimulation. Multiple units recorded on the same electrode in M38 showed increased discharge at approximately 10 ms latency (Fig. 5.3 A), whereas some units recorded from M41 showed facilitation at a shorter latency of around 2-4 ms (Fig. 5.3 B). Again, for the latter PSTH the spike waveforms corresponding to the histogram peaks were close to, but distinct from the stimulus artefact (Fig. 5.3 C).

Finally, no stimulus-related suppression of either M1 or dentate unit activity was observed in the current data set.

The demonstration of increased discharge of single M1 units during focal stimulation in the dentate nucleus with a latency between 2-10 ms, and of increased dentate unit discharge through M1 stimulation confirms findings from a previous study (Holdefer and Miller, 2000) and and is consistent with evidence that these two structures are reciprocally connected by excitatory pathways. However, these effects were rarely observed.

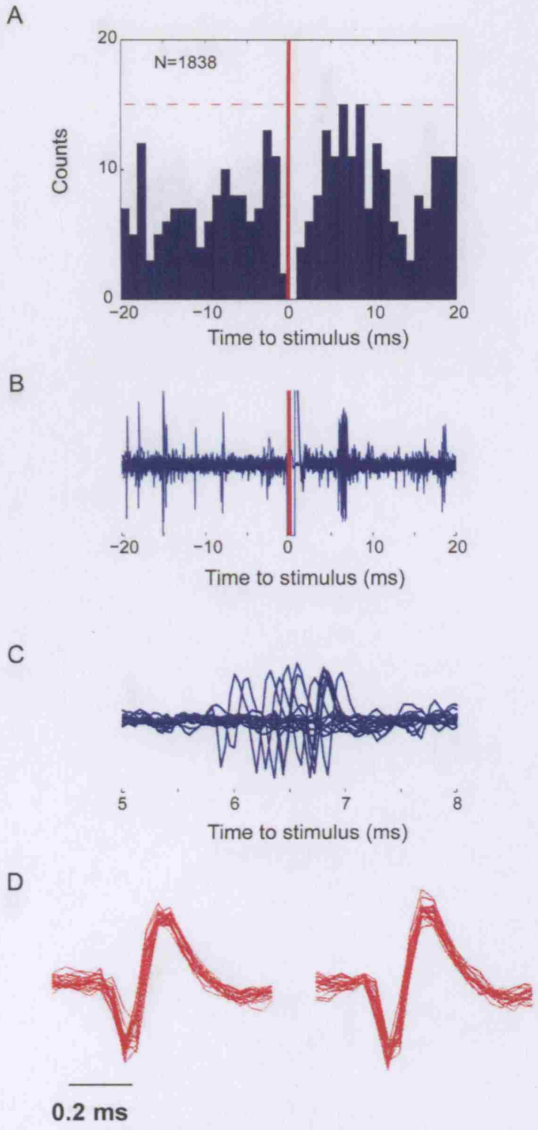

Figure 5.1. Stimulus triggered average of M1 unit, 1. A, PSTH showing short latency (6-9ms) facilitation of an unidentified M1 neuron during focal stimulation in dentate nucleus, for 1838 stimuli. Dashed line indicates 99% significance limit based on mean bin count before stimulation, vertical red line indicates time of stimulation. **B**, superimposition of 100 traces from raw spike recording, aligned to time of spike counts comprising peak in the PSTH. Spiking was observed at approx 6ms post stimulus. **C**, time expansion showing waveform of spikes in B. **D**, waveform of spikes discriminated offline (20 superimposed traces from beginning and end of spike file) to compile PSTH matches waveform of stimulus triggered spikes in B, indicating that peak in PSTH was due to facilitation of this discriminated unit.

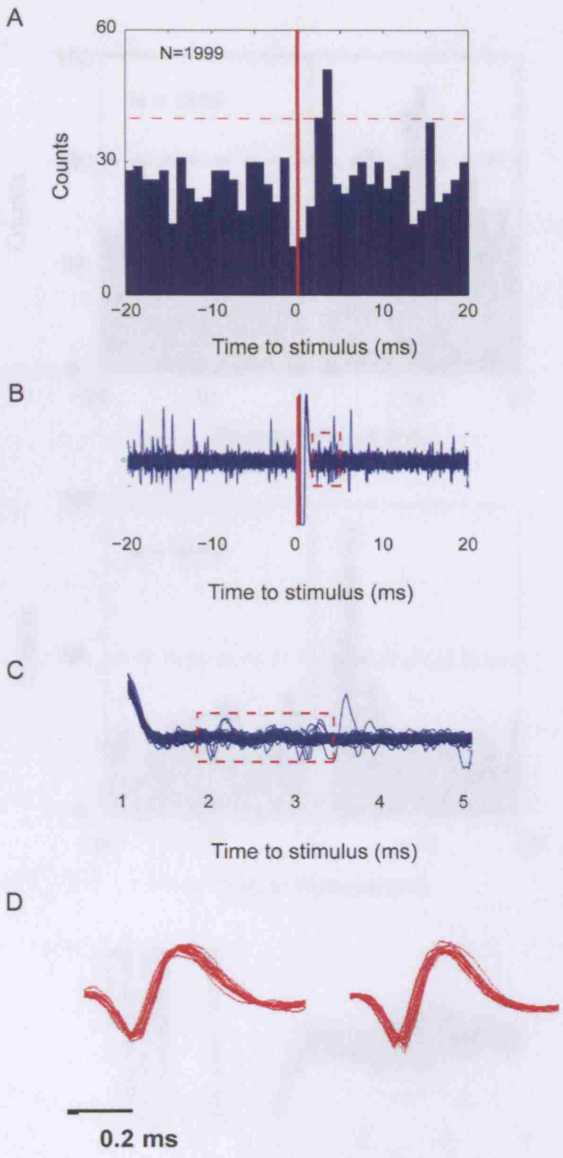

Figure 5.2. Stimulus triggered average of M1 unit, 2. A, short latency (2-4ms) facilitation of unidentified M1 unit during dentate stimulation, for 1999 stimuli. Same conventions as for fig 1. **B**, dashed red box indicates presence of small spikes in raw recording at time of PSTH peak (100 superimposed sweeps). **C**, time expansion indicates that spikes were separate from stimulus artefact. **D**, waveform of discriminated spikes used to compile PSTH matches spikes in C.

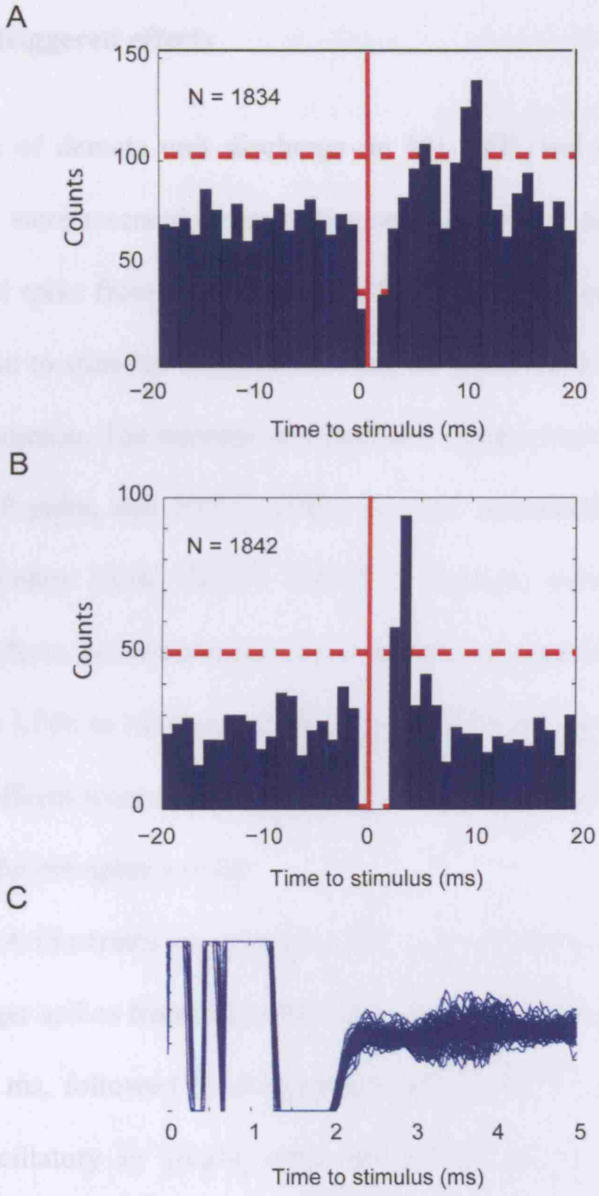

Figure 5.3. Stimulus triggered average of dentate units. A, facilitation of multiple dentate units at ~10ms during stimulation in M1, 1834 stimuli. **B,** facilitation of multiple dentate units at 2-4ms, 1842 stimuli. **C,** 100 sweeps of raw spike recording aligned to PSTH peak indicate multiunit activity distinct from stimulus artefact.

5.3.2 Spike-triggered effects

The effects of dentate unit discharge on M1 LFP, and of M1 unit discharge on dentate LFP, were assessed by averaging sections of LFP aligned to the time of each discriminated spike from a single neuron, for 100 ms pre-spike to 100 ms post-spike. In comparison to stimulus-triggered effects, the occurrence of spike-triggered effects was more common. The number of significant effects was 82/161 (51%) for dentate unit–M1 LFP pairs, and 70/515 (14%) for M1 unit-dentate LFP pairs in monkey M41. In monkey M38, 38/103 (46%) of dentate unit-M1 LFP pairs showed significant effects. M1unit-dentate LFP SpTAs were not compiled for this monkey, since dentate LFPs in M38 were unfortunately contaminated with mechanical noise. Significant effects were assessed using 99% significance limits based on the mean LFP during the pre-spike period.

Figure 5.4 A illustrates an example of M1 LFP from monkey M41 averaged using 168,968 trigger spikes from a dentate unit. A significant positivity preceded the spike by about 10 ms, followed by a significant negativity 10 ms post-spike. The effect was also oscillatory in nature, with two further significant positivities after the central peak each separated by approximately 45 ms, corresponding to a frequency of 22 Hz.

Four separate averages were compiled, each from a quarter of the available trigger spikes. In each of these quarters, the central peak-trough at time = 0 could still be discerned, indicating that the overall effect was not due to contamination by artefacts in a small number of sweeps.

Another oscillatory spike triggered average (hereafter referred to as SpTA) was observed in a separate dentate unit –M1 LFP pair (Fig. 5.4 B). A clear negativity was

evident at time 0, with oscillatory sidelobes before and after the spike. This activity did not exceed 99% significance. However, the significance of strong oscillatory effects present in time series such as fig 4B can also be assessed through analysis in the frequency domain, which is the focus of the following chapter.

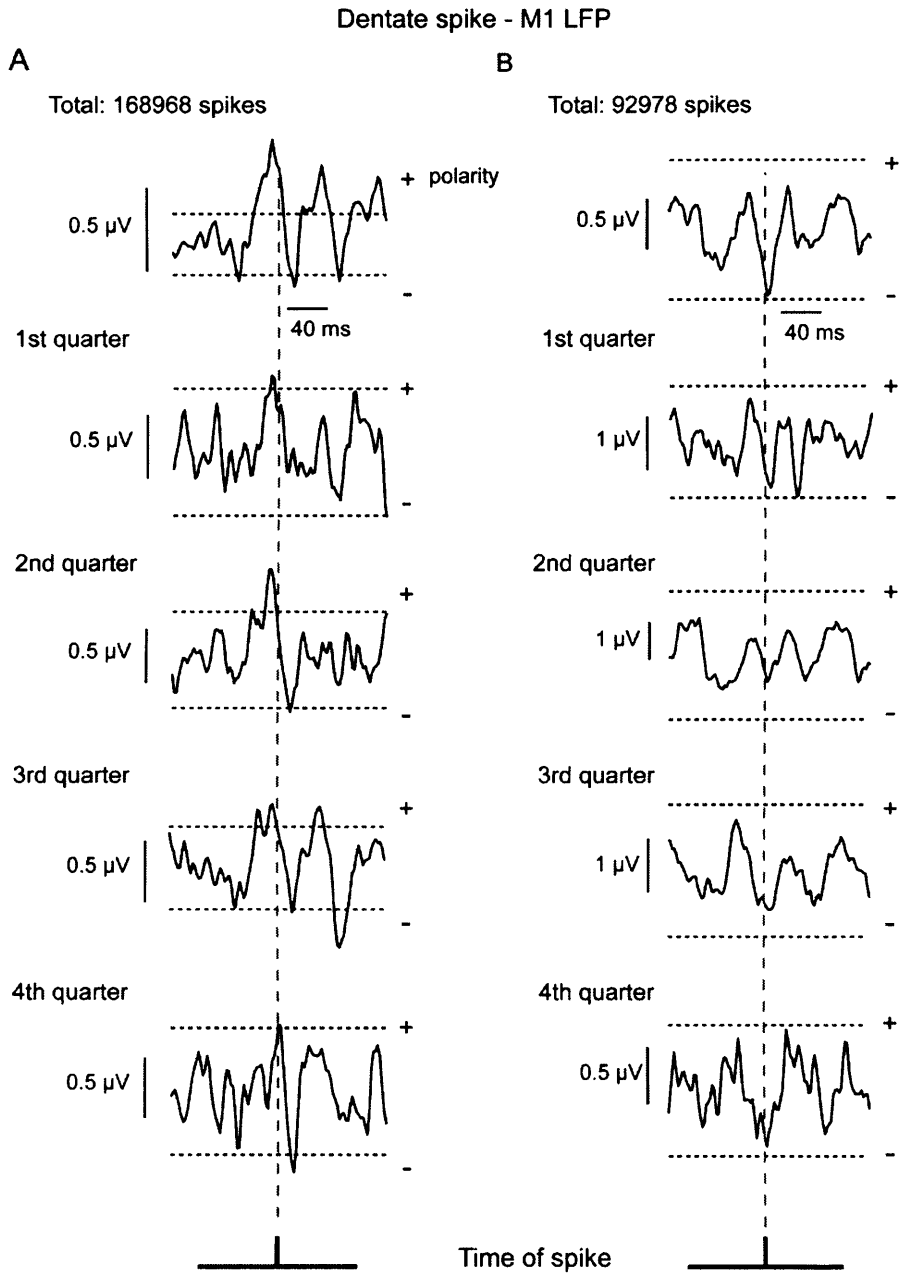

Figure 5.4. Spike triggered averaging of M1 LFP. A, post-spike effect in spike triggered average of M1 LFP from dentate neuron. Horizontal dashed lines indicate 99% significance calculated from pre-spike period. To assess the reliability of this affect, averages were compiled separately from each quarter of the trigger spikes. **B**, effect in M1 LFP for a separate LFP-spike pair.

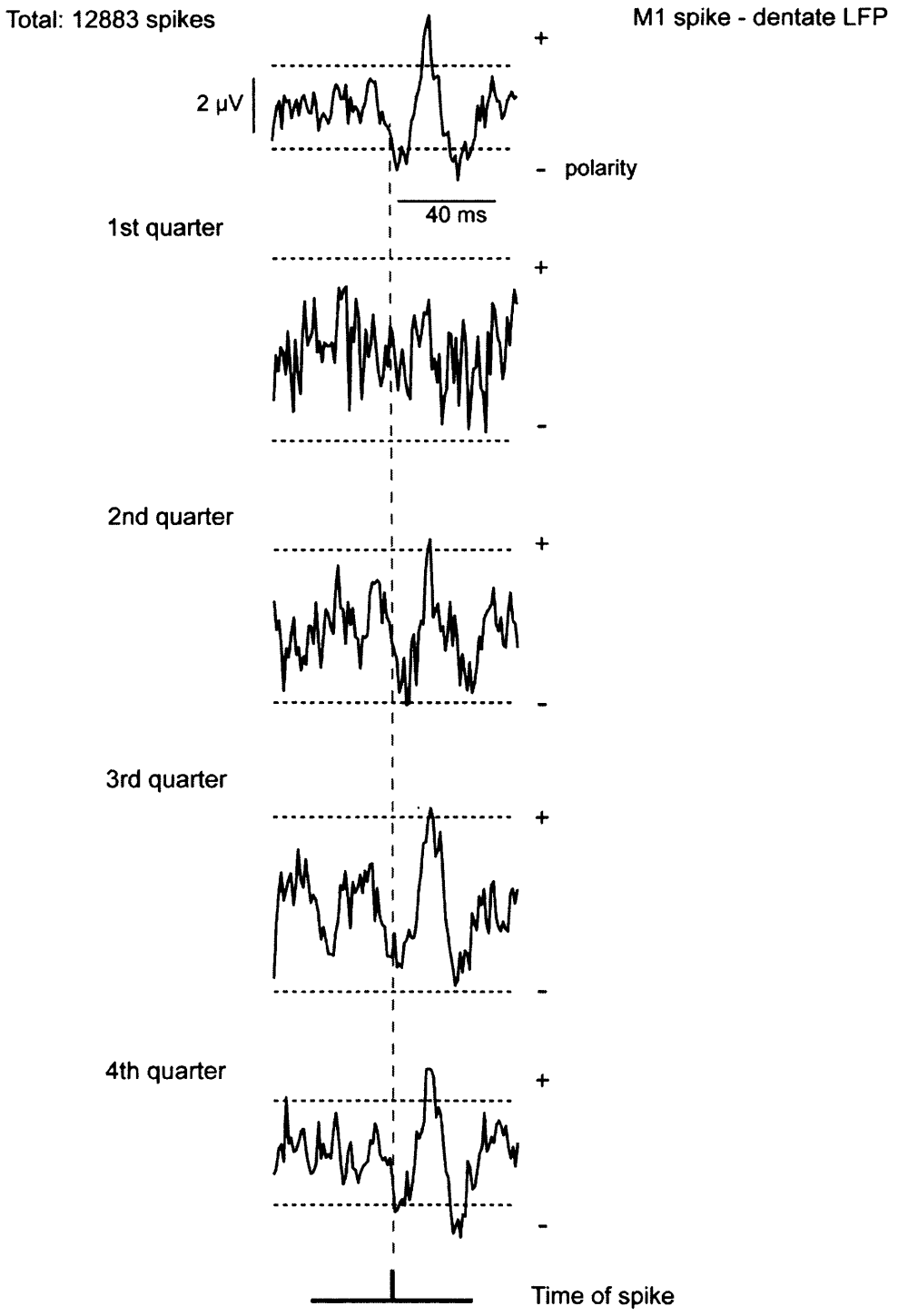

Figure 5.5. Spike triggered averaging of dentate LFP. Post-spike effect in spike triggered average of dentate LFP from M1 unit. Conventions same as for Fig. 5.4.

The observation of significant negativity in M1 LFP after averaging from dentate unit activity is also consistent with Holdefer et al. (2000). In addition, their findings were extended in the present experiment through the demonstration of significant effects on dentate nucleus LFP averaged from single M1 units (Fig. 5.5). A significant positivity was evident in the trace at approximately 15 ms post-spike, a similar latency to the effects described above.

5.3.3 Population data

Since similar effects were observed at multiple sites across recording sessions, an attempt was made to combine these SpTAs in order to describe the average influence of spiking activity in one area on LFP activity in the other.

Further, to assess the extent to which these interactions were "functional", reflecting task-related communication between the two structures, averages were compiled separately for each of the four spring forces which the monkey worked against (three forces for monkey M41). However, as individual SpTAs could be quite noisy (e.g. Fig. 5.5) these population averages were noisy, and there seemed to be no apparent relationship between SpTA amplitude and force (frequency effects are analysed in the next chapter).

As illustrated in figures 5.4B, averaging LFP from all the cell's spikes could sometimes lead to weaker effects than compiling averages from smaller numbers of spikes. It is possible that the temporal coupling of cell spiking to LFP revealed by spike triggered averaging was to some extent masked or reduced, by incorporating in the SpTA large numbers of spikes with little or no relationship to the LFP. Similar

effects are seen when compiling SpTAs of hand muscle EMGs using CM cell spikes: only a small proportion of the cell's spikes are exactly time-locked to motoneuron discharge, and the influence of spiking on the EMG (or LFP) signal is probabilistic in nature. Thus to examine these LFP SpTAs more clearly, averages were compiled using selected spikes, chosen according to the amplitude of the LFP signal during a short time window around the spike (peak-trough amplitude from 4 ms pre-spike to 7 ms post spike). The top 25% of the cell's spikes that 'produced' the largest effects were then used to average the LFP as described above.

An example average for a dentate unit – M1 LFP pair is shown in figure 5.6 A. This was the same pair as the SpTA in figure 5.4 B, and demonstrates the result of the spike selection process on the SpTA. Most striking is its oscillatory nature, which was already quite clear in the standard average; after sorting, prominent side-lobes could be seen which corresponded to ~20 Hz LFP oscillations. Interestingly, the phase of these oscillations relative to the spike appeared to shift in the clean compared to the standard SpTA. In addition, a large pre-spike positivity and post-spike negativity were evident, consistent with previous SpTAs of M1 LFP from nuclear units(Holdefer et al., 2000). Note also the large amplitude (peak to peak ~ 60μV), presumably due to selecting and averaging sweeps with large amplitude effects. As with the standard SpTAs, non-oscillatory averages were also observed, i.e the selection process favoured spikes producing large amplitude biphasic peaks, and some of these were also associated with 15-30 Hz oscillations. Not all of these averages were oscillatory (Fig. 5.6B). Similar effects were found for dentate LFP – M1 unit spiking (Fig 5.6 C,D).

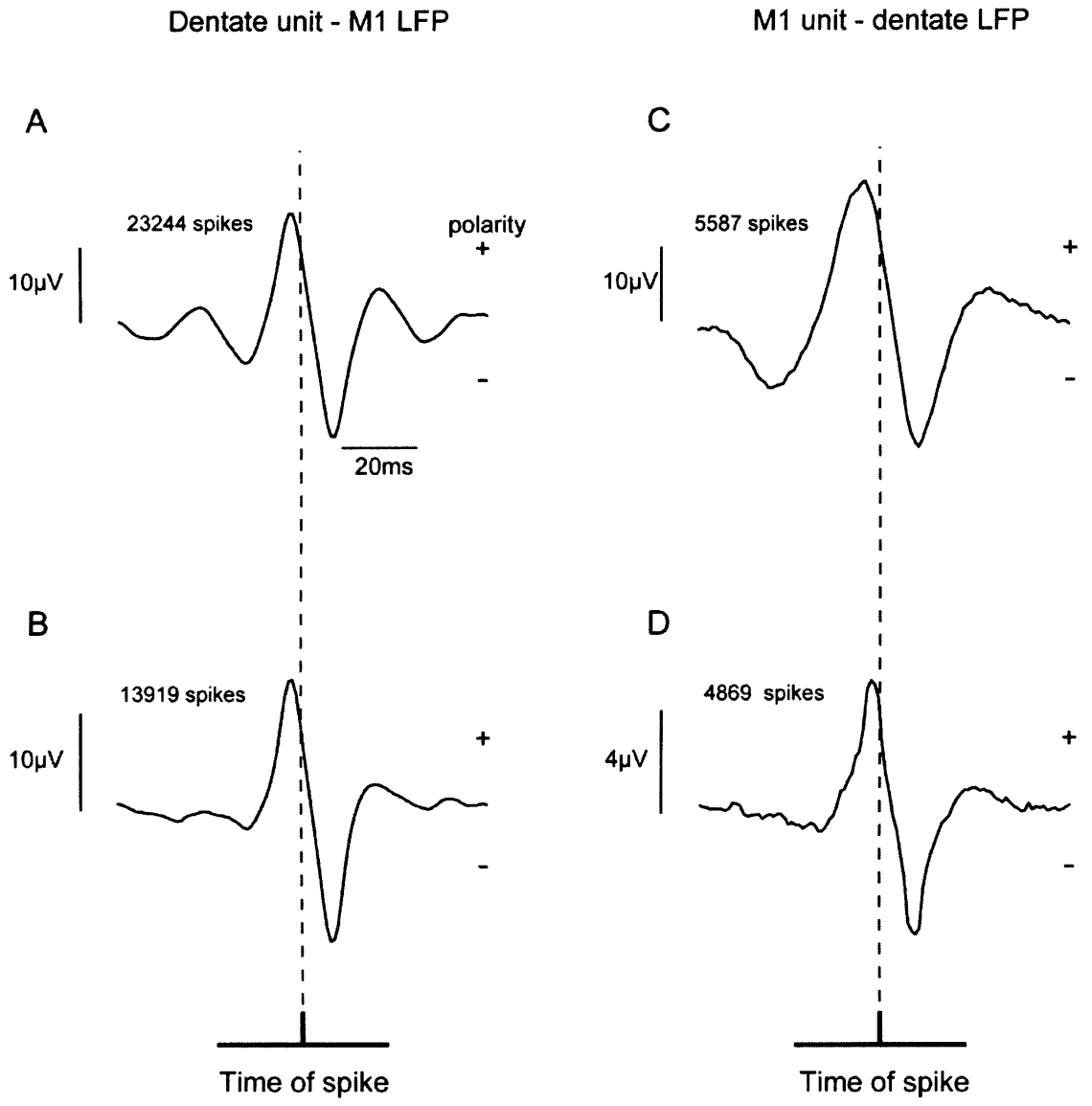

Figure 5.6. "Clean" spike triggered averages. **A**, oscillatory spike triggered average of M1 LFP from M41 calculated by sorting spikes according to amplitude of post spike effect. Each trace represents average compiled from top 25% of total spikes. **B**, non-oscillatory spike triggered average of M1 LFP from dentate unit spikes in M38. **C, D** oscillatory and non-oscillatory averages of dentate LFP from M1 spikes (M41).

These "clean" SpTAs were averaged across pairs, separately for dentate unit – M1 LFP and M1 unit – dentate LFP. Figure 5.7 A shows the average SpTA for 161 dentate unit – M1 LFP pairs from monkey M41: like the single SpTA, this combined SpTA contained pronounced ~20 Hz oscillations. The dashed lines represent ± 1 standard deviation of the mean and indicate that there was little variance in the shape of these effects across pairs. Thus in this monkey, a significant proportion of dentate spiking appeared to be strongly coupled to 15-30 Hz rhythms in M1 LFP. In contrast, the same average for monkey M38 showed a clear central biphasic peak but only very small oscillatory side lobes suggesting that across pairs, oscillatory spike-LFP coupling was observed less frequently (Fig. 5.7 B). An average SpTA for 440 M1 unit –dentate LFP pairs was also compiled (Fig. 5.7 C): this also comprised a biphasic peak although its shape was different to the other two averages, and there was more variation in the shape of these effects across pairs.

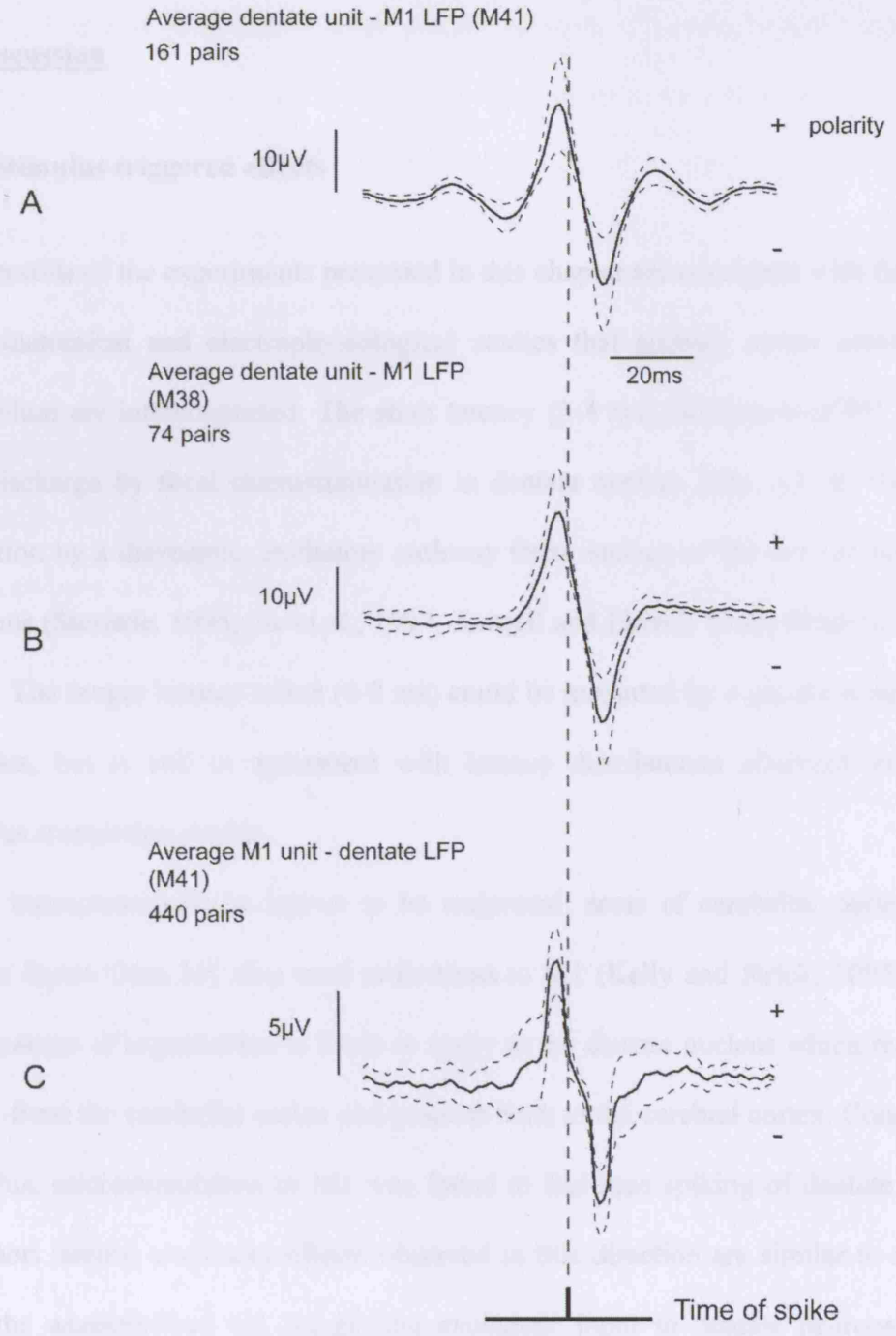

Figure 5.7. Population spike triggered averages. A, mean spike-triggered average of M1 LFP from dentate unit spiking for M41, calculated by combining single "clean" averages (e.g. Fig 5.6) from multiple pairs of sites. Note oscillatory profile. Dashed lines indicate 1 standard deviation from the mean. **B, C**, averages of M1 LFP from dentate spikes in M38, and of dentate LFP from M1 spikes in M41, respectively.

5.4 Discussion

5.4.1 Stimulus triggered effects

The results of the experiments presented in this chapter are consistent with findings from anatomical and electrophysiological studies that primary motor cortex and cerebellum are interconnected. The short latency (3-4 ms) facilitation of M1 single unit discharge by focal microstimulation in dentate nucleus (Fig. 5.1 A) suggests activation by a disynaptic, excitatory pathway from nucleus to M1 via ventrolateral thalamus (Steriade, 1995; Na et al., 1997; Jorntell and Ekerot, 1999; Holdefer et al., 2000). The longer latency effect (6-9 ms) could be mediated by a greater number of synapses, but is still in agreement with latency distributions observed in these previous stimulation studies.

This interconnectivity is known to be reciprocal: areas of cerebellar cortex that receive inputs from M1 also send projections to M1 (Kelly and Strick, 2003). The same pattern of organisation is likely to apply to the dentate nucleus which receives output from the cerebellar cortex and projects back to the cerebral cortex. Consistent with this, microstimulation in M1 was found to facilitate spiking of dentate units. The short latency excitatory effects observed in this direction are similar to results from the anaesthetized cat, suggesting excitatory input to dentate neurons from mossy fibre collaterals of ponto-cerebellar axons (Shinoda et al., 1992). This pathway could potentially contribute towards the modulation of neural activity in the dentate, and could explain the observed similarities in the task-related firing of single M1 and dentate units that were described in chapter 3 (for example, M1 and dentate neurons were found to have similar discharge onset times in relation to EMG

activity). However, it should be noted that the strength of these collateral projections from the pontine nuclei are somewhat weak in comparison to collaterals from NRTP (Mihailoff 1993; Gerrits and Voogd 1987, Shinoda et al 1992) and GABAergic collaterals of climbing fibres from the inferior olive (DeZeeuw et al 1997). Also, only around 20% of all stained PN projections show evidence of nuclear collaterals (Shinoda et al 1992). These factors might therefore limit the ability of pontine outputs to modulate neural activity in dentate nucleus, so the theory that dentate units were activated by these collaterals in the current experiment should be interpreted with some caution. It has been suggested, however, that relatively weak inputs could still have an effect (Shinoda et al 1992).

The dearth of significant effects found here is probably due in part to the low stimulus intensities that were used (25μA), which were limited by the impedances of the recording electrodes. This might also explain why no significant suppression effects were observed. In previous work, a larger proportion (10%) of significant effects, both facilitation and suppression, was found when stimulating at 100μA (Holdefer et al., 2000). Furthermore, a smaller number of sites were investigated in comparison to the Holdefer et al study (131 nuclear stimulation sites compared to 210 sites), so it remains a possibility that stimulating at further locations might provide a greater yield of significant effects. On a similar note, Holdefer et al also considered their yield to be a relatively small proportion, and attributed this to difficulties in achieving optimum alignment between M1 and nuclear sites, due to a high degree of topographical specificity in corticocerebellar interconnections. The present stimulation findings support this hypothesis.

5.4.2 Spike-trigged effects

The demonstration of significant spike-triggered effects in LFP in both directions is also in agreement with reciprocal connectivity, and provides evidence for M1-cerebellar interactions at the population level, since LFP signals represent the distributed synaptic activity of populations of neurons. The "clean" SpTAs in figure 5.6, 5.7 and 5.8 were generated by an arbitrary spike sorting process, and should not be taken as a direct representation of inter-area communication. However, they do highlight the probabilistic nature of spike-triggered effects: not all spikes contributed equally to the average, but rather the SpTA shape could be attributed to the influence of a small proportion of the total spiking events. As they are derived from synaptic activity, LFP signals can be thought of as representing the synaptic input to the region from which they are recorded (Scherberger et al., 2005). In contrast, spike signals represent the output of a region, since electrophysiological recordings are biased towards sampling from large, pyramidal output cells (Humphrey and Corrie, 1978). Hence, the presence of spike triggered effects in both normal (unprocessed) and "clean" SpTAs, is evidence for the influence of spiking activity in one region on the local synaptic processing taking place in another region: i.e., M1-cerebellar communication.

Furthermore, in both standard and clean SpTAs, LFP changes sometimes preceded the spike (e.g. Fig. 5.4 B, Fig. 5.6). This can be interpreted as a change in activity in the region of the LFP recording, leading to the occurrence of a spike at the other location (Holdefer et al., 2000), which is evidence for reciprocal connectivity. Taken together, these results suggest a partial synchronisation of spiking activity in each structure with LFP activity in the other. This could be a consequence of phase-

locking of cell firing within a region to local 15-30 Hz oscillatory activity in the LFP, which can be found in both M1 and cerebellum (Albus, 1971; Pellerin and Lamarre, 1997; Hari and Salenius, 1999). Alternatively, both centres could be synchronised to a third, common source of input. In either case, LFP signals from each area should then show significant coherence or phase locking. Supporting this are the observations of ~20 Hz oscillations in the standard and clean SpTAs of M1 LFP from dentate unit activity in monkey M41. However, a lack of such oscillations for the same SpTAs in monkey M38, and also for SpTAs of dentate LFP from M1 units, could indicate that spike synchronisation to LFP is either less oscillatory in these instances or is achieved by other means. It is generally known that the degree of oscillatory 15-30 Hz synchrony shown in the motor system can vary amongst individuals, in monkeys (Baker et al., 1997) and humans (Kilner et al., 1999). To investigate these various issues further, interactions between LFP signals recorded simultaneously from M1 and dentate nucleus were studied, and the results of this analysis are presented in the next chapter.

5.4.3 Comparison of stimulus-triggered and spike-triggered effects

Spike-triggered averages of LFP commonly showed evidence of M1-cerebellar connections, while PSTHs of spike activity rarely did. This difference suggests that the input to each region from the other is highly divergent, contacting many neurons, but with a weak influence on each individual cell. It would therefore be more readily observed at the population level rather than the single neuron level.

The difference in the proportion of significant LFP SpTA effects for M1 unit – dentate LFP (14%) compared to dentate unit M1- M1 LFP (51%) suggests an asymmetry in the efficacy of connectivity between M1 and dentate nucleus, with a stronger influence of dentate output on M1. Short latency, disynaptic pathways link these structures in both directions, as suggested by the stimulus-triggered averages: dentate is connected to M1 via VL thalamus, and M1 output can reach dentate through mossy fibre collaterals (Shinoda et al., 1992). The observed asymmetry could therefore be taken as evidence that, from a functional point of view, the principle pathway by which M1 influences dentate is via a longer, more convoluted route through cerebellar cortex and inhibitory cortico-nuclear connections (c.f. figure 1.2) so that M1 activity would tend to suppress discharge of dentate neurons. Arguing against this interpretation however is the observed similarity between M1 and dentate responses demonstrated in chapter 3, which would favour communication through the excitatory MF collateral pathway. To properly assess the extent of this difference it will be necessary to compare LFP SpTA effects in more animals.

5.5 Chapter summary

In this chapter, a preliminary assessment of interactions between primary motor cortex and dentate nucleus during task performance has been made. Using microstimulation it was possible to demonstrate functional connectivity between these structures, supporting and extending the findings of previous studies. As these effects were scarce, spike triggered averaging was successfully used to study the coupling of single neuron activity in each area with population activity in the other.

Altogether, these approaches indicate that cerebro-cerebellar communication in the awake monkey can be readily observed via conventional methods, with a particular emphasis on the analysis of interactions between LFP signals, which will be described in the following chapter.

Chapter 6: Interactions between M1 and cerebellum.

II – Single unit data and spectral analysis

6.1 Introduction

As described in Chapter 1, oscillations in the 15-30 Hz range have been observed in M1, cerebellar cortex and deep cerebellar nuclei. Coherence of M1 and cerebellar oscillations has been proposed to underlie cortico-cerebellar communication (O'Connor et al., 2002; Courtemanche and Lamarre, 2005). Such communication would be necessary given the role of the cerebellum in motor learning (Wolpert et al., 1998; Ito, 2005) and the sensory guidance of movement (Stein and Glickstein, 1992). In particular, the cerebellum is a likely candidate for the location of forward models which are thought to underlie skilled motor behaviour (Miall et al., 1993; Imamizu et al., 2000; Miall et al., 2001; Imamizu et al., 2003), for example the feedforward anticipatory adjustment of grip force (Flanagan and Wing, 1997; Kawato et al., 2003).

Previous work in this laboratory found evidence for neural activity that was correlated with feedforward control (Jackson, 2002). Although M1 neurons are known to scale their firing rates with the level of force required to squeeze two levers in this task (Smith et al., 1975; Wannier et al., 1991; Maier et al., 1993; Baker and Baker, 2003), cells were found to exhibit this force dependence before the levers were moved i.e. in the absence of sensory feedback, when trials of a particular force were performed in large blocks of 50 or more. This feed-forward activity was abolished when the sequence of force conditions across trials was randomised, while

scaling during the movement and hold phases remained the same. Force-dependent 15-30 Hz oscillatory LFP activity during the hold was also observed in M1: power in the β band decreased with increasing force. This was consistent with scaling being exhibited at a population level, and it remained constant across block and random conditions. However, while preliminary cerebellar recordings found force *independent* beta LFP activity which was coherent with M1 oscillations, the effects of randomising conditions on cerebellar single unit and LFP activity, and M1-cerebellum coherence, were not tested. Therefore the characteristics of M1-cerebellar interactions under these different conditions were unclear.

The results presented in this chapter extend this work firstly by examining and comparing load-dependent activity of single units in M1 and cerebellar dentate nucleus during block and randomised trial sequences. If predictive behaviour during block sequences of trials was observed, then dentate neurons should demonstrate feedforward scaling of their activity in a similar fashion to M1.

Following this, the nature of communication between M1 and dentate during task performance was studied by spectral analysis of beta-frequency oscillatory LFP activity. 15-30 Hz oscillations should be observed in the hold period LFP recorded from both areas, which show force dependence. In addition, the observed disruption of feed-forward prediction during randomised trial sequences should lead to reduced cerebellar cortical activity (Miall et al 2001), and this might be reflected by concomitant changes in dentate nucleus LFP oscillations. In turn, changes in coherence between M1 and cerebellar LFPs during randomised sequences would be a strong indicator of altered communication between these structures.

6.2 Methods

6.2.1 Acceptance of trials

For analysis of spiking activity, trials were rejected if they did not meet the two criteria described in Chapter 2. For testing of LFP activity, a less stringent criterion was applied to ensure that there were larger trial numbers for the application of spectral analysis methods. Trials were rejected simply if finger position exceeded 1.4mm above baseline, before the time of movement onset. Again this accepted trials where the hold period was achieved on the first attempt and levers returned to rest quickly, and rejected trials where the hold was achieved after multiple attempts and the levers did not return to baseline properly. Examples of trials accepted and rejected by this criterion are illustrated in figure 6.1A and B, respectively.

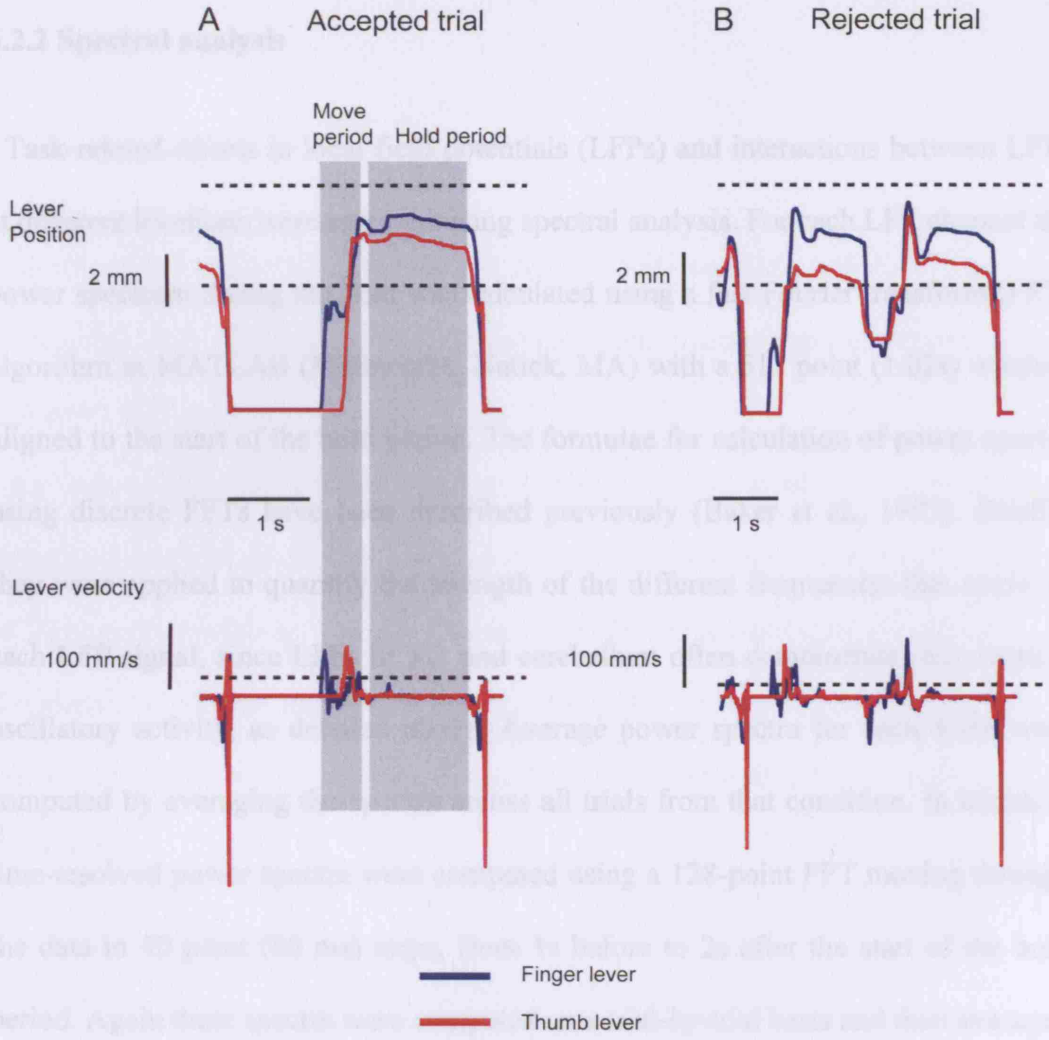

Figure 6.1. Trial selection for spectral analysis. **A**, position (top) and velocity (bottom) traces for a trial accepted according to criterion 3. **B**, equivalent plots for a rejected trial. Same conventions as figure 2.3.

6.2.2 Spectral analysis

Task-related effects in local field potentials (LFPs) and interactions between LFPs at different locations were assessed using spectral analysis. For each LFP channel the power spectrum during the hold was calculated using a fast Fourier transform (FFT) algorithm in MATLAB (Mathworks, Natick, MA) with a 512 point (1.02s) window aligned to the start of the hold period. The formulae for calculation of power spectra using discrete FFTs have been described previously (Baker et al., 1997). Briefly, they were applied to quantify the strength of the different frequencies that made up each LFP signal, since LFPs in M1 and cerebellum often demonstrate stereotypical oscillatory activity, as detailed above. Average power spectra for each force were computed by averaging the spectra across all trials from that condition. In addition, time-resolved power spectra were computed using a 128-point FFT moving through the data in 40 point (80 ms) steps, from 1s before to 2s after the start of the hold period. Again these spectra were computed on a trial-by-trial basis and then averaged for all trials in the recording session.

To quantify the level of interaction between LFP signals recorded simultaneously in M1 and dentate nucleus, the coherence spectrum was calculated for each signal pair. Coherence measures the amount of amplitude and phase correlation between two signals within a particular frequency band, and is bounded between 0 and 1. The calculations for coherence are described in Baker et al. (1997). Coherence was measured with a 512 point window aligned to hold start; it was computed for each trial and then averaged across all trials. This value C was considered significantly different from 0 if it exceeded the 95% level defined by Rosenberg et al. (1989):

$$C = 1 - \alpha^{1/(N-1)} \qquad (1)$$

where α=0.05 and N is the number of disjoint sections (i.e. number of trials) used to calculate the coherence. Time-resolved coherence spectra were computed using a 128 point FFT moving in 40 point steps.

As well as calculating coherence between single M1-dentate LFP pairs, average coherence was calculated across all the pairs of sites that were recorded over a total of 22 recording sessions. The significance of this average coherence was tested using the method of (Evans and Baker, 2003). Firstly, the probability density function of the single pair coherence values under the null hypothesis of zero coupling was calculated:

$$\text{prob}(C) = (1 - N)(1 - C)^{N-2} \qquad (2)$$

Equation (2) was derived by differentiating equation (1). The probability density of the average coherence across pairs was then estimated by convolution of the individual coherence densities; the 95th percentile of this probability distribution function was used as a significance level. The advantage of this method of averaging coherence, compared to previous studies incorporating Z-transformed values (Baker, 2000; Kilner et al., 2000) is that coherence retains its original bounding between 0 and 1, and thus the average has a more intuitive scale.

6.2.3 Phase and delay measurements

According to standard linear systems theory, the relationship between two coupled oscillators can be characterised by a phase shift and time delay (Rosenberg et al., 1989) . These were calculated from a linear regression line fitted to a plot of the cross-spectrum phase. The phase values at the frequency corresponding to peak coherence and the 3 adjacent points on either side were used for fitting. The mean value over this range determined the phase shift whilst the time delay was given by the slope of the regression line divided by 360°.

6.3 Results

6.3.1 Dataset

This chapter is based on data from M41, performing the precision grip task under three different load conditions, as described in section 2.1.3. In each recording session, trials for each condition were first presented in blocks, with each block comprising approximately 100 trials (Fig. 6.2, left panel). Then in the second part of the recording, each of the three forces was presented in smaller blocks of ten trials, and force varied randomly from block to block (Fig. 6.2, right panel), so the same force could sometimes be repeated for 20-30 trials. Each condition also comprised a total of 100 trials. Block size was chosen to be small enough for the force condition to be difficult to predict, but large enough for the animal to have to differentiate its behaviour sufficiently amongst the three conditions and perform the task accurately (if force is varied randomly on a single trial basis the task can become frustratingly difficult for the animal to perform properly, so that it develops a general strategy of producing the same motor output for each condition). Although small blocks of trials were used, this condition is henceforth referred to as the "random" condition. Data from a total of 11 sessions consisting of both block and random sequences are presented here.

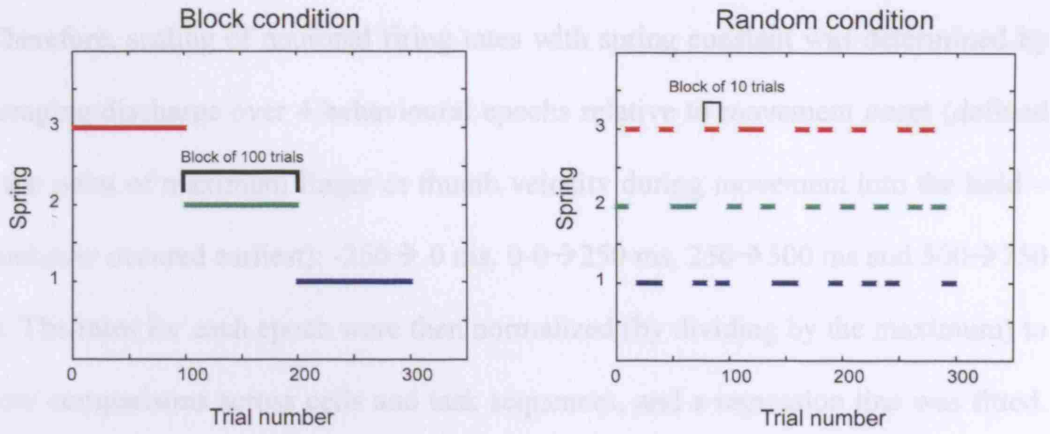

Figure 6.2. Sequence of spring forces in the block and random conditions.

Trials were accepted for analysis according to the criteria defined in Chapter 2 and above. Similar numbers of trials were selected for analysis in the block and random sequences, with an average of 41 trials (standard deviation =2) accepted per load condition.

The monkey could receive proprioceptive feedback about the current spring constant once it had moved the manipulandum levers. Movement initiation in all three conditions required application of the same 0.15N/mm force. Therefore scaling of neural or EMG activity with spring constant before movement onset were taken as indicators of feed-forward, predictive control. In a previous study, this predictive correlate was abolished in M1 neurons when force condition was randomized trial by trial (Jackson 2002). It was of interest in the present experiment to determine whether these feed-forward signals could again be observed, and if they were affected by a different type of random task sequence.

Therefore, scaling of neuronal firing rates with spring constant was determined by averaging discharge over 4 behavioural epochs relative to movement onset (defined as the point of maximum finger or thumb velocity during movement into the hold – whichever occured earliest): -250→ 0 ms, 0-0→250 ms, 250→500 ms and 500→750 ms. The rates for each epoch were then normalized (by dividing by the maximum) to allow comparisons across cells and task sequences, and a regression line was fitted. The absolute value of the slope of this line gave a measure of the degree of modulation of the cell's activity with force that was independent of direction (increase or decrease) and baseline firing rate, similar to the depth of modulation measure described in Chapter 4.

6.3.2 Kinematic data

Position and velocity profiles for finger and thumb levers during the block and random conditions are illustrated in figure 6.3. There was some variation in the final position achieved during the hold period amongst the different forces in both conditions, but this was small, in the order of ~1mm. From the force-displacement plot in figure 2.2 this variation would not cause a large difference in the force required to maintain lever position during the hold. Although finger velocity was slightly reduced during the random condition (Fig. 6.3 B), position and velocity profiles were basically similar between the two conditions. Note that in this example, movement of the thumb lever began slightly before the end of the first epoch, from approximately –40 → 0 ms), during the block condition. However, force-related scaling of EMG and neural activity before time 0 cannot be attributed to peripheral

feedback from lever movement, as sensory information could not be made available to M1 and/or cerebellum in order to influence movement, over such a short period. Instead, it probably reflects feed-forward control.

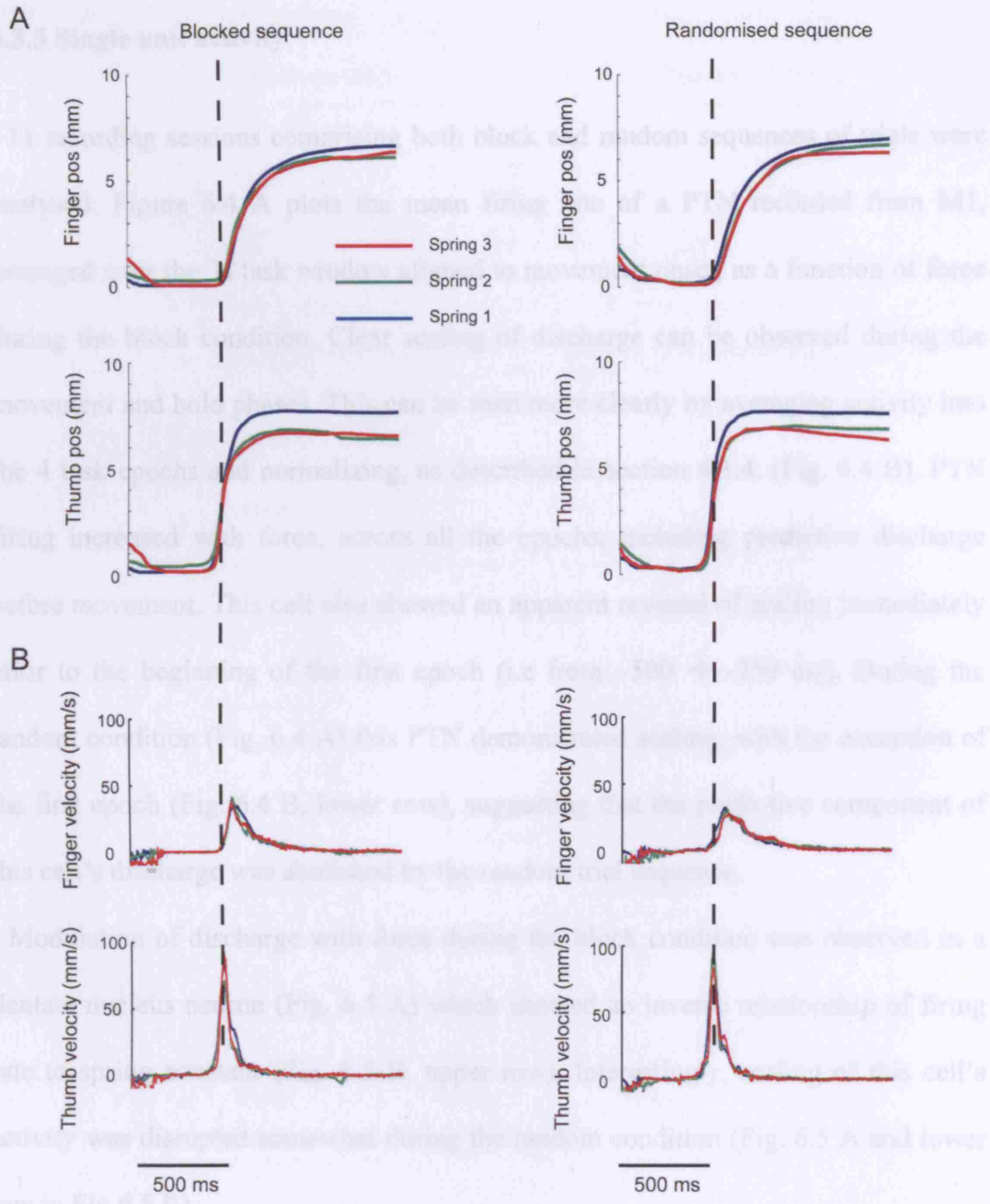

Figure 6.3 Kinematic data for block and random conditions. Averaged profiles of lever position (**A**) and lever velocity (**B**) aligned to movement onset for three spring-like conditions in block or random sequences (M41, 40 trials per condition).

6.3.3 Single unit activity

11 recording sessions comprising both block and random sequences of trials were analysed. Figure 6.4 A plots the mean firing rate of a PTN recorded from M1, averaged over the 3s task window aligned to movement onset, as a function of force during the block condition. Clear scaling of discharge can be observed during the movement and hold phases. This can be seen more clearly by averaging activity into the 4 task epochs and normalizing, as described in section 4.3.4. (Fig. 6.4 B). PTN firing increased with force, across all the epochs, including predictive discharge before movement. This cell also showed an apparent reversal of scaling immediately prior to the beginning of the first epoch (i.e from –500 → -250 ms). During the random condition (Fig. 6.4 A) this PTN demonstrated scaling, with the exception of the first epoch (Fig. 6.4 B, lower row), suggesting that the predictive component of this cell's discharge was abolished by the random trial sequence.

Modulation of discharge with force during the block condition was observed in a dentate nucleus neuron (Fig. 6.5 A) which showed an inverse relationship of firing rate to spring constant (Fig. 6.5 B, upper row). Interestingly, scaling of this cell's activity was disrupted somewhat during the random condition (Fig. 6.5 A and lower row in Fig 6.5 B).

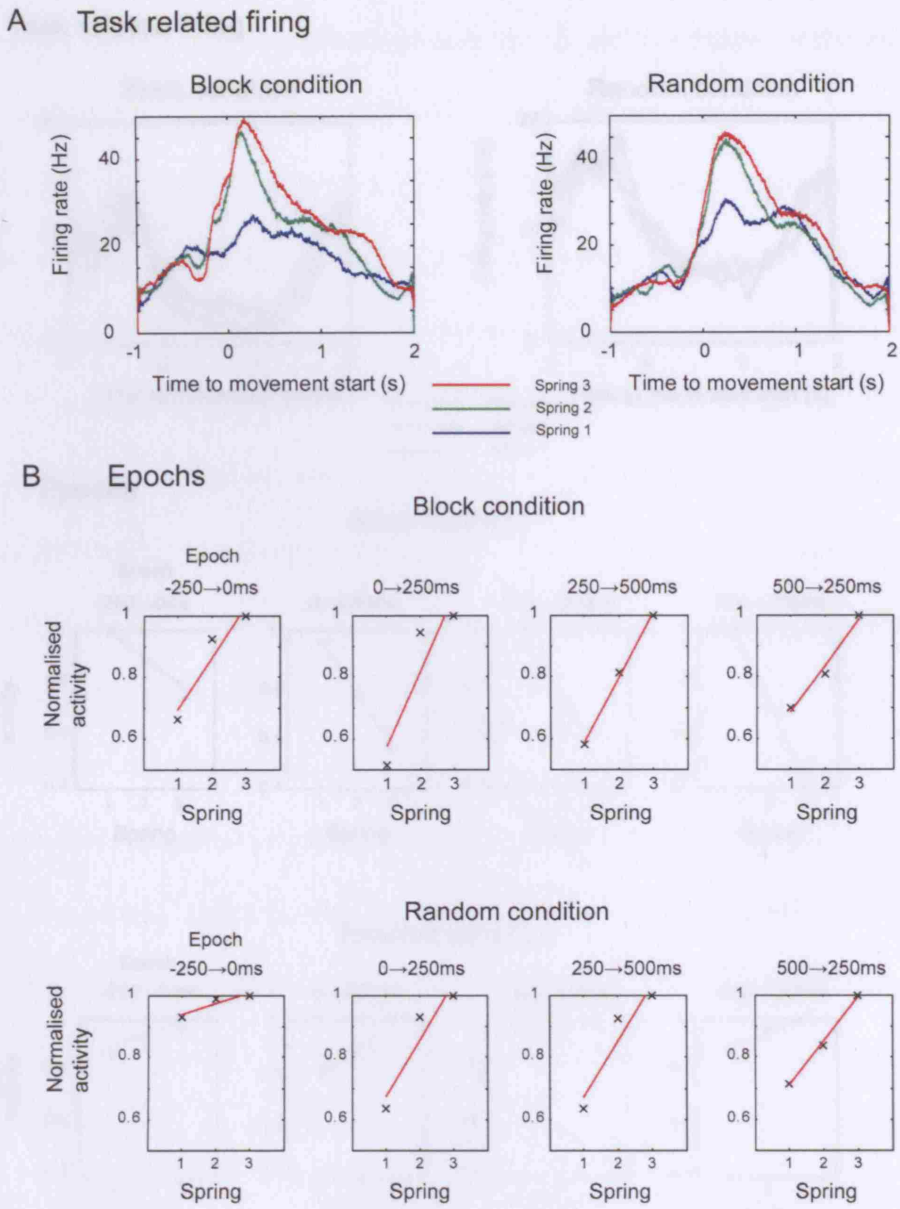

Figure 6.4. Load dependance of PTN activity during block and random trial sequences. A, left panel: task related firing for a M1 PTN aligned to movement onset during the block condition. Each trace represents mean firing rate during trials for each spring force, average of approximately 50 trials per trace. Some scaling of activity with force was evident during the 250ms prior to movement onset. Right panel: task related firing for the same cell during the random condition. **B**, scaling during block and random conditions compared by averaging activity into 250ms epochs as described in the previous chapter.

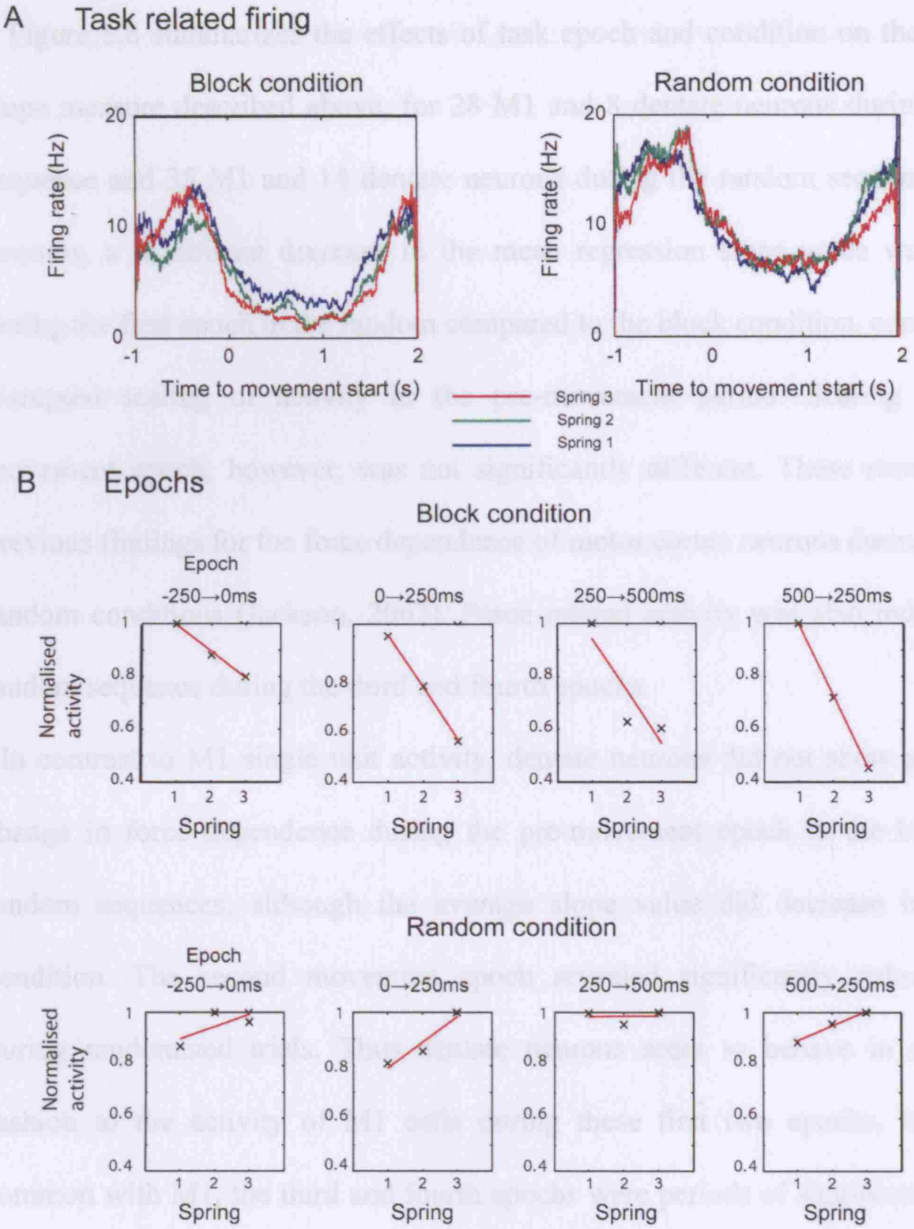

Figure 6.5. Load dependance of dentate unit activity during block and random trial sequencyes. A, task related firing as a function of spring force, for dentate nucleus neuron recorded during the block and random conditions. **B**, epoch analysis: note that this cell showed an inverse discharge-force relationship. Task related firing was disrupted during the random condition.

Figure 6.6 summarizes the effects of task epoch and condition on the regression slope measure described above, for 28 M1 and 8 dentate neurons during the block sequence and 35 M1 and 14 dentate neurons during the random sequence. For M1 neurons, a significant decrease in the mean regression slope value was observed during the first epoch in the random compared to the block condition, consistent with disrupted scaling of activity in the pre-movement period. Scaling during the movement epoch, however, was not significantly different. These results confirm previous findings for the force dependence of motor cortex neurons during block and random conditions (Jackson, 2002). Force related activity was also reduced in the random sequence during the third and fourth epochs.

In contrast to M1 single unit activity, dentate neurons did not show a significant change in force dependence during the pre-movement epoch in the block versus random sequences, although the average slope value did decrease in the latter condition. The second movement epoch revealed significantly reduced scaling during randomized trials. Thus dentate neurons seem to behave in an opposite fashion to the activity of M1 cells during these first two epochs. However, in common with M1, the third and fourth epochs were periods of significantly reduced force dependence in the random condition. This contrasts with the findings of the previous experiment (Jackson, 2002) and may reflect differences between the random sequences implemented in these two studies.

It should be noted that the order of presentation of force conditions in the block sequence was not balanced across the sessions analysed here, due to an idiosyncrasy in the monkey's performance. Its motivation to do the task was greatest at the start of the recording session, so it tended to apply excessive force to the levers, making it difficult to complete trials in the weakest force condition. The order of condition

presentation was therefore strongest→medium→weakest. Thus it is possible that the apparent force dependence described above for block sequences was simply a result of slow drifts in neuronal discharge across each session. To counteract this effect, average firing rates as a function of session time were calculated for all cells, and those which demonstrated this type of activity within a particular force block were rejected from the analysis. In the block condition 26/62 neurons were rejected this way, and 27/67 neurons were rejected in the random condition. Furthermore, analysis of M1 force dependence for 5 neurons during a single session where block order was medium→strongest→weakest shows that it was qualitatively similar to the findings in the population data.

Overall these results suggest differences in the coding of force between M1 and cerebellum during block and randomized task conditions, in single cells. For a better understanding of this neural activity at the population level, and in particular how these structures interact during this task, local field potentials (LFPs) recorded from these areas were analysed. The results of this analysis are set out below.

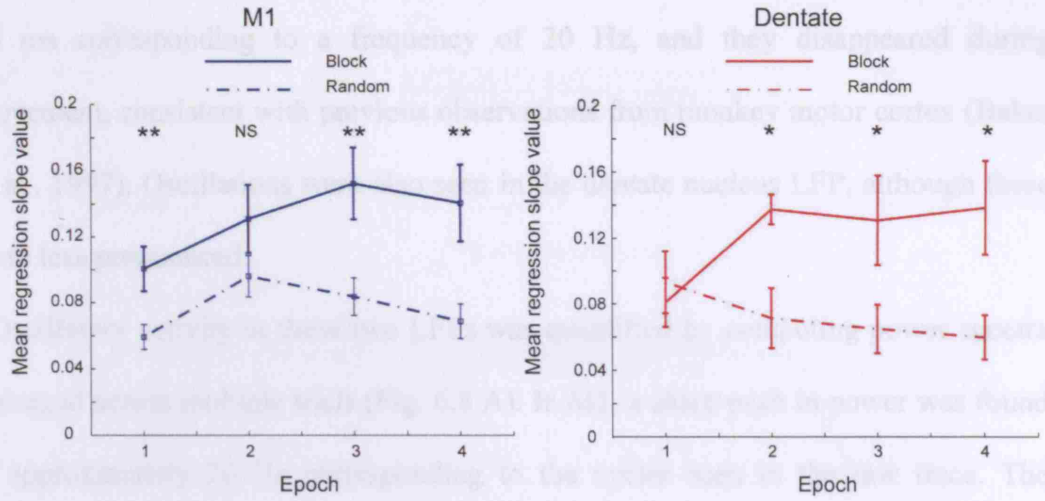

Figure 6.6. Average force-related discharge in M1 and dentate nucleus. Summary of force related discharge (measured from regression slope) as a function of task epoch, during block and random conditions, for M1 and dentate neurons (for n values see text). Asterisks indicate significant differences (1 tailed t-test, * $p<0.05$, ** $p<0.01$). Note that for M1, mean slope value was reduced during random condition in pre-movement epoch, but not during the movement epoch, whereas dentate neurons showed the opposite effect. Force dependence during the hold period (epochs 3 and 4) was significantly reduced for neurons from both areas.

6.3.4 Task relationship of LFP activity in M1 and dentate

LFPs were recorded from a total of 73 sites in M1 and 94 sites in dentate nucleus (e.g. site equals a recording from a separate electrode) across a total of 22 recording sessions using the standard block force sequence. Trials were accepted for analysis according to less stringent criteria than those imposed for the single unit data (see methods). Figure 6.7 shows example traces of simultaneously recorded local field potentials from M1 and dentate nucleus, together with finger and thumb position traces, during performance of a single trial. Clear oscillatory activity was observed in M1 LFP during the hold period. The period of these oscillations was approximately

50 ms corresponding to a frequency of 20 Hz, and they disappeared during movement, consistent with previous observations from monkey motor cortex (Baker et al., 1997). Oscillations were also seen in the dentate nucleus LFP, although these were less pronounced.

Oscillatory activity in these two LFPs was quantified by computing power spectra averaged across multiple trials (Fig. 6.8 A). In M1, a sharp peak in power was found at approximately 20 Hz corresponding to the cycles seen in the raw trace. The dentate nucleus spectrum also showed a peak at 20 Hz, and overall the spectrum was broader than in M1, indicating that higher frequencies contributed towards a greater proportion of the total power in the dentate LFP signal (Fig. 6.8 B). Note however that the overall power was far greater in M1 than in dentate at all frequencies (Fig. 6.8 C) indicating that the amplitude of oscillations was more greater in M1 than in dentate. This can be discerned in the raw traces in figure 6.7, and is consistent with previous findings (Jackson, 2002). Nevertheless, a significant peak in coherence between M1 and dentate was observed at ~20 Hz (Fig. 6.8 D).

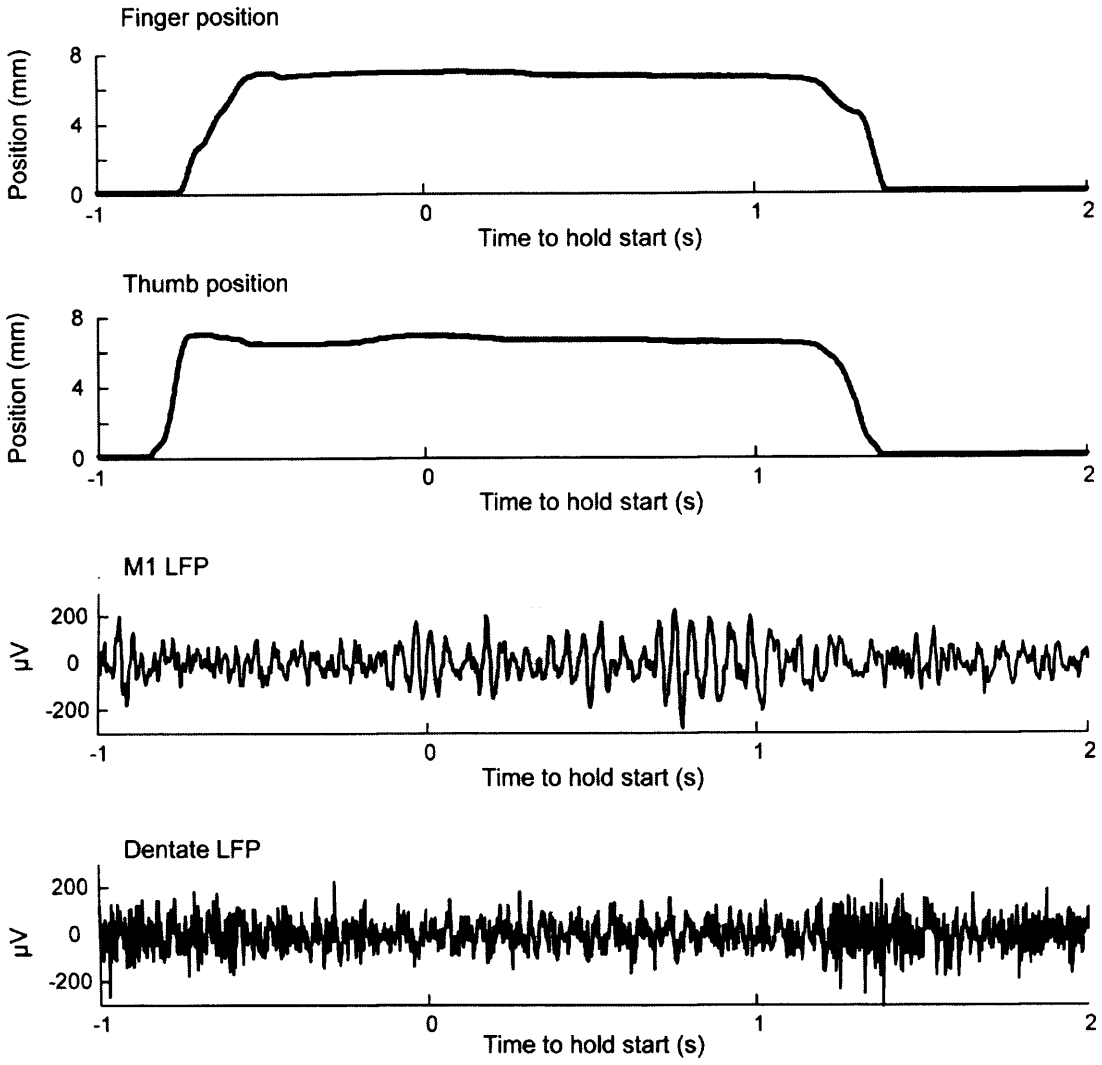

Figure 6.7 M1 and dentate nucleus LFP oscillations. Simultaneous LFP recording from M1 and cerebellar dentate nucleus during performance of a single precision grip trial. Grey shading highlights prominent oscillations in raw LFP during 1s hold period. Note that dentate oscillations are less pronounced than in M1.

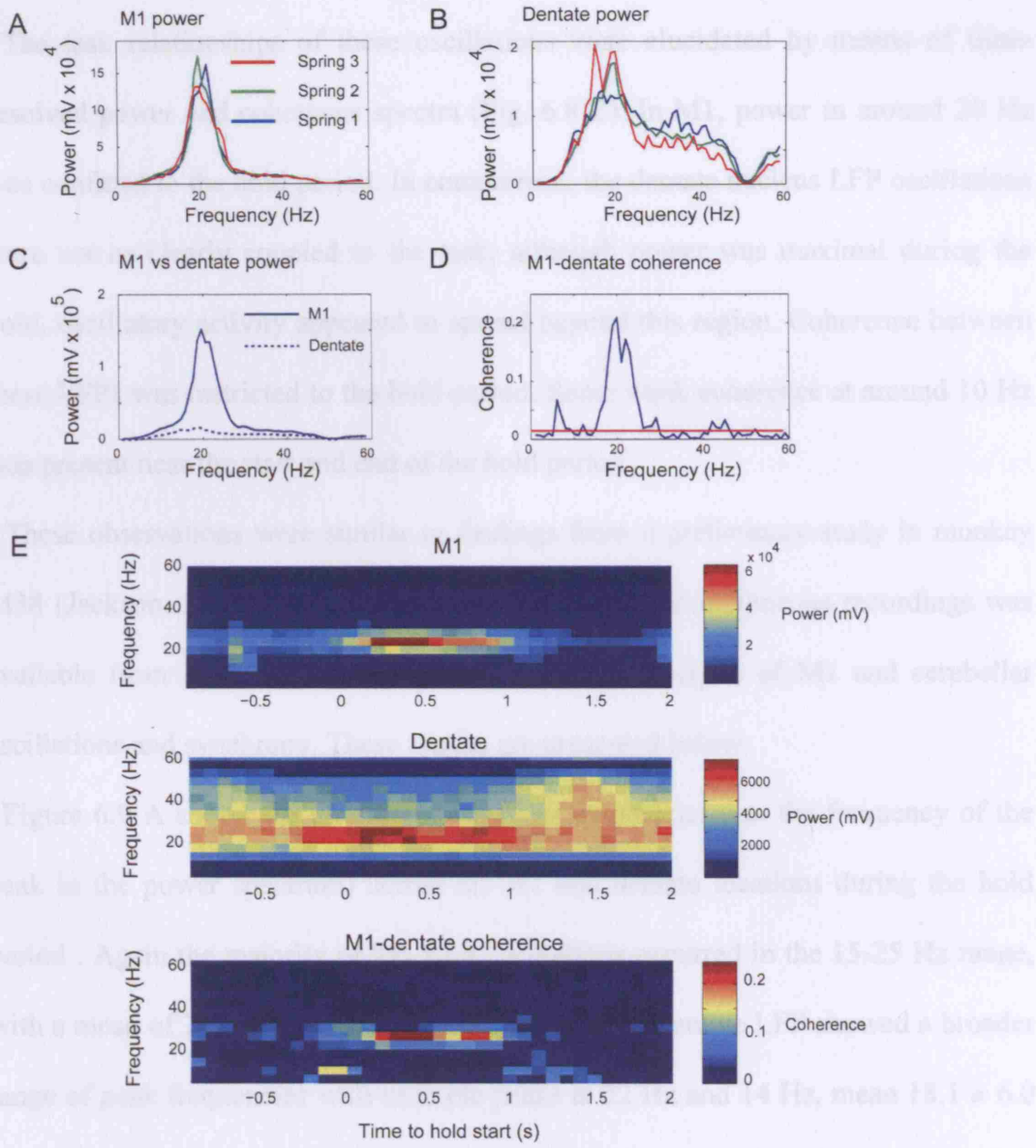

Figure 6.8 Comparison of M1 and dentate oscillations. **A, B** power spectra for LFPs recorded from M1 and dentate nucleus respectively. 70 trials per condition. **C**, comparison of power in M1 and dentate. Average of 220 trials across all 3 conditions. **D**, significant coherence between M1 and dentate LFP during the hold period, peak at approx. 20 Hz. Solid red line in coherence spectrum indicates theoretical 95% significance limit. **E**, time-resolved power and coherence spectra for the same signals, aligned to hold start. M1 power was clearly confined to the hold period, unlike dentate power.

The task relationships of these oscillations were elucidated by means of time-resolved power and coherence spectra (Fig. 6.8 E). In M1, power in around 20 Hz was confined to the hold period. In comparison, the dentate nucleus LFP oscillations were not as clearly coupled to the task: although power was maximal during the hold, oscillatory activity appeared to spread beyond this region. Coherence between these LFPs was restricted to the hold period. Some weak coherence at around 10 Hz was present near the start and end of the hold period

These observations were similar to findings from a preliminary study in monkey M38 (Jackson, 2002). However, a larger database of simultaneous recordings was available from M41, facilitating a more extensive analysis of M1 and cerebellar oscillations and synchrony. These results are presented below.

Figure 6.9 A shows the distribution of peak frequencies (i.e. the frequency of the peak in the power spectrum) across all M1 and dentate locations during the hold period . Again the majority of M1 LFP oscillations occurred in the 15-25 Hz range, with a mean of 20.5 ± 1.9 Hz (± standard deviation). Dentate LFP showed a broader range of peak frequencies with multiple peaks at 22 Hz and 14 Hz, mean 18.1 ± 6.0 Hz. A highly significant difference between these distributions suggests that the M1 and dentate oscillations were distinct (1 tailed Kolmogorov-Smirnov test, $P<1x10^{-8}$), and thus may have been generated by separate neuronal circuitry. Nevertheless, they were tightly coupled: averaging coherence values across a total of 317 M1-dentate pairs resulted in a clear, significant peak in coherence at approximately 20 Hz (Fig. 6.9 B). These findings support observations in previous experiments which pooled LFP oscillations from cerebellar cortex and the deep nuclei as they were found to be similar (Jackson, 2002). However, the 20 Hz peak found in the present, dentate-only

data does seem to be more prominent in comparison with the previous data. Note also the presence of separate peaks at 10 Hz and 40 Hz.

A population time-resolved coherence spectrum was computed by averaging coherence values across locations (Fig. 6.9 C): this bears many of the features of the single-pair plot in figure 6.8 E and indicates that across multiple sites, a similar task relationship of M1-dentate coherence was found. In contrast to the single pair plot, strong coherence was seen on average, between 5-10 Hz at around 2s after hold start. This time-resolved coherence spectrum comprises data from a smaller number of pairs (157) than the frequency spectrum plot, selected according to the degree of task-related coherence observed between single pairs.

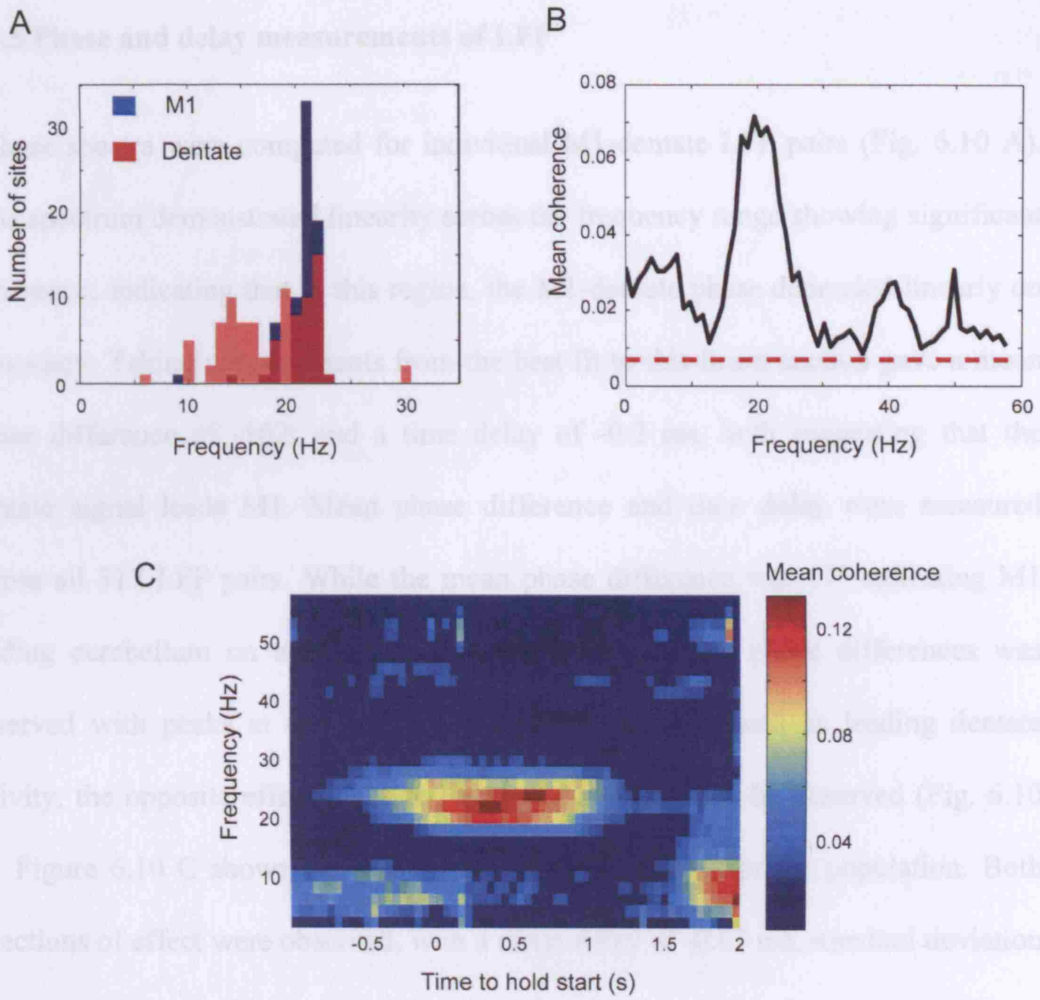

Figure 6.9. Population measures of oscillatory activity. A, distribution of peak frequencies of hold period oscillations for 73 M1 sites (blue shading) and 94 dentate nucleus sites (red shading). Note the broader distribution of frequencies for dentate LFPs. **B**, mean coherence calculated for 317 pairs of M1-dentate sites during the hold period. A prominent peak was observed at ~20Hz. Dotted line indicates theoretical 95% significance limit. Sharp peak at 50Hz represents contamination by mains noise. **C**, mean time-resolved coherence computed for 157 pairs of sites.

6.3.5 Phase and delay measurements of LFP

Phase spectra were computed for individual M1-dentate LFP pairs (Fig. 6.10 A). This spectrum demonstrated linearity across the frequency range showing significant coherence, indicating that in this region, the M1-dentate phase depended linearly on frequency. Taking measurements from the best fit to this linear section gave a mean phase difference of -102° and a time delay of -0.2 ms, both suggesting that the dentate signal leads M1. Mean phase difference and time delay were measured across all 317 LFP pairs. While the mean phase difference was 17° indicating M1 leading cerebellum on average, a bimodal distribution of phase differences was observed with peaks at 40° and -100° indicating that as well as leading dentate activity, the opposite effect (dentate leading M1) could also be observed (Fig. 6.10 B). Figure 6.10 C shows the distribution of phase delays for the population. Both directions of effect were observed, with a mean delay of -0.07 ms, standard deviation 0.7 ms, consistent with dentate activity leading M1 by only a short period of time. Note that this short delay does not represent the actual physiological latency for communication between M1 and dentate nucleus: the stimulation data from the previous chapter found that transmission delays were between approximately 3 – 10 ms.

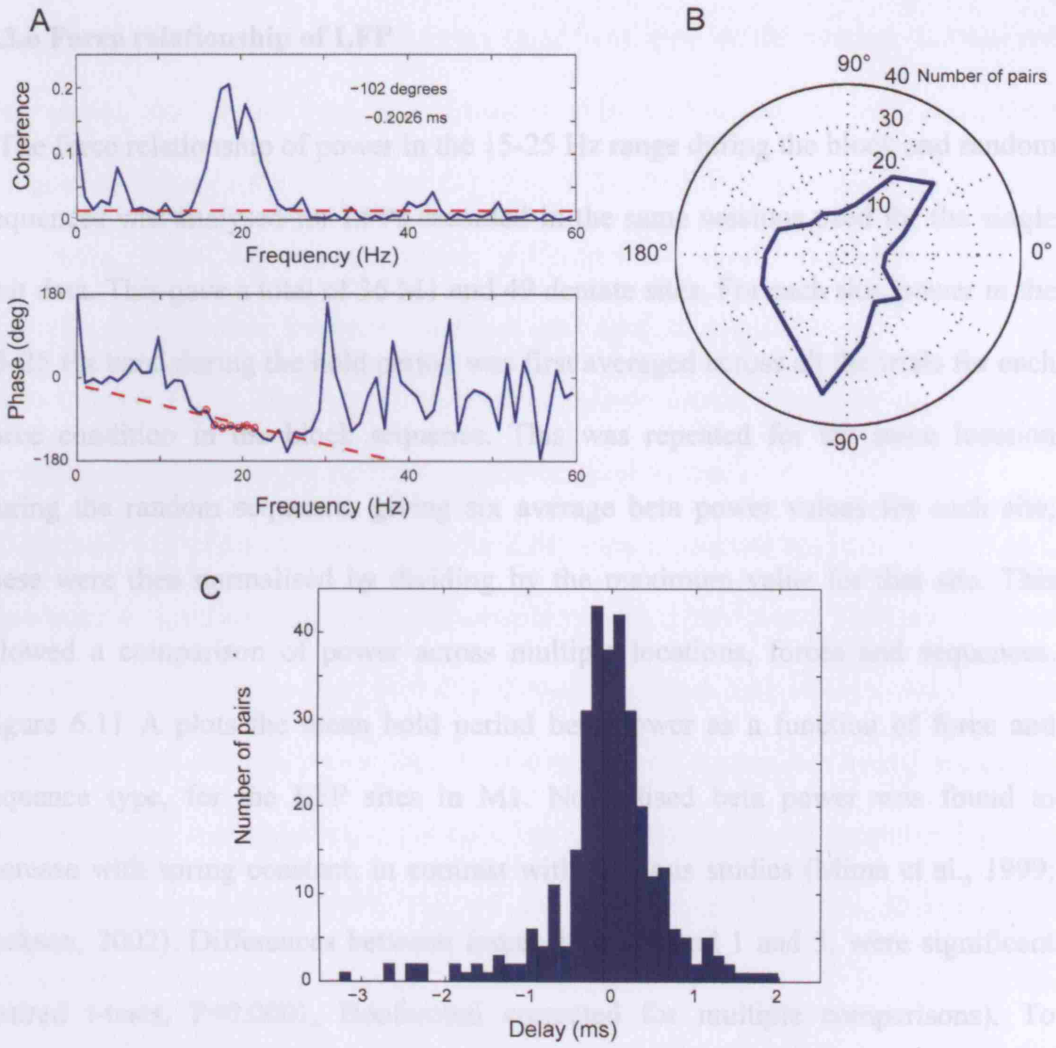

Figure 6.10. Phase relationship of M1-dentate LFP coherence. A, top panel: coherence spectra for same M1-dentate LFP pair as fig 6.8. Bottom panel: phase plot of corresponding cross spectrum from which phase and delay measurements were made. **B**, distribution of phase measurements for 317 M1-dentate LFP pairs. Note bimodal distribution. **C**, distribution of phase delays for these pairs. Mean delay –0.07ms.

6.3.6 Force relationship of LFP

The force relationship of power in the 15-25 Hz range during the block and random sequences was analysed for LFPs recorded in the same sessions used for the single unit data. This gave a total of 36 M1 and 49 dentate sites. For each site, power in the 15-25 Hz band during the hold period was first averaged across all the trials for each force condition in the block sequence. This was repeated for the same location during the random sequence, giving six average beta power values for each site; these were then normalised by dividing by the maximum value for that site. This allowed a comparison of power across multiple locations, forces and sequences. Figure 6.11 A plots the mean hold period beta power as a function of force and sequence type, for the LFP sites in M1. Normalised beta power was found to increase with spring constant, in contrast with previous studies (Mima et al., 1999; Jackson, 2002). Differences between forces 1 and 2, and 1 and 3, were significant (paired t-tests, $P<0.0001$, Bonferonni corrected for multiple comparisons). To confirm that the effect on power was due to hold period force and not another movement parameter such as lever displacement, trials were sorted into three new "conditions" according to the size of maximum finger lever displacement during the hold (i.e. condition 1: trials with smallest displacement, condition 3: trials with largest displacement). Average beta power did not vary significantly with finger position (paired t-tests, $P>0.05$).

Alternatively, the variation of power observed here could be caused by non-movement related factors. As stated above, for block sequences the order of force presentation was not balanced across sessions, and the increase in power could simply represent changes in attention, fatigue and/or motivation as the recording

progressed. However, exactly the same trend was seen in the average normalised beta power during the random sequences (Fig 6.11A), again with significant differences, between forces 1-3 and 2-3 ($P<0.0001$, $P<0.05$ respectively; Bonferonni corrected). There was no significant difference in mean normalised and un-normalised beta power between the block and random sequences for M1 LFP (1-tailed t-test, $P>0.05$). Thus power increase with force cannot simply be explained by variation in non-movement parameters as a function of time.

Figure 6.11 B plots the same data for LFP sites in dentate nucleus. Unlike M1, there was no significant difference in mean normalised beta power between different force conditions (paired t-tests, $P>0.05$). However, of particular interest was the clear overall decrease in mean power for all force conditions during the random sequence. This difference was significant for both the normalised and un-normalised power values (1-tailed t-tests, $P<0.05$). This cannot simply be explained by differences in movement performance during the random sequence since M1 LFP remained the same in both conditions. Thus there is a dissociation between M1 and cerebellum for LFP activity under different load conditions and trial sequences.

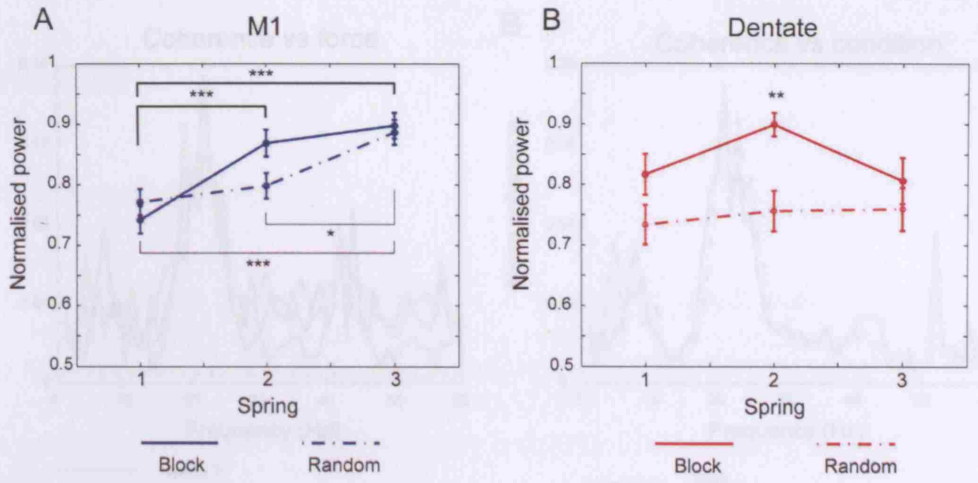

Figure 6.11. Force relationsip of M1 and dentate LFP oscillations. **A**, summary of dependence of normalised 15-25 Hz power during the hold period on spring force, in the block (solid line) and random (dash dot line) conditions, for LFP recordings from 36 sites in M1. Asterisks indicate significant differences (1 tailed paired t-test, * $p<0.05$, ** $p<0.001$, *** $p<0.0001$). **B**, summary for 49 dentate sites. Power did not vary significantly with force, but power averaged across all three forces during the block condition was significantly greater than during the random condition. Also note ** significantly higher power for spring 2 condition, $p<0.001$ (paired 1 tailed t-test).

In contrast to the effects seen in beta power, average M1-dentate LFP coherence in the beta range did not show any consistent scaling with force condition during the block sequence (Fig. 6.12 A), nor did the level of coherence change between the block and random conditions (Fig. 6.12 B). This suggests that despite changes in activity in M1 and cerebellum during different conditions of task performance, the degree of interaction between these areas remained the same.

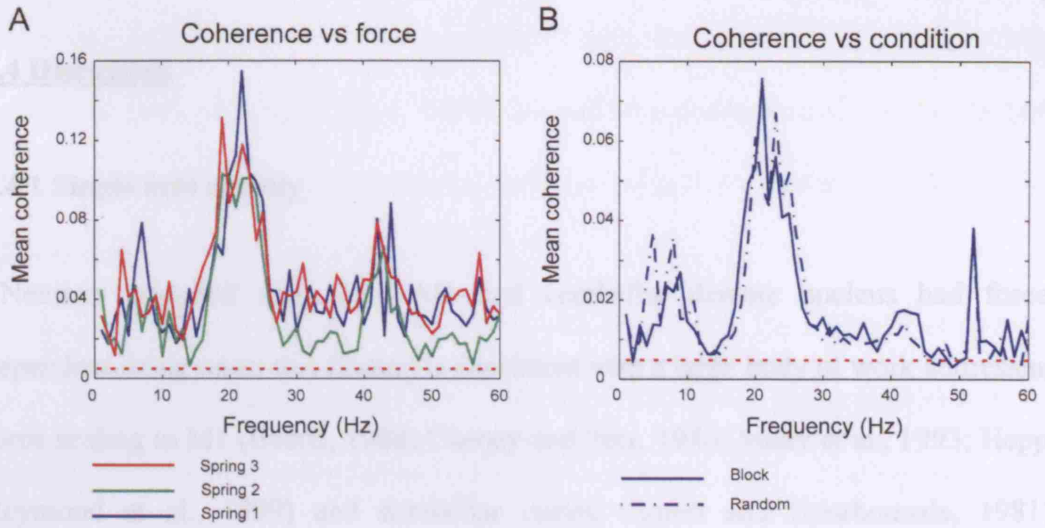

Figure 6.12. Force relationship of M1-dentate LFP coherence. A, mean coherence during the block condition for 317 M1-dentate pairs, as a function of spring force (see legend). A clear peak was observed at ~20Hz for all three forces, but no clear relationship of coherence to force level was found. **B**, mean coherence for 54 M1-dentate pairs compared during the block (solid line) and random (dash dot line) conditions. Again, coherence peaked at ~20Hz but did not differ between the two conditions. Red dotted lines indicate theoretical 95% significance limit.

6.4 Discussion

6.4.1 Single unit activity

Neurons recorded from both M1 and cerebellar dentate nucleus had force-dependent firing rates; this finding is consistent with a large body of work addressing force scaling in M1 (Evarts, 1968; Cheney and Fetz, 1980; Maier et al., 1993; Hepp-Reymond et al., 1999) and cerebellar cortex (Smith and Bourbonnais, 1981), together with similarities in movement related activity between M1 and dentate (Thach, 1975, 1978). The correlation of spike rate with force, before movement onset, suggests a neural correlate of feed-forward control associated with predictive scaling of EMG activity in muscles of the hand and forearm during task performance (see previous chapter).

This scaling must be implemented by feedforward control, since until lever movement begins there is no proprioceptive and cutaneous sensory feedback about the current force level. While it has been demonstrated previously in M1 (Jackson, 2002), its observation in the dentate nucleus is not surprising given that forward models are probably implemented in the cerebellum. Although they appear to be located in cerebellar cortex, based on evidence from human imaging studies (Imamizu et al., 2000; Miall et al., 2001; Imamizu et al., 2003; Kawato et al., 2003; Ito, 2005), the dentate nucleus is a key component of cerebellar control (Darlot et al., 1996). It receives input from lateral cerebellar cortical areas related to hand and arm movements (Voogd and Glickstein, 1998) and sends extensive projections to M1 via the ventrolateral thalamus (Dum and Strick, 2003). Inactivation of dentate nucleus by cooling disrupts predictive muscle activation which normally counteracts

perturbing torque pulses in an arm movement task, and reduces M1 activity related to this response (Vilis and Hore, 1980). In addition, under normal conditions both M1 and dentate show pre-movement activity related to movement preparation (Evarts and Tanji, 1976; Strick, 1983).

Although the "random" condition force condition varied in small blocks of 10 trials rather than on a single trial basis, it still abolished predictive activity in M1 (Figs. 6.4 B and 6.6 A) in line with previous findings (Jackson, 2002). Scaling during the movement epoch was preserved, since peripheral feedback was available to guide movement. In contrast, pre-movement dentate scaling was slightly reduced in the random condition but did not vary significantly. This difference is puzzling given that predictive information reaches M1 from the dentate nucleus; but a speculative hypothesis is that it could represent a partially developed forward model in the cerebellum which is not yet used to modify motor cortex. The development of a model could be possible under semi random compared to fully random task conditions: indeed, dentate is capable of processing and learning (Darlot et al., 1996) so may be able to gate the flow of information to M1 rather than simply relaying cerebellar cortical activity. The significantly reduced force dependence of dentate neurons during the movement epoch might also reflect the focus of cerebellum on feed-forward as opposed to feed-back control.

6.4.2 M1 and cerebellar oscillations

The existence of 15-30 Hz oscillatory activity in dentate nucleus LFP was confirmed, which was analagous to oscillations in cerebellar cortex (Pellerin and

Lamarre, 1997; Hartmann and Bower, 1998) as well as the established beta rhythms in M1. Whereas previous research has suggested a role of cerebellar oscillations in attention (Courtemanche et al., 2002; Courtemanche and Lamarre, 2005) the results of the present experiments support a role for both M1 and dentate beta rhythms in movement control.

Firstly, the amplitude of beta oscillations in M1 were found to show a significant increase with increasing force required to maintain the digits in a stable grip. This trend is the opposite of observations from two previous monkeys under similar task conditions (Jackson, 2002). It might be due to a genuine difference in oscillatory activity in the subject from which the current data were collected: individual differences in the extent of beta rhythmicity are often encountered, for example when measuring cortico-muscular coherence (Riddle and Baker, 2005). Supporting this is the fact that the size of the force effect in monkey M38 was relatively weak (Jackson, 2002). It should also be noted that in the literature, no significant relationship between M1 beta power and force has been found: for example, Mima et al. (1999) and Kilner et al. (2000) both failed to find significant scaling of these rhythms with force in human EEG/MEG recordings. Furthermore, there is no reason *a priori* to assume that LFP power must be scaled in a particular direction in relation to force. Firing rates of M1 neurons can both increase and decrease with increasing force, and LFPs do not simply reflect spiking activity in a particular region of cortex but rather synaptic activity on dendrites of the constituent neurons. Variation of beta frequency power might be related to changes in corticomuscular 15-30 Hz coherence as a function of spring compliance (Kilner et al., 2000), which also varied amongst the three conditions together with hold period force.

In contrast to M1, dentate LFPs in the 15-30 Hz band showed no significant variation with force, even though single unit activity was similar. This is consistent with results from (Jackson, 2002) for combined cerebellar cortex and dentate LFPs from two monkeys.

6.4.3 Sources of M1 and cerebellar oscillations

The significant differences in the frequency distributions of beta LFP rhythms (Fig. 6.9 A and Jackson 2002) suggest that M1 and cerebellar rhythms are generated by distinct, local sources. M1 beta frequency LFP oscillations are though to result from the influence of inhibitory interneurons on the cortical network, which according to computer modelling and in vivo recording studies (Lytton and Sejnowski, 1991; Jackson, 2002) may induce oscillatory activity of pyramidal cells (e.g. PTNs) in response to aperiodic input. M1 PTNs are phase locked to 15-30 Hz LFP oscillations (Baker et al., 1997; Baker et al., 2003). The functional implications of M1 rhythmicity are discussed in the Introduction to this chapter.

In cerebellum, there is some evidence that the cortex can act as a rhythm generator. As mentioned above, beta frequency LFP oscillations have been observed here on numerous occasions (Pellerin and Lamarre, 1997; Hartmann and Bower, 1998; Courtemanche et al., 2002; O'Connor et al., 2002; Courtemanche and Lamarre, 2005). Again, an inhibitory interneuron – the Golgi cell – is thought to be responsible for their generation, as modelling and slice preparation work suggest that this neuron can induce synchronous oscillatory behaviour in populations of reciprocally connected golgi cell – granule cell pairs, in response to random mossy fibre input (Dieudonne, 1998; Maex and Schutter, 1998). This in turn could induce

synchronised parallel fibre activity (Isope et al., 2002) which would be capable of producing coordinated firing of Purkinje cell simple spikes, although whether or not it would occur at beta frequencies is unclear since Purkinje cell –Purkinje cell synapses are poorly characterised in terms of their strength and time course of activity (Maex and De Schutter, 2005). Purkinje cells tend to have high spontaneous discharge rates of between 160-200 Hz , but their firing rate is suppressed during maintained contractions in precision grip (Smith and Bourbonnais, 1981), which is precisely when 15-30 Hz oscillations in cerebellar cortex and dentate are most prominent. In theory, Purkinje cell spiking could then entrain similar oscillatory activity in the deep nuclei through inhibitory cortico-nuclear projections, which could explain periodicity observed in the spiking of single dentate and interpositus neurons (Aumann and Fetz, 2004). Lastly, from a functional point of view, oscillatory activity in cerebellar cortex may serve a role in the precise temporal coding of information, for example modifying the processing of mossy fibre input (Maex and De Schutter, 2005) or altering plasticity at the parallel fibre-Purkinje cell synapse (De Schutter, 1995), which would be of particular importance for the development of forward models (see below).

In relation to this last point, it is interesting that instead of demonstrating a clear modulation with force, power in the 15-30 Hz band in dentate LFP showed a significant decrease in the random versus the block condition (Figure 6.11 B). This novel observation cannot be explained simply by task-related behavioural changes, since overall M1 power remained the same. Given this striking contrast between M1 and cerebellar activity, it is tempting to speculate that the change in the amplitude of beta oscillations observed in dentate nucleus may relate to the decreased predictability of force level in the random condition. There are a number of possible

alternatives: It could reflect altered activity in the cerebellar cortex, for example disruption of a forward model, which has previously been linked with reduced cortical activity (inferred from the BOLD signal) during a coordinated hand-eye tracking task in humans (Miall et al., 2001). In the current experiment, the failure of a forward model in the cortex could be associated with decreased rhythmical activity of coupled Golgi cell – granule cell pairs, which through their influence on Purkinje cells could be detected in dentate nucleus LFP. Alternatively, it could reflect altered activity in the dentate itself, rather than simply an echo of events taking place in the cortex above; perhaps the dentate is the locus of a model, or is able to modify cortical activity through nucleo-cortical and nucleo-olivary connections. The extensive interconnectivity of these areas to form a "corticonuclear complex" (Ito, 1984) makes it difficult to pinpoint the precise location of these changes. To better relate changes in oscillatory activity to cerebellar structure and function, simultaneous recordings of cortical and nuclear LFP should be compared in the block and random conditions.

6.4.4 M1 – cerebellar coherence

Although the sources of oscillatory activity in M1 and dentate were somewhat different, these oscillations were found to be significantly and closely temporally coupled at around 20 Hz. Coherent M1-cerebellar oscillations at this frequency may underlie cerebro-cerebellar communication (O'Connor et al., 2002; Courtemanche and Lamarre, 2005), since oscillatory synchrony is thought to facilitate widespread synaptic coupling of selected groups of neurons, permitting reliable communication

between motor areas (Konig et al., 1995; Donoghue et al., 1998; Baker et al., 1999). The phase distribution and mean delay measured from these coherence spectra were bimodal and small respectively, consistent with reciprocal connectivity between these structures and parallel processing during movement control, as opposed to sequential activation (Thach, 1975; Schwarz and Thier, 1999). The small mean delay (0.7 ms) would tend to suggest synchronisation of activity in the two structures by a third, common source of input. However, this contrasts with the evidence from the power spectra, which suggests intrinsic sources for M1 and cerebellar oscillations. Therefore, the precise mechanism by which LFP oscillations in these structures become synchronised remains unclear. Partial directed coherence (Schelter et al., 2005) provides a more accurate tool for measuring the direction of coherence effects; this method could be combined with LFP recordings from additional sites such as VL thalamus or the pontine nuclei, in order to help resolve this issue.

Unlike corticomuscular coherence, this synchrony showed no relationship to force level or randomisation of conditions, suggesting that while the temporal coupling between M1 and muscle can vary (Feige et al., 2000; Kilner et al., 2000), the extent of its internal communication with the cerebellum remains the same.

The importance of significant coherence in other frequency bands is unclear. Coherence in the alpha range (~10 Hz) in the population time-resolved coherence spectrum (Fig. 6.9 C) was observed during the hold period. Oscillations in M1 in this frequency band have been found previously in the macaque, and PTNs show phase locking of their spiking activity to these rhythms (Baker et al 2003). Similar frequency oscillations could be present in dentate as a result of activity in the inferior olive: there is evidence from in vitro and anaesthetised preparations that this structure is capable of generating ~10Hz activity (Llinas and Yarom 1986). Such

activity could propagate through to the deep cerebellar nuclei through climbing fibre collaterals, which in turn send mossy fibres to cerebellar cortex (Tolbert et al 1976, 1978; Chan-Palay 1977). This therefore provides a mechanism by which 10Hz activity in the olive could influence cerebellar nuclear and cortical processing, and hence movement control. Coherence in this range might then represent another mechanism for M1-cerebellar interactions. For further discussion of this issue, see section 7.3 in the following chapter.

6.5 Chapter summary

As noted in chapter 3, there are similarities in the activity of M1 and cerebellar dentate nucleus during the precision grip task, at the single unit level. Neurons in both these areas were shown to encode muscle activity and force level in their firing rates. But by comparing this activity under randomised conditions, subtle differences in the single unit data could be resolved. These became more clear when activity was analysed at the population level, using LFP signals. As well a providing further support for the hypothesis that LFP oscillations encode parameters of movement, the results from this chapter demonstrated a clear dissociation between M1 and dentate encoding that is consistent with the role of the cerebellum in feed-forward predictive control. Furthermore, interactions between populations of neurons in these structures were widespread, and could be demonstrated across a variety of conditions, indicating that M1 and cerebellum work in close cooperation to control finger movements.

Chapter 7: General Discussion

7.1 Single unit activity

A consistent feature of the single unit data analysed in these experiments was a basic similarity of responses recorded from different types of identified neuron, in M1 and cerebellar dentate nucleus. For example in chapter 3, M1 and dentate cells showed the same basic relationships to muscle activity, spring force and kinematics. In chapter 4, neurons within M1 with different patterns of subcortical connectivity were similarly correlated with spring force and discharged at about the same time relative to movement. These results can be readily interpreted through the underlying functional connectivity which links these neuronal populations into a cerebro-cerebellar loop. For example, collaterals of mossy fibre input from the pontine nuclei to the dentate nucleus (Shinoda et al., 1992), relaying input from M1, could feasibly underlie the movement-related discharge of dentate neurons which closely parallels activity in M1. The similarities between PTNs and CPNs observed in chapter 4 are a feature of the cortical interconnectivity, shown by cross-correlation histograms, that links them together into the same network. The approaches developed in chapters 3 and 4 could complement each other further – by characterising muscle encoding by CPNs, or comparing PTNs and CPNs with simultaneously recorded dentate units – to provide more insights into the features of this loop. Overall, the single neuron findings suggest a tight functional coupling between M1 and dentate nucleus: a firm basis for studying how they interact.

Nevertheless, M1 and cerebellum cannot simply be doing the same thing, otherwise there would be no need for them to communicate in the first place. The cerebellum has its own contribution to make towards the control of hand movements: principally, one of motor learning and predictive control. Under the highly trained task conditions studied here, this contribution may only reveal itself through quite small differences in the responses of single units to basic movement parameters. For example, a predictive component of grip control was demonstrated, but this was seen in both M1 and dentate responses. By introducing randomised sequences of trials in chapter 6, however, it was possible to disrupt predictive control and begin to tease apart the relative roles of M1 and cerebellum in precision grip.

Another way to probe the roles of these two structures and how they interact was to study activity at the population level, by analysing local field potential (LFP) signals recorded from each area. The general implications of these results will now be discussed.

7.2 Oscillatory activity within M1

In chapter 6, the level of β frequency power in LFPs recorded from M1 was found to scale positively with increasing force during the block condition, and a concomitant increase during random trial sequences made it less likely that this relationship was simply due to other, non-movement factors. Within the context of findings from previous experiments, however, interpretation of this result is less straightforward.

Firstly, it is not clear why an increase or decrease in these rhythms should occur during generation of higher or lower levels of force output by M1. Perhaps these oscillations correspond in a relatively simple way to the firing rates of motor cortical neurons, and simply reflect the correlation of firing rate with force?

There is a good understanding of how oscillatory LFP activity can arise in a population of cortical neurons. LFP oscillations represent the summed, synchronous synaptic potentials in a large number of cells (Singer, 1994). As a consequence a substantial proportion of the input to a given PTN is synchronised with this LFP (Baker et al., 2003), and in turn PTNs emit action potentials that are partially phase locked to these rhythms (Murthy and Fetz, 1996b; Donoghue et al., 1998; Baker et al., 2003).

Yet it is also recognised that oscillatory spiking patterns do not translate into oscillatory LFP patterns in a straightforward, linear way. The LFP signal itself is more likely to reflect dendritic synaptic activity (Singer, 1994; Konig et al., 1995) and the conversion of this activity into a sequence of action potentials is non-linear due to the spike threshold (Baker et al., 2003). Thus it does not follow *a priori* that increased firing rates of PTNs due to increased force should lead to greater power in the β frequency range. Moreover, single neurons were observed that changed their firing rates in either direction as spring force increased, consistent with previous work showing negative correlations with precision grip force (Werner et al., 1991; Maier et al., 1993). Since both directions of effect were observed with similar frequency in M1, the two should have cancelled giving zero net modulation across the population. Also, individual dentate neurons were found to show similar force correlations as those in M1, yet no force relationship was apparent in 15-30 Hz dentate LFP.

A second hypothesis is that, rather than being an artefact of firing rates, the observed trend in the LFP reflects adaptation in the motor cortex during the block condition. Such adaptation was demonstrated behaviourally and in terms of anticipatory EMG and neural discharge scaled to each spring force, in chapters 4 and 6. Increased β oscillations at higher spring forces could indicate a change in the M1 input-output gain relationship due to this adaptation. But arguing against this is the finding that the same LFP trend was found during the random condition, when spring force alternated more rapidly and was less predictable. However, it should be noted that the block and random conditions were only compared during the hold period, and so an adaptive change could already have occurred in M1 during the initial lever movement when current spring force could be determined from sensory feedback.

Thirdly, it has been suggested that synchronous discharge of cortico-motoneuronal cells represents a more efficient synaptic drive for recruitment of motoneurons (Baker et al., 1997; Kilner et al., 2000). Measurements from pairs of CM cells however, found no significant difference in the size of post-spike facilitation of EMG for synchronous versus asynchronous spikes, casting doubts on this hypothesis (Jackson et al., 2003). But since only a small proportion of the full extent of pairwise synchrony was assessed, synchronisation of cell activity at a level large enough to produce effects in the LFP could enhance motoneuron recruitment, which would be useful when gripping against a stronger spring constant. This might explain the slight trend for β power to show a corresponding increase since this reflects greater synchronisation of neural activity.

The fundamental problem with interpreting the functional significance of force-related β synchronisation is that it does not show a systematic change under similar conditions in separate studies. Mima et al. (1999) and Kilner et al. (2000) using EEG

and MEG recordings in humans respectively, failed to find a correlation of M1 β frequency power with grip force, while (Jackson, 2002) found decreasing synchronisation at higher forces in macaque M1.

In contrast, Kilner et al. demonstrated a strong and consistent relationship of synchronisation between cortex and muscle to spring compliance (the spring force:displacement ratio). This difference between intrinsic M1 oscillations and cortico-muscular coherence needs to be clarified, since it has been demonstrated that in humans the two can be dissociated (Baker and Baker, 2003). Diazepam, a $GABA_a$ antagonist, was found to increase ~20 Hz synchrony in M1, in line with the theory that LFP oscillations result from the action of local inhibitory interneurons. Cortico-muscular coherence, on the other hand, was unaffected by drug administration. Thus cortico-muscular coherence might be a functional entity in its own right, representing an interaction between oscillatory descending outputs and ascending afferent inputs used by the motor system for "sensorimotor integration" (Riddle and Baker, 2005). Whereas the β frequency oscillations observed here and in a preliminary study (Jackson, 2002) in macaque M1 might be less functionally related to parameters of movement control, which would be consistent with the observation that β rhythms in M1 LFP are suppressed during movement (Baker et al., 1997; Donoghue et al., 1998) arguing against a role in motor programming. Indeed, Gilbertson et al. (2005) found that finger movements triggered during periods of β synchrony were slowed relative to movements elicited at other times. M1 oscillations may instead be useful for promoting existing motor set and maintaining stability of grasp, which would explain their prevalence during the hold period.

To investigate this distinction further, rhythmical M1 activity, cortico-motoneuronal cell synchrony and M1-EMG coherence need to be measured within

the same monkey across a range of spring constants. Consistent changes in β frequency power related to spring force should be evidenced at the single neuron level by changes in synchrony between cortico-motoneuronal cell pairs. At the same time, measured M1-EMG coherence would be expected to vary independently with spring compliance. Oral administration of diazepam in a similar manner to Baker and Baker's study should then enhance β frequency power and cortico-muscular cell synchrony, while M1-EMG coherence should remain unchanged.

7.3 Oscillatory activity within cerebellum

Oscillatory activity has been extensively studied in LFPs recorded from the granular layer of the cerebellar cortex, where it is chiefly in the 15-30 Hz range. Its proposed functions include attention and the processing of sensory input through mossy fibres. Another important source of cerebellar oscillations is the inferior olive, where the membrane potential of individual neurons and the distributed activity across populations of neurons can show rhythmic 10 Hz activity (Llinas and Yarom 1986). Synchronous climbing fibre activity may be important for the control of skilled movements (Welsh et al 1995, Kazantsev et al 2004), and has been shown to control the temporal dynamics of simple spike firing in populations of Purkinje cells in cerebellar cortex of ketamine anaesthetized rats, by modulating mossy fibre throughput during stimulation of M1 (Schwarz and Welsh 2001). Modulation of mossy fibre system would be achieved in part through climbing fibre collaterals to the nuclei, which in turn send mossy fibres to cerebellar cortex (nucleo-cortical projections: Tolbert et al 1976, 1978; Chan-Palay 1977). Coherence between dentate

and M1 in the 10Hz range observed in Chapter 6 could be taken as support for theories of motor control through precisely timed olivary activity. However, these are controversial (Keating and Thach 1997; Kitazawa and Wolpert 2005; Baker and Edgely 2006). At the very least, the importance of the inferior olive in motor control and in the M1-cerebellar interactions discussed here should not be overlooked, since lesions to this structure severely disrupt movements (Soechting et al 1976b).

There has been less of a focus on the existence of oscillatory activity in deep cerebellar nuclei, until recently (Aumann and Fetz, 2004). The findings in chapter 6 confirm a previous observation of 15-30 Hz activity in dentate LFP and extend this finding with the novel observation of increased β frequency power during the random condition. This could be the neural correlate of adaptation – an altered input-output gain relationship – which was not found in M1. Such a dissociation would implicate the dentate nucleus as the locus of adaptive changes during control of force in precision grip, which would be consistent with its role in motor learning and as a substrate for internal models. It was also speculated that this activity might underlie failure, or modification of a forward model related to prediction of grip force.

7.4 Interactions between M1 and cerebellum: coherence effects

The observation of significant coherence between M1 and dentate LFP which does not vary across force conditions or trial sequences (block vs random) might seem paradoxical, given that there is a dissociation in the task relationships of each area's LFP oscillations. Significant differences between these structures were also found at

the single cell level, in the encoding of muscle activity and kinematic parameters (Chapter 3). However, in a similar vein to the findings on cortico-muscular coherence, this result could be used to support the interpretation of M1-dentate coherence as an independent variable representing genuine communication between these structures which is separate from the ongoing activity within them.

Furthermore, it should be noted that internal communication may not signal parameters of movement when assessed by a simple correlation with these parameters. For example, O' Connor et al. (2002) demonstrated coherence between cerebellar cortical and primary somatosensory cortex LFP during whisking movements in rats: coherence was tied to the presence of whisking, just as M1-dentate coherence was seen during the hold period, but did not correlate with the phase of whisking movements. In contrast, cortico-muscular coherence, which reflects more the output of cortical motor areas, correlates directly with a parameter of movement (spring compliance), although a precise function for this phenomenon remains to be established (Salenius and Hari, 2003).

The invariance of coherence that we observed may in part be due features of the analysis. An important limitation of the current work was the calculation of coherence by averaging spectra across many trials, under the assumption that M1-cerebellar interactions are stereotyped and do not vary on a trial to trial basis, as performance during the precision grip task was highly stereotyped. It should be recognised that under these task conditions, particularly during block trial sequences, the need for close cooperation of M1 and cerebellar activity may be somewhat reduced.

7.5 Communication through synchronisation or rate coding?

At this point, however, it is useful to inquire: to what extent do the coherence and spike-triggered average effects demonstrated here actually represent "interactions" or "communication" between brain structures? This question relates to the larger issue of the functional significance of synchronised neural activity in the brain. It has been proposed as a mechanism for solving the binding problem - how different features of an object are bound together into a single coherent percept (von der Malsburg, 1994). More generally, synchronisation could provide a way of disambiguating distributed codes which are superimposed within the same network (Treisman, 1999). Synchrony could also facilitate conversions from one distributed code to another, and so could provide a means by which regions of the brain, with different distributed codes, could communicate with one another (Singer, 1999). Central to these concepts are findings from modelling studies showing that temporally correlated activity of neurons presents a more effective drive to those cells' target structures (Abeles, 1991; Singer, 1999), and that neurons are sensitive to the second order temporal structure of their inputs (Rudolph and Destexhe, 2001). Specifically, these models suggest that precisely temporally correlated synaptic inputs (in the order of a few milliseconds) can influence neuronal activity in a variety of ways, including switching neuronal responses on or off, and modulating the gain of their response functions (Salinas and Sejnowski, 2000, 2001).

It is thought that oscillatory synchronisation might facilitate longer range communication since it would render synaptic input optimally timed and maximally effective. Oscillatory activity may serve to propagate synchrony beyond the range of direct connections (Konig et al., 1995; Schoffelen et al., 2005). Thus, within the

framework of these theoretical considerations, the demonstration of spike triggered average effects and significant coherence between M1 and cerebellum is evidence that these structures interact during precision grip.

However, there are two limitations to what this approach can tell us. Firstly, it has not been conclusively demonstrated *in vivo* that synchronised synaptic inputs are more effective than asynchronous inputs at driving neural activity in target structures; see the discussion on cortico-muscular synchrony above. Secondly, these findings demonstrate *how* interactions might take place *in vivo* and that they are related to hand control, but they do not show *what* is communicated. This is in part due to the type of analysis that was used. The basic coherence measure in chapter 6 assessed the extent of correlated activity between the two areas in the frequency domain, but the direction of this coherence was ambiguous, because a bimodal distribution of phase lags was found. Thus we were not able to characterise how (or if) activity in M1 influenced that in dentate, and vice versa, under these circumstances. Application of partial directed coherence (Schelter et al., 2005) could provide a better estimate of directionality, from which causality could be inferred, providing clues to the information content of this communication. It would be interesting to measure partial coherence between M1, dentate and cerebellar cortical LFPs, during development of or switching between internal models, for example in the grip force paradigm used by Kawato and collegues (Kawato et al., 2003). Under these conditions it should be possible to study how cerebellar processing influences the encoding of movement parameters by M1.

But more fundamentally, the limitations of the present findings are due to limitations in what synchrony can currently tell us about the transfer of information between brain areas. The concept of communication through synchronisation is

certainly intuitive, and widespread. Synchronised LFP activity between remote brain regions has been observed in other locations than between M1 and cerebellum – for example between SI and MI (Murthy and Fetz, 1996a) and between dorsal premotor cortex and area MIP of parietal cortex (Pesaran et al., 2005). Oscillatory synchronisation of single units has also been shown over long distances (>2mm) in cat visual cortex (Konig et al., 1995).

But the transfer of information through synchronisation must be properly quantified to assess whether it is a valid means of interaction between brain structures. So far, possible encoding through synchrony has only been studied within individual regions. Theory and experimental recordings have shown that broad correlations in the firing rates of multiple cortical neurons across trials can encode significantly more information than is available from their firing rates alone, including coding of movement direction and movement sequences by pairs of M1 neurons (Lee et al., 1998; Abbott and Dayan, 1999; Maynard et al., 1999; Hatsopoulos et al., 2003). On a related note, temporal structure in LFP recorded from the parietal reaching region over similar time scales can encode information about arm reaching movements, which compliments information available from neural spiking (Scherberger et al., 2005). LFP signals are easier to record over long periods of time than spike signals, so from the point of view of designing a brain-machine interface (BMI) they might represent a more useful source of information about movement encoding in this area. These examples demonstrate how synchrony can be an important factor in neural computation.

However, precise millisecond synchrony between pairs of neurons does not encode more information than a combination of firing rate and broad correlations (Oram et al., 2001). Thus over shorter time scales (20-50 ms), current evidence suggests that

populations of neurons within M1 and cerebellum encode parameters through distributed patterns of their firing rates and not through temporal synchronisation of their activity.

In light of this distinction between two basic types of synchrony, one can return to the question of what M1-cerebellar coherence represents. Since it is a feature of broadly correlated activity between neurons, the studies by Maynard et al. (1999) and Hatsopoulos et al. (2003) could subsequently be taken as support for a functional role of this coherence in the computations executed through M1-cerebellar interactions. But this mechanism would seem to be of little use across the short time scales during which the cerebellum would be expected to update M1 movement representations, in its capacity as a feed-forward predictor. The lack of coherence during precise movements of the fingers is consistent with this.

Instead, it may simply reflect an underlying "priming" or initiation of communication between M1 and cerebellum, which could be readily achieved during periods that are less computationally intensive, such as the hold period. Alternatively, given that coherence can be observed between dorsal premotor cortex and area PRR during planning of reaching movements (Pesaran et al 2005), the 15-30 Hz coherence observed in the current work might reflect M1-cerebellar communication underlying control of upcoming rather than ongoing movements, although arguing against this is the observation that coherence remained unchanged by the experimental manipulations described here.

In contrast, the presence of a peak or trough at relatively short latencies (20-50 ms) in spike triggered averages of LFP indicates the influence of spiking in one region on activity in another over a shorter time scale. Based on our understanding of spike triggered effects in the corticomotoneuronal system, we might expect this influence

to manifest itself as synchronised spiking of the trigger neuron with one or more neurons around the electrode in the target region. However, this interpretation is complicated by the effects of other neurons synchronised to the trigger cell, the variety of pathways by which this spiking could come to exert its influence, and the fact that LFP reflects more the sum of synaptic activity at dendrites of neurons in the target region. Given these factors, it might be better to interpret the spike triggered effects demonstrated here more conservatively as the influence of spiking activity in one region on "local synaptic activity" in the target area. Nevertheless, these effects are separate from temporally broader 15-30 Hz synchronisation, since the two could be dissociated in the averages.

7.6 Future work

Together, the various issues which have been discussed here provide a strong motivation for conducting future simultaneous recordings of both M1 and dentate single unit and LFP activity during a basic learning paradigm, for example learning to move in different force field conditions such as those used by Krouchev and Kalaska (2003). As mentioned above, the nature of M1-cerebellar oscillatory activity and coherence are difficult to interpret under the current task, and could potentially be clarified by adopting more sophisticated analyses. One concern is that the techniques used in this chapter may have overlooked some features of M1-cerebellar interactions, by averaging data across many hundreds of trials. This was true for both single unit and LFP analysis. Of course, the use of a highly trained task and the collection of data across repeated trials were needed to ensure that sufficient neural

data could be sampled and correlated with the animal's behaviour in a meaningful way. Nonetheless, future work may be able to pinpoint more accurately the contribution of the cerebellum during hand movements by looking at smaller numbers of trials. For example, multi-taper analysis of LFP-LFP coherence can provide similar estimates of time-resolved power and coherence spectra, but without requiring averaging over large numbers of trials (Jarvis and Mitra, 2001). A more dynamic M1-dentate coherence might then reveal itself. Through these methods, it would be more feasible to investigate how forward models develop in the cerebellum, how they are used to modulate processing of movement commands in M1, and how they might be calibrated through communication with M1 in order to remain accurate.

Spike triggered effects in particular warrant further investigation, for two reasons. Firstly, they may represent a mechanism for M1-cerebellar communication over shorter time scales, relating more to the online guidance of movement and the role of the cerebellum in feed-forward control. Secondly, according to the conservative interpretation of these effects, there is no inherent need to assume short term neural synchrony, which so far has not been shown to provide information within the brain that cannot not simply be encoded through firing rates alone (Oram et al., 2001; Rolls and Deco, 2002). While no parametric relationship to spring force of these spike triggered effects was found, other parameters such as muscle activity, digit position and velocity should be tested. However, many of these effects were revealed after averaging and sorting of large numbers of spikes. Through more extensive mapping of M1 and dentate, optimally aligned paired sites or "hot spots" might provide stronger effects. It would also be instructive to compile SpTAs by incorporating only transient bursts of spikes related to movement execution, and

excluding tonic spiking activity during the hold – these were found to be common patterns of activity amongst different types of M1 and dentate neurons (Chapters 3 and 4). The contribution of spikes across trials must also be determined, which was not tested here, as observations of spike triggered effects over small numbers of trials would provide another basis for monitoring M1-cerebellar interactions during learning.

The spike triggered approach could be complemented by the firing rate encoding model that was studied in chapter 3. Here, we attempted to quantify the coding of muscle activity and kinematic parameters by single M1 and dentate neurons. It would be straightforward to extend this model to include the activity of simultaneously recorded cells, to quantify the contribution of network activity towards this encoding, as was demonstrated within M1 by Paninski et al. (2004c). The next logical step would be to study the contribution of dentate activity towards encoding of muscle activity in M1, and vice versa, in comparison to coding of kinematics. Thus, interactions between the two areas could be studied within the domain of theories of rate coding, which would allow better quantification of the information transfer between these areas related to movement control.

7.7 Summary of main findings

1. During precision grip, the encoding of muscle activity in the firing rates of single neurons in M1 and dentate nucleus is linear. The same cells were equally well correlated with basic kinematic parameters (finger position and velocity). Predictions of cell activity fitted using these parameters were significantly more accurate when applied to M1 neurons, particularly PTNs, suggesting a more direct role for M1 in the initiation and control of skilled finger movements.

2. Different output pathways of M1 were identified and studied in the awake behaving monkey, at the single neuron level. Output cells with axons passing through the pyramids (PTNs, putative corticospinal neurons) and cells projecting only as far as the cerebral peduncles but not in the pyramids (putative cortico-pontine neurons) showed essentially the same activity patterns, although subtle differences in hold related activity and force encoding were found. Again, these results indicate that PTNs are more directly linked to movement control and that cerebellum can receive movement-related input through multiple channels from M1.

3. When trials of the same load condition were presented in large blocks, predictive scaling of discharge with force was observed in single M1 and dentate units consistent with feed-forward control of grip force. During random trial sequences this predictive signal was disrupted in M1 but not dentate nucleus.

4. 15-30 Hz oscillations were observed in dentate nucleus as well as M1. In random compared to block trial conditions, M1 oscillations were unchanged whereas dentate rhythms showed a significant increase in power.

5. This dissociation of M1 and dentate nucleus activity at the single neuron and population levels between block and random conditions highlights the role of the cerebellum in predictive control of grip force.

6. A close temporal association of M1 and dentate activity could be observed at narrow and broad time scales through spike triggered averaging of LFP and coherent LFP oscillations, respectively. The task invariance of these effects suggests that interactions between M1 and cerebellum occur across a range of conditions.

References

Abbott LF, Dayan P (1999) The effect of correlated variability on the accuracy of a population code. Neural Comput 11:91-101.

Abeles M (1991) Corticonics: neural circuits of the cerebral cortex. Cambridge: Cambridge University Press.

Adelson EH, Bergen JR (1985) Spatiotemporal energy models for the perception of motion. J Opt Soc Am A 2:284-299.

Albus J (1971) A theory of cerebellar function. Math Biosci 10:25-61.

Allen GI, Tsukahara N (1974) Cerebrocerebellar communication systems. Physiol Rev 54:957-1006.

Andersen P, Hagan PJ, Phillips CG, Powell TP (1975) Mapping by microstimulation of overlapping projections from area 4 to motor units of the baboon's hand. Proc R Soc Lond B Biol Sci 188:31-36.

Asanuma C, Thach WT, Jones EG (1983a) Cytoarchitectonic delineation of the ventral lateral thalamic region in the monkey. Brain Res 286:219-235.

Asanuma C, Thach WT, Jones EG (1983b) Distribution of cerebellar terminations and their relation to other afferent terminations in the ventral lateral thalamic region of the monkey. Brain Res 286:237-265.

Aumann TD, Fetz EE (2004) Oscillatory activity in forelimb muscles of behaving monkeys evoked by microstimulation in the cerebellar nuclei. Neurosci Lett 361:106-110.

Baker MR, Baker SN (2003) The effect of diazepam on motor cortical oscillations and corticomuscular coherence studied in man. J Physiol 546:931-942.

Baker, MR, Edgley, SA (2006). Non-uniform olivocerebellar conduction time in the vermis of the rat cerebellum. J Physiol: 570: 501-506.

Baker SN (2000) 'Pooled coherence' can overestimate the significance of coupling in the presence of inter-experiment variability. J Neurosci Methods 96:171-172.

Baker SN, Lemon RN (1998) Computer simulation of post-spike facilitation in spike-triggered averages of rectified EMG. J Neurophysiol 80:1391-1406.

Baker SN, Olivier E, Lemon RN (1997) Coherent oscillations in monkey motor cortex and hand muscle EMG show task-dependent modulation. J Physiol 501:225-241.

Baker SN, Pinches EM, Lemon RN (2003) Synchronization in monkey motor cortex during a precision grip task. II. effect of oscillatory activity on corticospinal output. J Neurophysiol 89:1941-1953.

Baker SN, Kilner JM, Pinches EM, Lemon RN (1999) The role of synchrony and oscillations in the motor output. Exp Brain Res 128:109-117.

Baker SN, Spinks R, Jackson A, Lemon RN (2001) Synchronization in monkey motor cortex during a precision grip task. I. Task-dependent modulation in single-unit synchrony. J Neurophysiol 85:869-885.

Baker SN, Philbin N, Spinks R, Pinches EM, Wolpert DM, MacManus DG, Pauluis Q, Lemon RN (1999) Multiple single unit recording in the cortex of monkeys using independently moveable microelectrodes. J Neurosci Methods 94:5-17.

Bastian AJ, Mugnaini E, Thach WT (1999) Cerebellum. In: Fundamental Neuroscience (Zigmond MJ, Bloom FE, Landis SC, Roberts JL, Squire LR, eds). San Diego: Academic Press.

Bauswein E, Fromm C, Preuss A (1989) Corticostriatal cells in comparison with pyramidal tract neurons: contrasting properties in the behaving monkey. Brain Res 493:198-203.

Bauswein E, Fromm C, Werner W, Ziemann U (1991) Phasic and tonic responses of premotor and primary motor cortex neurons to torque changes. Exp Brain Res 86:303-310.

Bennett KM, Lemon RN (1996) Corticomotoneuronal contribution to the fractionation of muscle activity during precision grip in the monkey. J Neurophysiol 75:1826-1842.

Berry MJ, 2nd, Meister M (1998) Refractoriness and neural precision. J Neurosci 18:2200-2211.

Bloedel JR, Courville J (1981) A review of cerebellar afferent systems. In: Handbook of Physiology, Vol. II. Motor Control (Brooks VB, ed). Baltimore: Williams and Wilkins.

Boyden ES, Katoh A, Raymond JL (2004) Cerebellum-dependent learning: the role of multiple plasticity mechanisms. Annu Rev Neurosci 27:581-609.

Brenner N, Bialek W, de Ruyter van Steveninck R (2000) Adaptive rescaling maximizes information transmission. Neuron 26:695-702.

Brochier T, Spinks R, Umilta MA, Lemon RN (2004). Patterns of muscle activity underlying object-specific grasp by the macaque monkey. J Neurophysiol 92: 1770-1782.

Brodal A (1981) Neurological anatomy: in relation to clinical medicine, 3rd Edition. New York; Oxford: Oxford University Press.

Brodal P (1978) The corticopontine projection in the rhesus monkey. Origin and principles of organization. Brain 101:251-283.

Brodal P, Bjaalie JG (1992) Organisation of the pontine nuclei. Neurosci Res 13: 83-118.

Brodal P, Bjaalie JG (1997) Salient anatomic features of the cortico-ponto-cerebellar pathway. Prog Brain Res 114:227-249.

Brooks VB, Thach WT (1981) Cerebellar control of posture and movement. In: Handbook of Physiology, Vol. II. Motor Control (Brooks VB, ed). Baltimore: Williams and Wilkins.

Brown EN, Kass RE, Mitra PP (2004) Multiple neural spike train data analysis: state-of-the-art and future challenges. Nat Neurosci 7:456-461.

Buys EJ, Lemon RN, Mantel GW, Muir RB (1986) Selective facilitation of different hand muscles by single corticospinal neurones in the conscious monkey. J Physiol 381:529-549.

Cajal SR (1952) Histologie du Systéme Nerveux de l' Homme et des Vertébrés, Centenary edition Frañcaise, translated by L Azoulay. Madrid: Consejo Superior de Investigaciones Cientificas.

Carpenter, MB, Nova, HR (1960). Descending division of the. brachium conjunctivum in the cat: A cerebello-reticular. system. J. Comp. Neurol. 114, 295-305.

Chan-Palay V (1977) Cerebellar dentate nucleus: organization, cytology and transmitters. Berlin; New York: Springer-Verlag.

Chapman CE, Spidalieri G, Lamarre Y (1986) Activity of dentate neurons during arm movements triggered by visual, auditory, and somesthetic stimuli in the monkey. 55:203-226.

Chen S, Hillman DE (1993) Colocalisation of neurotransmitters in the deep cerebellar nuclei. J Neurocytology 22: 81-91.

Cheney PD, Fetz EE (1980) Functional classes of primate corticomotoneuronal cells and their relation to active force. J Neurophysiol 44:773-791.

Chichilnisky EJ (2001) A simple white noise analysis of neuronal light responses. Network 12:199-213.

Classen J, Liepert J, Wise SP, Hallett M, Cohen LG (1998) Rapid plasticity of human cortical movement representation induced by practice. J Neurophysiol 79:1117-1123.

Conrad B, Brooks VB (1974) Effects of dentate cooling on rapid alternating arm movements. J Neurophysiol 37:792-804.

Conway BA, Halliday DM, Farmer SF, Shahani U, Maas P, Weir AI, Rosenberg JR (1995) Synchronization between motor cortex and spinal motoneuronal pool during the performance of a maintained motor task in man. J Physiol 489 (Pt 3):917-924.

Courtemanche R, Lamarre Y (2005) Local field potential oscillations in primate cerebellar cortex: synchronization with cerebral cortex during active and passive expectancy. J Neurophysiol 93:2039-2052.

Courtemanche R, Pellerin JP, Lamarre Y (2002) Local field potential oscillations in primate cerebellar cortex: modulation during active and passive expectancy. J Neurophysiol 88:771-782.

Darlot C, Zupan L, Etard O, Denise P, Maruani A (1996) Computation of inverse dynamics for the control of movements. Biol Cybern 75:173-186.

Davidson PR, Wolpert DM (2005) Widespread access to predictive models in the motor system: a short review. J Neural Eng 2:S313-319.

De Schutter E (1995) Cerebellar long-term depression might normalize excitation of Purkinje cells: a hypothesis. Trends Neurosci 18:291-295.

De Zeeuw CI, Berrebi AS (1995). Postsynaptic targets of Purkinje cell terminals in the cerebellar and vestibular nuclei of the rat. Eur J Neurosci 7: 2322-33.

De Zeeuw CI, Yeo CH (2005) Time and tide in cerebellar memory formation. Curr Opin Neurobiol 15:667-674.

Dhanarajan P, Ruegg DG, Wiesendanger M (1977) An anatomical investigation of the corticopontine projection in the primate (Saimiri sciureus). The projection from motor and somatosensory areas. Neuroscience 2:913-922.

Dieudonne S (1998) Submillisecond kinetics and low efficacy of parallel fibre-Golgi cell synaptic currents in the rat cerebellum. J Physiol 510 (Pt 3):845-866.

Donoghue JP, Sanes JN (1988) Organization of adult motor cortex representation patterns following neonatal forelimb nerve injury in rats. J Neurosci 8:3221-3232.

Donoghue JP, Leibovic S, Sanes JN (1992) Organization of the forelimb area in squirrel monkey motor cortex: representation of digit, wrist, and elbow muscles. Exp Brain Res 89:1-19.

Donoghue JP, Sanes JN, Hatsopoulos NG, Gaal G (1998) Neural discharge and local field potential oscillations in primate motor cortex during voluntary movements. J Neurophysiol 79:159-173.

Dum RP, Strick PL (2003) An unfolded map of the cerebellar dentate nucleus and its projections to the cerebral cortex. J Neurophysiol 89:634-639.

Dum RP, Strick PL (2005) Frontal lobe inputs to the digit representations of the motor areas on the lateral surface of the hemisphere. J Neurosci 25:1375-1386.

Ebner TJ, Fu Q (1997) What features of visually guided arm movements are encoded in the simple spike discharge of cerebellar Purkinje cells? Prog Brain Res 114:431-447.

Eggermont JJ (1990) The Correlative Brain. Theory and Experiment in Neural Interaction. Berlin: Springer.

Ethier C, Brizzi L, Darling WG and Capaday C (2006). Linear summation of cat motor cortex outputs. J Neurosci 26: 5574-5581.

Evans CM, Baker SN (2003) Task-dependent intermanual coupling of 8-Hz discontinuities during slow finger movements. Eur J Neurosci 18:453-456.

Evarts EV (1968) Relation of pyramidal tract activity to force exerted during voluntary movement. J Neurophysiol 31:14-27.

Evarts EV, Tanji J (1976) Reflex and intended responses in motor cortex pyramidal tract neurons of monkey. J Neurophysiol 39:1069-1080.

Feige B, Aertsen A, Kristeva-Feige R (2000) Dynamic synchronization between multiple cortical motor areas and muscle activity in phasic voluntary movements. J Neurophysiol 84:2622-2629.

Fetz EE, Cheney PD (1980) Postspike facilitation of forelimb muscle activity by primate corticomotoneuronal cells. J Neurophysiol 44:751-772.

Flament D, Hore J (1986) Movement and electromyographic disorders associated with cerebellar dysmetria. J Neurophysiol 55:1221-1233.

Flanagan JR, Wing AM (1997) The role of internal models in motion planning and control: evidence from grip force adjustments during movements of hand-held loads. J Neurosci 17:1519-1528.

Fortier PA, Kalaska JF, Smith AM (1989) Cerebellar neuronal activity related to whole-arm reaching movements in the monkey. J Neurophysiol 62:198-211.

Fu QG, Flament D, Coltz JD, Ebner TJ (1995) Temporal encoding of movement kinematics in the discharge of primate primary motor and premotor neurons. J Neurophysiol 73:836-854.

Fu QG, Flament D, Coltz JD, Ebner TJ (1997) Relationship of cerebellar Purkinje cell simple spike discharge to movement kinematics in the monkey. 78:478-491.

Georgopoulos AP, Schwartz AB, Kettner RE (1986) Neuronal population coding of movement direction. Science 233:1416-1419.

Gerrits NM, Voogd J (1987) The projection of the nucleus reticularis tegmenti pontis and adjacent regions of the pontine nuclei to the central cerebellar nuclei in the cat. J Comp Neurol 258:52-69.

Geyer S, Matelli M, Luppino G, Zilles K (2000) Functional neuroanatomy of the primate isocortical motor system. Anat Embryol (Berl) 202:443-474.

Ghosh S, Porter R (1988a) Morphology of pyramidal neurones in monkey motor cortex and the synaptic actions of their intracortical axon collaterals. J Physiol 400:593-615.

Ghosh S, Porter R (1988b) Corticocortical synaptic influences on morphologically identified pyramidal neurones in the motor cortex of the monkey. J Physiol 400:617-629.

Ghosh S, Brinkman C, Porter R (1987) A quantitative study of the distribution of neurons projecting to the precentral motor cortex in the monkey (M. fascicularis). J Comp Neurol 259:424-444.

Gilbert PF, Thach WT (1977) Purkinje cell activity during motor learning. Brain Res 128:309-328.

Gilbertson T, Lalo E, Doyle L, Di Lazzaro V, Cioni B, Brown P (2005) Existing motor state is favored at the expense of new movement during 13-35 Hz oscillatory synchrony in the human corticospinal system. J Neurosci 25:7771-7779.

Glickstein M (1997) Mossy-fibre sensory input to the cerebellum. Prog Brain Res 114:251-259.

Glickstein M (2000) How are visual areas of the brain connected to motor areas for the sensory guidance of movement? Trends Neurosci 23:613-617.

Glickstein M (2006). Thinking about the cerebellum.Brain 129: 288-290.

Glickstein M, May JG, 3rd, Mercier BE (1985) Corticopontine projection in the macaque: the distribution of labelled cortical cells after large injections of horseradish peroxidase in the pontine nuclei. J Comp Neurol 235:343-359.

Glickstein M, Waller J, Baizer JS, Brown B, Timmann D (2005) Cerebellum lesions and finger use. Cerebellum 4:189-197.

Goodkin HP, Thach WT (2003a) Cerebellar control of constrained and unconstrained movements. I. Nuclear inactivation. J Neurophysiol 89:884-895.

Goodkin HP, Thach WT (2003b) Cerebellar control of constrained and unconstrained movements. II. EMG and nuclear activity. J Neurophysiol 89:896-908.

Gould HJ, 3rd, Cusick CG, Pons TP, Kaas JH (1986) The relationship of corpus callosum connections to electrical stimulation maps of motor, supplementary motor, and the frontal eye fields in owl monkeys. J Comp Neurol 247:297-325.

Hari R, Salenius S (1999) Rhythmical corticomotor communication. Neuroreport 10:R1-10.

Hartmann-von Monakow K, Akert K, Kunzle H (1981) Projection of precentral, premotor and prefrontal cortex to the basilar pontine grey and to nucleus reticularis tegmenti pontis in the monkey (Macaca fascicularis). Schweiz Arch Neurol Neurochir Psychiatr 129:189-208.

Hartmann MJ, Bower JM (1998) Oscillatory activity in the cerebellar hemispheres of unrestrained rats. J Neurophysiol 80:1598-1604.

Hatsopoulos N, Joshi J, O'Leary JG (2004) Decoding continuous and discrete motor behaviors using motor and premotor cortical ensembles. J Neurophysiol 92:1165-1174.

Hatsopoulos NG, Paninski L, Donoghue JP (2003) Sequential movement representations based on correlated neuronal activity. Exp Brain Res 149:478-486.

Henneman E, Cooke PM, Snider RS (1952) Cerebellar projections to the cerebral cortex. Res Publ Assoc Res Nerv Ment Dis 30:317-333.

Hepp-Reymond M, Kirkpatrick-Tanner M, Gabernet L, Qi HX, Weber B (1999) Context-dependent force coding in motor and premotor cortical areas. Exp Brain Res 128:123-133.

Holdefer RN, Miller LE (2002) Primary motor cortical neurons encode functional muscle synergies. Exp Brain Res 146:233-243.

Holdefer RN, Houk JC, Miller LE (2005) Movement-related discharge in the cerebellar nuclei persists after local injections of GABA(A) antagonists. J Neurophysiol 93:35-43.

Holdefer RN, Miller LE, Chen LL, Houk JC (2000) Functional connectivity between cerebellum and primary motor cortex in the awake monkey. J Neurophysiol 84:585-590.

Hoover JE, Strick PL (1999) The organization of cerebellar and basal ganglia outputs to primary motor cortex as revealed by retrograde transneuronal transport of herpes simplex virus type 1. J Neurosci 19:1446-1463.

Huang CS, Hiraba H, Sessle BJ (1989) Input-output relationships of the primary face motor cortex in the monkey (Macaca fascicularis). J Neurophysiol 61:350-362.

Hummel FC, Cohen LG (2005) Drivers of brain plasticity. Curr Opin Neurol 18:667-674.

Humphrey DR, Corrie WS (1978) Properties of pyramidal tract neuron system within a functionally defined subregion of primate motor cortex. J Neurophysiol 41:216-243.

Humphrey DR, Schmidt EM, Thompson WD (1970) Predicting measures of motor performance from multiple cortical spike trains. Science 170:758-762.

Huntley GW, Jones EG (1991) Relationship of intrinsic connections to forelimb movement representations in monkey motor cortex: a correlative anatomic and physiological study. J Neurophysiol 66:390-413.

Imamizu H, Kuroda T, Miyauchi S, Yoshioka T, Kawato M (2003) Modular organization of internal models of tools in the human cerebellum. Proc Natl Acad Sci U S A 100:5461-5466.

Imamizu H, Miyauchi S, Tamada T, Sasaki Y, Takino R, Putz B, Yoshioka T, Kawato M (2000) Human cerebellar activity reflecting an acquired internal model of a new tool. Nature 403:192-195.

Isope P, Dieudonne S, Barbour B (2002) Temporal organization of activity in the cerebellar cortex: a manifesto for synchrony. Ann N Y Acad Sci 978:164-174.

Ito M (1984) The cerebellum and neural control. New York: Raven Press.

Ito M (2000) Mechanisms of motor learning in the cerebellum. Brain Res 886:237-245.

Ito M (2005) Bases and implications of learning in the cerebellum--adaptive control and internal model mechanism. Prog Brain Res 148:95-109.

Jackson A (2002) Synchrony in the primate motor system. In: Institute of Neurology. London: UCL.

Jackson A, Gee VJ, Baker SN, Lemon RN (2003) Synchrony between neurons with similar muscle fields in monkey motor cortex. Neuron 38:115-125.

Jacobs KM, Donoghue JP (1991) Reshaping the cortical motor map by unmasking latent intracortical connections. Science 251:944-947.

Jarvis MR, Mitra PP (2001) Sampling properties of the spectrum and coherency of sequences of action potentials. Neural Comput 13:717-749.

Jones EG (1986) Connectivity of the primate sensory motor cortex. In: Cerebral Cortex (Jones EG, Peters A, eds). New York; London: Plenum.

Jones EG, Wise SP (1977) Size, laminar and columnar distribution of efferent cells in the sensory-motor cortex of monkeys. J Comp Neurol 175:391-438.

Jorntell H, Ekerot CF (1999) Topographical organization of projections to cat motor cortex from nucleus interpositus anterior and forelimb skin. J Physiol 514 (Pt 2):551-566.

Jueptner M, Frith CD, Brooks DJ, Frackowiak RS, Passingham RE (1997) Anatomy of motor learning. II. Subcortical structures and learning by trial and error. J Neurophysiol 77:1325-1337.

Kakei S, Hoffman DS, Strick PL (1999) Muscle and movement representations in the primary motor cortex. Science 285:2136-2139.

Kang Y, Endo K, Araki T (1988) Excitatory synaptic actions between pairs of neighboring pyramidal tract cells in the motor cortex. J Neurophysiol 59:636-647.

Kang Y, Endo K, Araki T (1991) Differential connections by intracortical axon collaterals among pyramidal tract cells in the cat motor cortex. J Physiol 435:243-256.

Kawamura K, Chiba M (1979) Cortical neurons projecting to the pontine nuclei in the cat. An experimental study with the horseradish peroxidase technique. Exp Brain Res 35:269-285.

Kawato M, Kuroda T, Imamizu H, Nakano E, Miyauchi S, Yoshioka T (2003) Internal forward models in the cerebellum: fMRI study on grip force and load force coupling. Prog Brain Res 142:171-188.

Kazantsev VB, Nekorkin VI, Makarenko VI, Llinas R (2004) Self-referential phase reset based on inferior olive oscillator dynamics. Proc Natl Acad Sci U S A 101:18183-18188.

Keat J, Reinagel P, Reid RC, Meister M (2001) Predicting every spike: a model for the responses of visual neurons. Neuron 30:803-817.

Keating JG, Thach WT (1997). No clock signal in the discharge of neurons in the deep cerebellar nuclei. J Neurophysiol 77: 2232-2234.

Kelly AM, Garavan H (2005) Human functional neuroimaging of brain changes associated with practice. Cereb Cortex 15:1089-1102.

Kelly RM, Strick PL (2003) Cerebellar loops with motor cortex and prefrontal cortex of a nonhuman primate. J Neurosci 23:8432-8444.

Kilner JM, Baker SN, Salenius S, Hari R, Lemon RN (2000) Human cortical muscle coherence is directly related to specific motor parameters. J Neurosci 20:8838-8845.

Kilner JM, Baker SN, Salenius S, Jousmaki V, Hari R, Lemon RN (1999) Task-dependent modulation of 15-30 Hz coherence between rectified EMGs from human hand and forearm muscles. J Physiol 516 (Pt 2):559-570.

Kirkwood PA (1979) On the use and interpretation of cross-correlations measurements in the mammalian central nervous system. J Neurosci Methods 1:107-132.

Kitazawa S, Wolpert DM (2005) Rhythmicity, randomness and synchrony in climbing fiber signals. Trends Neurosci 28:611-619.

Konig P, Engel AK, Singer W (1995) Relation between oscillatory activity and long-range synchronization in cat visual cortex. Proc Natl Acad Sci U S A 92:290-294.

Krouchev NI, Kalaska JF (2003) Context-dependent anticipation of different task dynamics: rapid recall of appropriate motor skills using visual cues. J Neurophysiol 89:1165-1175.

Kurata K (2005) Activity properties and location of neurons in the motor thalamus that project to the cortical motor areas in monkeys. J Neurophysiol 94:550-566.

Kuypers HG, Lawrence DG (1967) Cortical projections to the red nucleus and the brain stem in the Rhesus monkey. Brain Res 4:151-188.

Lawrence DG, Kuypers HG (1968) The functional organization of the motor system in the monkey. I. The effects of bilateral pyramidal lesions. Brain 91:1-14.

Lawrence DG, Porter R, Redman SJ (1985) Corticomotoneuronal synapses in the monkey: light microscopic localization upon motoneurons of intrinsic muscles of the hand. J Comp Neurol 232:499-510.

Lee D, Port NL, Kruse W, Georgopoulos AP (1998) Variability and correlated noise in the discharge of neurons in motor and parietal areas of the primate cortex. J Neurosci 18:1161-1170.

Leergard TB, Alloway KD, Pham TAT, Bolstad I, Hoffer ZS, Pettersen C, Bjaalie JG (2004). Three-dimensional topography of corticopontine projections from rat sensorimotor cortex: comparisons with corticostriatal projections reveal diverse integrative organisation. J Comp Neurol 478: 306-322.

Lemon R (1988) The output map of the primate motor cortex. Trends Neurosci 11:501-506.

Lemon RN (1981) Functional properties of monkey motor cortex neurones receiving afferent input from the hand and fingers. J Physiol 311:497-519.

Lemon RN (1999) Neural control of dexterity: what has been achieved? Exp Brain Res 128:6-12.

Lemon RN, Muir RB, Mantel GW (1987) The effects upon the activity of hand and forearm muscles of intracortical stimulation in the vicinity of corticomotor neurones in the conscious monkey. Exp Brain Res 66:621-637.

Li CS, Padoa-Schioppa C, Bizzi E (2001) Neuronal correlates of motor performance and motor learning in the primary motor cortex of monkeys adapting to an external force field. Neuron 30:593-607.

Liu X, Robertson E, Miall RC (2003) Neuronal activity related to the visual representation of arm movements in the lateral cerebellar cortex. J Neurophysiol 89:1223-1237.

Llinas R (1981) Electrophysiology of the cerebellar networks. In: Handbook of Physiology, Vol. II. Motor Control (Brooks VB, ed). Baltimore: Williams and Wilkins.

Llinas R, Yarom Y (1986). Oscillatory properties of guinea-pig inferior olivary neurones and their pharmacological modulation: an in vitro study. J Physiol 376: 163-182.

Lytton WW, Sejnowski TJ (1991) Simulations of cortical pyramidal neurons synchronized by inhibitory interneurons. J Neurophysiol 66:1059-1079.

Maex R, Schutter ED (1998) Synchronization of golgi and granule cell firing in a detailed network model of the cerebellar granule cell layer. J Neurophysiol 80:2521-2537.

Maex R, De Schutter E (2005) Oscillations in the cerebellar cortex: a prediction of their frequency bands. Prog Brain Res 148:181-188.

Maier MA and Hepp-Reymond MC (1995). EMG activation patterns in precision grip. I.Contribution of 15 finger muscles to isometric force. *Exp Brain Res* 103: 108-122.

Maier MA, Bennett KM, Hepp-Reymond MC, Lemon RN (1993) Contribution of the monkey corticomotoneuronal system to the control of force in precision grip. J Neurophysiol 69:772-785.

Mano N, Yamamoto K (1980) Simple-spike activity of cerebellar Purkinje cells related to visually guided wrist tracking movement in the monkey. J Neurophysiol 43:713-728.

Marr D (1969) A theory of cerebellar cortex. J Physiol 202:437-470.

Martin RF, Bowden DM (2000) Primate Brain Maps: Structure of the Macaque Brain. New York: Elsevier.

Mason CR, Miller LE, Baker JF, Houk JC (1998) Organization of reaching and grasping movements in the primate cerebellar nuclei as revealed by focal muscimol inactivations. J Neurophysiol 79:537-554.

Matelli M, Luppino G, Fogassi L, Rizzolatti G (1989) Thalamic input to inferior area 6 and area 4 in the macaque monkey. J Comp Neurol 280:468-488.

Maynard EM, Hatsopoulos NG, Ojakangas CL, Acuna BD, Sanes JN, Normann RA, Donoghue JP (1999) Neuronal interactions improve cortical population coding of movement direction. J Neurosci 19:8083-8093.

McKiernan BJ, Marcario JK, Karrer JH, Cheney PD (1998) Corticomotoneuronal postspike effects in shoulder, elbow, wrist, digit, and intrinsic hand muscles during a reach and prehension task. J Neurophysiol 80:1961-1980.

McKiernan BJ, Marcario JK, Karrer JH, Cheney PD (2000) Correlations between corticomotoneuronal (CM) cell postspike effects and cell-target muscle covariation. J Neurophysiol 83:99-115.

Miall RC, Reckess GZ, Imamizu H (2001) The cerebellum coordinates eye and hand tracking movements. Nat Neurosci 4:638-644.

Miall RC, Weir DJ, Wolpert DM, Stein JF (1993) Is the Cerebellum a Smith Predictor? J Mot Behav 25:203-216.

Middleton FA, Strick PL (2000) Basal ganglia and cerebellar loops: motor and cognitive circuits. Brain Res Brain Res Rev 31:236-250.

Mihailoff GA (1993). Cerebellar nuclear projections from the basilar pontine nuclei and nucleus reticularis tegmenti pontis as demonstrated with PHA-L tracing in the rat. J Comp Neurol 330: 130-146.

Mihailoff GA, McArdle CB (1981) The cytoarchitecture, cytology, and synaptic organization of the basilar pontine nuclei in the rat. II. Electron microscopic studies. J Comp Neurol 195:203-219.

Miller LE, Sinkjaer T (1998) Primate red nucleus discharge encodes the dynamics of limb muscle activity. J Neurophysiol 80:59-70.

Miller LE, van Kan PL, Sinkjaer T, Andersen T, Harris GD, Houk JC (1993) Correlation of primate red nucleus discharge with muscle activity during free-form arm movements. J Physiol 469:213-243.

Mima T, Simpkins N, Oluwatimilehin T, Hallett M (1999) Force level modulates human cortical oscillatory activities. Neurosci Lett 275:77-80.

Monzee J, Drew T, Smith AM (2004) Effects of muscimol inactivation of the cerebellar nuclei on precision grip. J Neurophysiol 91:1240-1249.

Moran DW, Schwartz AB (1999) Motor cortical representation of speed and direction during reaching. J Neurophysiol 82:2676-2692.

Morrow MM, Miller LE (2003) Prediction of muscle activity by populations of sequentially recorded primary motor cortex neurons. J Neurophysiol 89:2279-2288.

Murthy VN, Fetz EE (1996a) Oscillatory activity in sensorimotor cortex of awake monkeys: synchronization of local field potentials and relation to behavior. J Neurophysiol 76:3949-3967.

Murthy VN, Fetz EE (1996b) Synchronization of neurons during local field potential oscillations in sensorimotor cortex of awake monkeys. J Neurophysiol 76:3968-3982.

Mushiake H, Strick PL (1993) Preferential activity of dentate neurons during limb movements guided by vision. J Neurophysiol 70:2660-2664.

Mussa-Ivaldi FA (1988) Do neurons in the motor cortex encode movement direction? An alternative hypothesis. Neurosci Lett 91:106-111.

Na J, Kakei S, Shinoda Y (1997) Cerebellar input to corticothalamic neurons in layers V and VI in the motor cortex. Neurosci Res 28:77-91.

Nicolelis MA, Ghazanfar AA, Faggin BM, Votaw S, Oliveira LM (1997) Reconstructing the engram: simultaneous, multisite, many single neuron recordings. Neuron 18:529-537.

O'Connor SM, Berg RW, Kleinfeld D (2002) Coherent electrical activity between vibrissa sensory areas of cerebellum and neocortex is enhanced during free whisking. J Neurophysiol 87:2137-2148.

Oram MW, Hatsopoulos NG, Richmond BJ, Donoghue JP (2001) Excess synchrony in motor cortical neurons provides redundant direction information with that from coarse temporal measures. J Neurophysiol 86:1700-1716.

Palay S, Chan-Palay V (1987) Cerebellar cortex. In: Encyclopedia of neuroscience (Adelman G, ed). Boston: Birkhèauser.

Paninski L (2003) Convergence properties of three spike-triggered analysis techniques. Network 14:437-464.

Paninski L, Fellows MR, Hatsopoulos NG, Donoghue JP (2004a) Spatiotemporal tuning of motor cortical neurons for hand position and velocity. J Neurophysiol 91:515-532.

Paninski L, Pillow JW, Simoncelli EP (2004b) Maximum likelihood estimation of a stochastic integrate-and-fire neural encoding model. Neural computation.16:2533-2561.

Paninski L, Shoham S, Fellows MR, Hatsopoulos NG, Donoghue JP (2004c) Superlinear population encoding of dynamic hand trajectory in primary motor cortex. J Neurosci 24:8551-8561.

Pascual-Leone A, Amedi A, Fregni F, Merabet LB (2005) The plastic human brain cortex. Annu Rev Neurosci 28:377-401.

Pauluis Q, Baker SN (2000) An accurate measure of the instantaneous discharge probability, with application to unitary joint-even analysis. Neural Comput 12:647-669.

Pellerin JP, Lamarre Y (1997) Local field potential oscillations in primate cerebellar cortex during voluntary movement. J Neurophysiol 78:3502-3507.

Penhune VB, Doyon J (2005) Cerebellum and M1 interaction during early learning of timed motor sequences. Neuroimage 26:801-812.

Pesaran B, Nelson MJ, Andersen RA (2005) Coherence in dorsal premotor cortex and area MIP during free choice and instructed behaviours. Abstract Viewer/Itinerary Planner Washington, DC: Society for Neuroscience, 2005 Online Program No. 363.11. 2005.

Pfurtscheller G, Stancak A, Jr., Neuper C (1996a) Post-movement beta synchronization. A correlate of an idling motor area? Electroencephalogr Clin Neurophysiol 98:281-293.

Pfurtscheller G, Stancak A, Jr., Neuper C (1996b) Event-related synchronization (ERS) in the alpha band--an electrophysiological correlate of cortical idling: a review. Int J Psychophysiol 24:39-46.

Pillow JW, Simoncelli EP (2003) Biases in white noise analysis due to non-Poisson spike generation. Neurocomputing 52:109-115.

Poliakov AV, Schieber MH (1999) Limited functional grouping of neurons in the motor cortex hand area during individuated finger movements: A cluster analysis. J Neurophysiol 82:3488-3505.

Pope P, Wing AM, Praamstra P, Miall RC (2005) Force related activations in rhythmic sequence production. Neuroimage 27:909-918.

Porter R, Lemon R, Physiological Society. (1993) Corticospinal function and voluntary movement. Oxford: Clarendon Press.

Renaud LP, Kelly JS (1974) Simultaneous recordings from pericruciate pyramidal tract and non-pyramidal tract neurons; response to stimulation of inhibitory pathways. Brain Res 79:29-44.

Renaud LP, Kelly JS, Provini L (1974) Synaptic inhibition in pyramidal tract neurons: membrane potential and conductance changes evoked by pyramidal tract and cortical surface stimulation. J Neurophysiol 37:1144-1155.

Riddle CN, Baker SN (2005) Manipulation of peripheral neural feedback loops alters human corticomuscular coherence. J Physiol 566:625-639.

Rispal-Padel L, Cicirata F, Pons C (1982) Cerebellar nuclear topography of simple and synergistic movements in the alert baboon (Papio papio). Exp Brain Res 47:365-380.

Rolls ET, Deco G (2002) Computational neuroscience of vision. Oxford: Oxford University Press.

Rosenberg JR, Amjad AM, Breeze P, Brillinger DR, Halliday DM (1989) The Fourier approach to the identification of functional coupling between neuronal spike trains. Prog Biophys Mol Biol 53:1-31.

Rudolph M, Destexhe A (2001) Do neocortical pyramidal neurons display stochastic resonance? J Comput Neurosci 11:19-42.

Ruegg DG, Seguin JJ, Wiesendanger M (1977) Effects of electrical stimulation of somatosensory and motor areas of the cerebral cortex on neurones of the pontine nuclei in squirrel monkeys. Neuroscience 2:923-927.

Rust NC, Schwartz O, Movshon JA, Simoncelli EP (2005) Spatiotemporal elements of macaque v1 receptive fields. 46:945-946.

Salenius S, Hari R (2003) Synchronous cortical oscillatory activity during motor action. Curr Opin Neurobiol 13:678-684.

Salinas E, Sejnowski TJ (2000) Impact of correlated synaptic input on output firing rate and variability in simple neuronal models. J Neurosci 20:6193-6209.

Salinas E, Sejnowski TJ (2001) Correlated neuronal activity and the flow of neural information. Nat Rev Neurosci 2:539-550.

Schelter B, Winterhalder M, Eichler M, Peifer M, Hellwig B, Guschlbauer B, Lucking CH, Dahlhaus R, Timmer J (2005) Testing for directed influences among neural signals using partial directed coherence. J Neurosci Methods.

Scherberger H, Jarvis MR, Andersen RA (2005) Cortical local field potential encodes movement intentions in the posterior parietal cortex. Neuron 46:347-354.

Schieber MH (1999) Voluntary descending control. In: Fundamental Neuroscience (Zigmond MJ, Bloom FE, Landis SC, Roberts JL, Squire LR, eds). San Diego: Academic Press.

Schieber MH, Thach WT (1985) Trained slow tracking. II. Bidirectional discharge patterns of cerebellar nuclear, motor cortex, and spindle afferent neurons. 54:1228-1270.

Schieber MH, Hibbard LS (1993) How somatotopic is the motor cortex hand area? Science 261:489-492.

Schieber MH, Santello M (2004). Hand function: peripheral and central constraints on performance. J Appl Physiol 96: 2293-2300.

Schmahmann JD, Rosene DL, Pandya DN (2004) Motor projections to the basis pontis in rhesus monkey. J Comp Neurol 478:248-268.

Schoffelen JM, Oostenveld R, Fries P (2005) Neuronal coherence as a mechanism of effective corticospinal interaction. Science 308:111-113.

Schwarz C, Thier P (1999) Binding of signals relevant for action: towards a hypothesis of the functional role of the pontine nuclei. Trends Neurosci 22:443-451.

Scott SH (2000) Reply to 'One motor cortex, two different views'. Nat Neurosci 3:964-965.

Scott SH, Kalaska JF (1997) Reaching movements with similar hand paths but different arm orientations. I. Activity of individual cells in motor cortex. J Neurophysiol 77:826-852.

Schwarz C, Welsh JP (2001). Dynamic modulation of mossy fiber system throughput by inferior olive synchrony: a multielectrode study of cerebellar cortex activated by motor cortex. J Neurophysiol 86: 2489-2504.

Serruya MD, Hatsopoulos NG, Paninski L, Fellows MR, Donoghue JP (2002) Instant neural control of a movement signal. Nature 416:141-142.

Shadmehr R, Mussa-Ivaldi FA (1994) Adaptive representation of dynamics during learning of a motor task. J Neurosci 14:3208-3224.

Shinoda Y, Zarzecki P, Asanuma H (1979) Spinal branching of pyramidal tract neurons in the monkey. Exp Brain Res 34:59-72.

Shinoda Y, Yokota J, Futami T (1981) Divergent projection of individual corticospinal axons to motoneurons of multiple muscles in the monkey. Neurosci Lett 23:7-12.

Shinoda Y, Yamaguchi T, Futami T (1986) Multiple axon collaterals of single corticospinal axons in the cat spinal cord. J Neurophysiol 55:425-448.

Shinoda Y, Sugiuchi Y, Futami T, Izawa R (1992) Axon collaterals of mossy fibers from the pontine nucleus in the cerebellar dentate nucleus. J Neurophysiol 67:547-560.

Shoham S, Paninski LM, Fellows MR, Hatsopoulos NG, Donoghue JP, Normann RA (2005). Statistical encoding model for a primary motor cortical brain-machine interface. IEEE Trans Biomed Eng. 52: 1312-1322.

Simoncelli EP, Paninski L, Pillow JW, Schwartz O, Gazzaniga MS (2004) Characterization of neural responses with stochastic stimuli. In: The Cognitive Neurosciences III: MIT.

Singer W (1994) Time as coding space in neocortical processing: a hypothesis. In: Temporal Coding in the Brain (Buzsaki G, Christen Y, eds). Berlin; London: Springer-Verlag.

Singer W (1999) Neuronal synchrony: a versatile code for the definition of relations? Neuron 24:49-65, 111-125.

Smith AM, Bourbonnais D (1981) Neuronal activity in cerebellar cortex related to control of prehensile force. J Neurophysiol 45:286-303.

Smith AM, Hepp-Reymond MC, Wyss UR (1975) Relation of activity in precentral cortical neurons to force and rate of force change during isometric contractions of finger muscles. Exp Brain Res 23:315-332.

Snider RS, Eldred E (1952) Cerebrocerebellar relationships in the monkey. J Neurophysiol 15:27-40.

Soechting JF, Burton JE, Onoda N (1978) Relationships between sensory input, motor output and unit activity in interpositus and red nuclei during intentional movement. Brain Res 152:65-79.

Spidalieri G, Busby L, Lamarre Y (1983) Fast ballistic arm movements triggered by visual, auditory, and somesthetic stimuli in the monkey. II. Effects of unilateral dentate lesion on discharge of precentral cortical neurons and reaction time. J Neurophysiol 50:1359-1379.

Stein JF, Glickstein M (1992) Role of the cerebellum in visual guidance of movement. Physiol Rev 72:967-1017.

Steriade M (1995) Two channels in the cerebellothalamocortical system. J Comp Neurol 354:57-70.

Strick PL (1983) The influence of motor preparation on the response of cerebellar neurons to limb displacements. J Neurosci 3:2007-2020.

Sugihara I, Shinoda Y (2004) Molecular, topographic, and functional organization of the cerebellar cortex: a study with combined aldolase C and olivocerebellar labeling. J Neurosci 24:8771-8785.

Tanji J, Wise SP (1981) Submodality distribution in sensorimotor cortex of the unanesthetized monkey. J Neurophysiol 45:467-481.

Thach WT (1975) Timing of activity in cerebellar dentate nucleus and cerebral motor cortex during prompt volitional movement. Brain Res 88:233-241.

Thach WT (1978) Correlation of neural discharge with pattern and force of muscular activity, joint position, and direction of intended next movement in motor cortex and cerebellum. J Neurophysiol 41:654-676.

Thach WT, Goodkin HP, Keating JG (1992) The cerebellum and the adaptive coordination of movement. Annu Rev Neurosci 15:403-442.

Thomson AM, Deuchars J (1997) Synaptic interactions in neocortical local circuits: dual intracellular recordings in vitro. Cereb Cortex 7:510-522.

Todorov E (2000) Direct cortical control of muscle activation in voluntary arm movements: a model. Nat Neurosci 3:391.

Tolbert DL, Bantli H, Bloedel JR (1976) Anatomical and physiological evidence for a cerebellar nucleo-cortical projection in the cat. Neuroscience 1:205-217.

Tolbert DL, Bantli H, Bloedel JR (1978) Multiple branching of cerebellar efferent projections in cats. Exp Brain Res 31:305-316.

Tomasch J (1969) The numerical capacity of the human cortico-pontocerebellar system. Brain Res 13:476-484.

Touryan J, Lau B, Dan Y (2002) Isolation of relevant visual features from random stimuli for cortical complex cells. J Neurosci 22:10811-10818.

Treisman A (1999) Solutions to the binding problem: progress through controversy and convergence. Neuron 24:105-110, 111-125.

Truccolo W, Eden UT, Fellows MR, Donoghue JP, Brown EN (2005) A point process framework for relating neural spiking activity to spiking history, neural ensemble, and extrinsic covariate effects. J Neurophysiol 93:1074-1089.

Turner RS, DeLong MR (2000) Corticostriatal activity in primary motor cortex of the macaque. J Neurosci 20:7096-7108.

Ugolini G, Kuypers HG (1986) Collaterals of corticospinal and pyramidal fibres to the pontine grey demonstrated by a new application of the fluorescent fibre labelling technique. Brain Res 365:211-227.

van Kan PL, Houk JC, Gibson AR (1993) Output organization of intermediate cerebellum of the monkey. J Neurophysiol 69:57-73.

Vilis T, Hore J (1977) Effects of changes in mechanical state of limb on cerebellar intention tremor. J Neurophysiol 40:1214-1224.

Vilis T, Hore J (1980) Central neural mechanisms contributing to cerebellar tremor produced by limb perturbations. J Neurophysiol 43:279-291.

von der Malsburg C (1994) The correlation theory of brain function. In: Models of Neural Networks II (E. Domany JLvH, and K. Schulten, ed). Berlin: Springer.

Voogd J (1967) Comparative aspects of the structure and fibre connexions of the mammalian cerebellum. Prog Brain Res 25:94-134.

Voogd J, Glickstein M (1998) The anatomy of the cerebellum. Trends Neurosci 21:370-375.

Walker AE (1938) An oscillographic study of the cerebello-cerebral relationships. J Neurophysiol 1:16-23.

Wannier TM, Maier MA, Hepp-Reymond MC (1991) Contrasting properties of monkey somatosensory and motor cortex neurons activated during the control of force in precision grip. J Neurophysiol 65:572-589.

Welsh, J. P., Lang, E. J., Sugihara, I. & Llinas, R. (1995). Dynamic organization of motor control within the olivocerebellar system. Nature 374, 453-457.

Werner W, Bauswein E, Fromm C (1991) Static firing rates of premotor and primary motor cortical neurons associated with torque and joint position. Exp Brain Res 86:293-302.

Wetmore DZ, Baker SN (2004) Post-spike distance-to-threshold trajectories of neurones in monkey motor cortex. J Physiol 555:831-850.

Wetts R, Kalaska JF, Smith AM (1985) Cerebellar nuclear cell activity during antagonist cocontraction and reciprocal inhibition of forearm muscles. J Neurophysiol 54:231-244.

Wiesendanger R, Wiesendanger M (1982) The corticopontine system in the rat. I. Mapping of corticopontine neurons. J Comp Neurol 208:215-226.

Wolpert DM, Kawato M (1998) Multiple paired forward and inverse models for motor control. Neural Netw 11:1317-1329.

Wolpert DM, Miall RC, Kawato M (1998) Internal models in the cerebellum. Trends Cogn Sci 2:338-347.